

MULTI-STEP PHOTOIONIZATION SPECTROSCOPY OF Sm I

By

ALLAPPARAMBIL UNNI SEEMA

(Enrolment No: PHYS01201304042)

**Bhabha Atomic Research Centre,
Mumbai - 400085, India.**

*A thesis submitted to the
Board of Studies in Physical Sciences
In partial fulfillment of requirements
for the Degree of*

DOCTOR OF PHILOSOPHY

of

HOMI BHABHA NATIONAL INSTITUTE



October, 2018

Homi Bhabha National Institute

Recommendations of the Viva Voce Committee

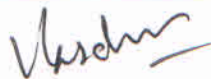
As members of the Viva Voce Committee, we certify that we have read the dissertation prepared by **Allapparambil Unni Seema** entitled "**Muti-step photoionization spectroscopy of Sm I**" and recommend that it may be accepted as fulfilling the thesis requirement for the award of Degree of Doctor of Philosophy.

Chairman - **Dr. N. K. Sahoo**



Date: 7/5/2019

Guide / Convener - **Dr. Vas Dev**



Date: 7/5/2019

Examiner - **Prof. Santhosh Chidangil**



Date: 7/05/19

Member 1- **Dr. S. K. Dixit**



Date: 7/5/19

Member 2- **Dr. S. G. Nakhate**



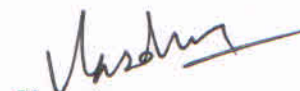
Date: 7/05/2019

Final approval and acceptance of this thesis is contingent upon the candidate's submission of the final copies of the thesis to HBNI.

I hereby certify that I have read this thesis prepared under my direction and recommend that it may be accepted as fulfilling the thesis requirement.

Date: 07/05/2019

Place: Mumbai



Signature
Guide

STATEMENT BY AUTHOR

This dissertation has been submitted in partial fulfillment of requirements for an advanced degree at Homi Bhabha National Institute (HBNI) and is deposited in the Library to be made available to borrowers under rules of the HBNI.

Brief quotations from this dissertation are allowable without special permission, provided that accurate acknowledgement of source is made. Requests for permission for extended quotation from or reproduction of this manuscript in whole or in part may be granted by the Competent Authority of HBNI when in his or her judgment the proposed use of the material is in the interests of scholarship. In all other instances, however, permission must be obtained from the author.



A.U. Seema.



DECLARATION

I, hereby declare that the investigation presented in the thesis has been carried out by me. The work is original and has not been submitted earlier as a whole or in part for a degree / diploma at this or any other Institution / University.



A.U. Seema.



List of publications arising from the thesis

Publications in Refereed Journal:

1. New even-parity high-lying levels of Sm I and measurement of isotope shifts by two-color resonance ionization mass spectrometry;
A.U.Seema, P.K. Mandal, Asawari D.Rath, Vas Dev;
Journal of Quantitative Spectroscopy & Radiative Transfer 145:197–204 (2014).
2. Polarization-based isotope-selective two-color photoionization of atomic samarium using broadband lasers;
A.U. Seema, Asawari D. Rath, P. K. Mandal and Vas Dev;
Appl. Phys. B 118:505–510 (2015).
3. Radiative lifetimes of even-parity high-lying levels of Sm I by delayed photoionization measurements;
A.U. Seema, P. K. Mandal, A. C. Sahoo, M. L. Shah, G. K. Bhowmick and Vas Dev;
Journal of Quantitative Spectroscopy & Radiative Transfer, 216: 1-5 (2018).

Publications in symposia:

1. Radiative lifetime measurements of even-parity high-lying levels of Sm I
A.U. Seema, P. K. Mandal, A. C. Sahoo, M. L. Shah, G. K. Bhowmick and Vas Dev.
Proceedings of NLS-26, 2017.
2. Isotope shift measurements of high-lying even parity levels of Sm I by multi-colour photoionization spectrometry.
A.U. Seema, P. K. Mandal, A. C. Sahoo, M. L. Shah, G. K. Bhowmick, Vas Dev.
Proceedings of NLS-25, 2016.
3. Polarisation Based Isotope Selective Excitation of Sm I using broad band lasers.
A.U. Seema, Asawari D. Rath, P. K. Mandal and Vas Dev; Proceedings of 23rd DAE-BRNS National Laser Symposium (NLS-23): Lasers Spectroscopy and Applications, Sri Venkateswara University, Tirupati, Dec. 3-6, 2014.
4. New even-parity high-lying levels of Sm I by two-colour photoionization spectroscopy.
A.U. Seema, P. K. Mandal, Asawari D. Rath and Vas Dev, Proceedings of National Laser Symposium-22, CP-10-64, PAGE 1-4, Manipal University, Manipal, Karnataka, Jan. 8-11, 2014.
5. Measurement of isotope shifts of even-parity high-lying levels of SmI by two-colour resonance ionization mass spectrometry.
A.U. Seema, P. K. Mandal, Asawari D. Rath and Vas Dev. Proceedings of National Laser Symposium-22, CP-10-65, PAGE 1-4, Manipal University, Manipal, Karnataka, Jan. 8-11, 2014.

Publications not included in the thesis

1. Observation of even-parity autoionization states of uranium by three-colour photoionization optogalvanic spectroscopy in U-Ne hollow cathode discharges, P. K. Mandal, **A. U. Seema**, R. C. Das, M. L. Shah, Vas Dev and B. M. Suri, Journal of Quantitative Spectroscopy & Radiative Transfer **124**, 79 (2013).
2. Radiative lifetimes, branching ratios and absolute transition probabilities of atomic uranium by delayed photoionization measurements", P. K. Mandal, R. C. Das, **A. U. Seema**, A. C. Sahoo, M. L. Shah, A. K. Pulhani, K. G. Manohar and Vas Dev, Applied Physics B **116**, 407 (2014).

Dedicated to

..... My beloved parents



Acknowledgments

*I take this opportunity to convey my heart-felt gratitude and respect to my guide **Prof. Vas Dev**, who has always stood up with me throughout the course of this work, cheerfully encouraging, supporting and guiding. His excellent knowledge about the subject, literature and instrumentation provided me the right guidance for the present work.*

*I gratefully acknowledge the insightful comments and suggestions rendered by my present and previous doctoral committee constituting senior scientists **Prof. N.K. Sahoo**, **Prof. S.K. Dixit**, **Prof. S.G. Nakhate**, **Prof. A. K. Das**, **Prof. P. A. Naik** and **Prof. K. Dasgupta**.*

*I am grateful to **Shri. R. K. Rajawat**, **AD BTDG & Head L&PTD**, for the encouragement and support. I thank **Dr. G. K. Bhowmick**, **Dr. A. K. Ray** and **Shri. S. Kundu** for the fruitful discussions, timely suggestions and encouragement. I am grateful to **Dr. B.N.Jagatap** and **Dr. K.G. Manohar** for mentoring me in the initial years of my work.*

*I am very grateful to **Dr. P. K. Mandal** for his untiring support especially during the experimental work carried out in MDRS lab. It is always motivating to work with an enthusiastic, encouraging and very lively colleague like him. I thankfully remember his sincere support during the preparation of the thesis.*

*It gives me pleasure in acknowledging the support, inspiration and guidance offered by my senior colleagues **Dr. Asawari Rath**, **Dr. A.K. Pulhani**, **Dr. M.L. Shah**, **Dr. R.C. Das**, **Shri. Someshwara Rao**, **Shri. Jinesh Thomas**, **Dr. S. Pradhan**, **Dr. V.S. Rawat** and **Dr. G. Shreedhar** during the course of this work.*

*I am thankful to the **workshop staff of Laser and Plasma Technology Division** for providing the technical support during the course of this work.*

*The ever willing moral support rendered by my friends **Rita Behera, Abdul Wahid, A. C. Sahoo, Shewta Roy, Remyadevi, Viju Chirayil, Shiju Varghese, Ajith, Rajesh, Nicy and Preeta** is remembered cheerfully.*

*I owe a lot to my **teachers**, right from my primary level to the Masters degree. It is their immense care and motivation that gave me the confidence to tread this complex route with perseverance.*

*I take this opportunity to express my gratitude to my parents, **Shri. A. K. Unni** and **Smt. M. K. Rathy**, for their immense love, everlasting care, unconditional support and constant encouragement without which I would not have reached here. I thank my brother **Naisan** and sister **Yamuna** for providing me the comfort space in my every need.*

*I thank with all my heart, my little wonders **Adarsh** and **Ananya** who always brighten up my life with their innocent smile and boundless love. Finally I reserve my deepest appreciation to my husband **Praveen Kumar** for his unconditional support. After all, I sincerely thank **all** those who have helped me directly or indirectly for the successful completion of this thesis.*

...A.U.Seema

CONTENTS

	Page no.
SYNOPSIS.....	XV
LIST OF FIGURES.....	1
LIST OF TABLES.....	5
CHAPTER 1: INTRODUCTION	9
1.1 Introduction to spectroscopy	9
1.1.1 Atomic Spectroscopy	10
1.1.2 Conventional Spectroscopic methods and its limitations	11
1.1.3 Laser Spectroscopy.....	12
1.1.3.1 Absorption spectroscopy with lasers	13
1.1.3.2 Laser induced Fluorescence	14
1.1.3.3 Ionisation Spectroscopy	15
1.1.3.3.1 Multi-step resonance photoionization and its importance to atomic spectroscopy	16
1.2 Atomic Spectroscopy of samarium: A literature review	21
1.3 Motivation for the present work	26
CHAPTER 2: EXPERIMENTAL SET-UP.....	33
2.1 Introduction	33
2.2 Different Laser systems employed in the multi-step photoionization set-up	34
2.2.1 Nd:YAG Laser	35
2.2.2 Dye Laser	37
2.3 Time-of-flight mass spectrometer	40
2.3.1 Flight time of TOFMS	43
2.3.2 Resolution of TOFMS	44

2.3.2.1 Space resolution of TOFMS.....	44
2.3.2.2 Energy resolution of TOFMS.....	45
2.4 Atomic Vapour Source	46
2.5 Experimental set-up for spectral calibration.....	47
2.5.1 Coarse calibration with Opto-galvanic signal.....	47
2.5.2 Fine calibration using Fabry-Perot Etalon.....	50
2.5.3 Photo diode	51
2.6 Signal detection and measurement systems.....	52
2.6.1 Micro Channel Plate (MCP) Detectors.....	52
2.6.2 Pre-amplifier	53
2.6.3 Boxcar averager	53
2.6.4 Wavelength meter	54
2.6.5 Laser power meter.....	55
 CHAPTER 3: DETERMINATION OF HIGH-LYING ENERGY LEVELS, TOTAL ANGULAR MOMENTA AND ISOTOPE SHIFTS BY TWO- COLOUR RESONANCE IONIZATION MASS SPECTROMETRY	 59
3.1 Introduction	59
3.2.1 Mass Shift	60
3.2.2 Field shift.....	62
3.3 Present work on the measurements of atomic parameters	63
3.3.1 Experimental details	64
3.3.2 Measurements of high-lying energy levels and the angular momenta.....	66
3.3.3 Determination of Isotope Shift.....	72
3.3.3.1 Measurements in the energy region 33136 cm ⁻¹ -33960 cm ⁻¹	72
3.3.3.2 Measurements in the energy region 35750 - 35450 cm ⁻¹	77
3.3.3.2.1 Odd-Even Staggering Effect	79
3.4 Conclusions	81

CHAPTER 4: RADIATIVE LIFETIMES OF EVEN-PARITY HIGH-LYING LEVELS OF SM I BY DELAYED PHOTOIONIZATION MEASUREMENTS 85

4.1 Introduction 85

4.2 Radiative lifetimes of excited atoms 85

4.3 Measurement Techniques..... 86

4.3.1 Techniques based on observation of exponential decay curve 87

4.3.1.1 Single-pulse excitation method 87

4.3.1.2 Delayed coincidence method..... 88

4.3.1.3 Beam foil method..... 88

4.3.1.4 Fast beam method 89

4.3.1.5 Pump-probe method..... 89

4.3.2 Techniques not based on observing exponential decay curve 90

4.3.2.1 Phase shift method 90

4.3.2.2 Hanle effect Method..... 90

4.4 Present work on radiative lifetime measurements 91

4.4.1 Experimental Method 92

4.4.2 Results and Discussion 97

4.4.3 Conclusions..... 102

CHAPTER 5: POLARIZATION-BASED ISOTOPE-SELECTIVE TWO-COLOR PHOTOIONIZATION OF ATOMIC SAMARIUM USING BROAD BAND LASERS 105

5.1 Introduction 105

5.2 Experimental scheme employed 106

5.3 Principle behind the process..... 108

5.4 Results and discussion 110

5.4.1 Population alignment on changing the quantisation axis 114

5.4.2 Dependence of relative polarisation angle on selectivity	117
5.5 Conclusions	118
CHAPTER 6: CONCLUSIONS AND FUTURE PROSPECTS.....	123
REFERENCES:.....	129

Homi Bhabha National Institute

SYNOPSIS OF Ph.D. THESIS

1. Name of the Student: **Allapparambil Unni Seema**
2. Name of the Constituent Institution: **Bhabha Atomic Research Centre**
3. Enrolment No.: **PHYS 01201304042**
4. Title of the Thesis: **Multi-step photoionization spectroscopy of Sm I**
5. Board of studies: **Physical Sciences**

SYNOPSIS

Spectroscopy is the branch of science which deals with the interaction of electromagnetic radiation with matter. It provides many possible ways by which the micro-world of atoms and molecules can be explored through light-matter interaction. The light emitted, absorbed, scattered or the photoions generated during the interaction process can be analyzed to study, identify and quantify matter since each element is characterized with its distinctive spectral features. The spectral data obtained through spectroscopic measurements can be utilized to understand electronic configuration, the energy level structure, as well as various other atomic/molecular properties. The quantitative measurements of these properties provide information useful for the diagnostics and quantification of atoms or molecules as well as it provide information about external parameters like electric field, magnetic field, temperature etc. Rapidly growing field of spectroscopy has made significant impact in many

areas of science including laser physics, analytical chemistry, environmental science, medicine, astrophysics etc.

In a broad perspective, spectroscopy is classified into various categories based on the factors like nature of interaction, detection method employed and the spectral range of interaction. Accordingly, depending on the nature of interaction, there are different classes termed as absorption spectroscopy, emission spectroscopy, scattering spectroscopy etc. and based on the detection method there are different classes such as photoionization spectroscopy, fluorescence spectroscopy, opto-galvanic spectroscopy, acousto-optic spectroscopy etc. and depending on the spectral range of interaction the classification includes micro wave spectroscopy, infrared spectroscopy, visible spectroscopy, UV spectroscopy, X-ray spectroscopy, gamma ray spectroscopy etc [1].

Conventionally, absorption or emission techniques were utilized for studying atomic spectra. These techniques were not suited for studying the high-lying atomic levels due to the following limitations: 1) absorption cross section decreases as one move up the excitation ladder making the detection of the high-lying levels difficult 2) inaccessibility of an excited state with the same parity as that of the ground state using single-photon excitation due to selection rules. Another experimental difficulty is that if the spectra lie in the vacuum ultra violet region, then complex vacuum ultra violet spectrometers have to be used for detection. The traditional atomic sources used in absorption/emission experiments are hollow cathode discharge lamps, electrode-less discharges, flames and plasmas. Spectroscopic investigations utilizing these sources put stringent conditions on the resolution of the spectrometer as these sources contain atoms, ions and multi-atomic species in diverse states. The complexity in assigning the atomic states also increases as many excited states can decay to low-lying

states. Hence it is tedious to get complete spectroscopic information using conventional techniques [2,3].

Invention of lasers have revolutionized the conventional spectroscopy and made it an excellent tool which finds application in diverse fields ranging from separation physics, analytical chemistry, chemical dynamics, cluster science, surface science, nuclear physics, bio-physics, geophysics, astrophysics, environmental science etc. The innovative applications evolved in these fields are strongly coupled with the incredible progress made in the development of various lasers. The spectral and temporal characteristics of the lasers – monochromaticity, high intensity, directionality, wavelength tunability, coherence and temporal flexibility have made it a versatile tool for spectroscopic applications compared to the conventional light sources. The development of high power tunable lasers has amplified the attractiveness and range of applications of lasers in the field of spectroscopy. Possibly, multi-step photoionization spectroscopy is one of these areas which have undergone great revolutions. Utilizing the increased intensity available with the laser sources, it is possible to probe highly excited states of atoms and molecules and with the increased spectral resolution of the laser sources, it is possible to probe the structural details. Commercially available lasers can be used to generate various wavelengths and intensities required for efficient photoionization schemes involving step-wise resonant excitation or non-resonant multi-photon excitations/ionization. Among the tunable lasers, dye lasers serve as the most common light source for multi-step photoionization spectroscopy with the possible wide tuning range covering from ultra violet through visible to far infrared. Progress made in the growth of dye lasers with specific characteristics like narrow band width, wide tuning range, ultra short pulse duration etc. had led to new experimental spectroscopic techniques. The increased power density available with the laser sources compared to the conventional

sources gives rise to many orders of magnitude enhancement in the detection sensitivity [4, 5, 6].

Spectroscopic studies of lanthanides are of fundamental importance in improving the understanding of basic atomic physics as well as in applied research because of its overriding scientific as well as technological applications in areas such as laser isotope separation, trace analysis, laser and medical industry, material science, astrophysics etc. Lanthanides and actinides are part of a distinct section of periodic table having partially filled f orbital. In the lanthanide and actinide series the 4f and 5f orbitals are gradually filled in with electrons. Due to the presence of unpaired electrons in the f orbital, the spectra of these elements are very rich and complex. The spectra produced by many of the lanthanides are intricate due to the presence of large number of isotopes of these elements. In addition, the presence of hyperfine structure for the odd isotopes further complicates the spectral analysis. These elements still have unexplored energy regions which cannot be accessed by conventional spectroscopic techniques due to the very low population in those levels making the signal detection very difficult.

Multi-step resonance ionization spectroscopy is well suited for studying the high-lying and autoionising atomic energy levels. Multi-step laser photoionization of atoms and molecules is currently a rapidly developing area of scientific exploration. This is an unparalleled method by which it is possible to characterize almost all the atomic and molecular properties and the dynamics. This method is sensitive enough to detect single atoms or ions. In this method, the high-lying atomic levels are accessed using one or more photons from tunable lasers depending on the ionization potential of the element. The excitation of these levels can be easily carried out using CW or pulsed tunable lasers as the photo-excitation cross sections involved in these processes involving resonant steps are

relatively high. Generally, the excited atoms are monitored by detecting either photoions, fluorescence from the excited levels or the change in the discharge impedance using the techniques of photoionization spectroscopy, laser-induced fluorescence and opto-galvanic spectroscopy respectively [7,8].

The present Ph. D thesis deals with the application of multi-step resonance ionization spectroscopic techniques for the measurement of various atomic parameters of samarium ($Z=62$), a representative of lanthanide series. The work described in the subsequent chapters involves the determination atomic parameters like energy levels, total angular momenta, isotope shifts and radiative life times of high-lying energy levels of samarium using multi-step resonance ionization spectroscopy. Most of these atomic parameters find application in many areas of science such as atomic physics, laser physics, plasma physics, laser chemistry, atmospheric science, astrophysics etc. It also describes in detail a novel isotope selective photoionization technique based on polarisation selection rule for efficient isotope-selective photoionization of the odd isotopes of samarium using broad band lasers. The thesis has been structured into six chapters, elaborating the work carried out in the above mentioned areas. The chapter-wise description of the work is given below:

Chapter 1 describes a brief introduction to atomic spectroscopy and its importance in atomic structure studies. Different conventional spectroscopic techniques and the problems associated with these techniques for studying the atomic structure of complex atoms, especially for studying the high-lying energy levels have been discussed. How the advent of laser spectroscopic techniques has overcome these difficulties and has offered a new outlook for the field has been outlined. In addition, literature survey of the laser spectroscopic work carried out previously relevant to the work reported in this thesis along with a brief description of the present studies is given at the end of this chapter.

Chapter 2 deals with the experimental set-up employed for the photoionization studies described in this thesis. It includes a detailed description of the Nd-YAG pumped dye laser systems used for photoionization studies, time-of-flight mass spectrometer, its working principle and its advantages over other conventional type mass spectrometers, hollow cathode discharge lamp used for coarse wavelength calibration of the photoionization spectra, Fabry-Perot etalon and photo diode unit used for fine wavelength calibration, signal detection and processing systems utilized in these experiments.

Chapter 3 deals with the measurement of energy level values, total angular momenta and isotope shifts of the high-lying levels of samarium using two-colour photoionization spectroscopy. Sm being one of the representatives of lanthanide series has a rich and complex spectrum due to its less than half filled 4f-shell. This chapter describes in detail the experimental methodologies followed in the measurement of high-lying energy levels, angular momenta and isotope shifts along with a brief description of the experimental set-up. Isotopic data on high-lying levels is a vital information required for determining isotopic selectivity in a multi-step excitation scheme.

Two-colour three-photon resonance photoionization spectra of atomic Sm (Sm I) are investigated in the energy region $33136 - 33960 \text{ cm}^{-1}$ and $35450 - 35750 \text{ cm}^{-1}$. The work resulted in the identification of more than twenty energy levels in these regions. The energy values of the newly identified energy levels have been assigned with an accuracy of $\pm 0.3 \text{ cm}^{-1}$. Based on the excitation scheme used, most of the new levels have been identified with a unique total angular momentum (J). In addition, by performing mass-resolved photoionization spectroscopy, the isotope shift of twenty eight high-lying levels of Sm I was measured. The details of this work will be presented in this chapter.

Chapter 4 deals with the radiative lifetime measurements of the even-parity high-lying levels of atomic samarium by delayed photoionization measurements using pump-probe spectroscopy. Radiative lifetime is an important atomic parameter when combined with branching ratio can provide another vital atomic parameter, the absolute transition probability which is required in many areas of science such as laser physics, plasma physics, astrophysics etc. These parameters also play crucial role in applications like laser vapour processing, trace elemental analysis, etc. To select a highly efficient ionization scheme, one must have reliable data on lifetimes and absolute transition probabilities for many levels and transitions. In addition, reliable atomic data is required for validating theoretical models which need detailed comparisons with experimental data especially in case of elements with complex spectra.

This chapter lists the radiative lifetimes of the even-parity high-lying levels of atomic samarium in the energy range 34000- 34815 cm^{-1} measured for the first time. The measurements were carried out by detecting time resolved delayed three-colour photoionization signal by pump-probe technique in an atomic beam coupled with a time-of-flight mass spectrometer. The measured values are in the range of 35 to 349 ns. Accuracy of the measurements was validated by measuring the lifetime of the first excited level used in the excitation scheme by employing two-colour pump-probe photoionization spectroscopy and comparing the measured value with that reported in the literature. The details of the measurement technique will be presented in the chapter.

Chapter 5 describes the experimental demonstration of polarization based isotope selective photoionization technique for selective photoionization of odd isotopes of samarium using broad band lasers. Generally, in laser isotope separation (LIS) process, isotope-selective photoionization of the target isotope is achieved by utilizing the isotope shift or the difference

in the hyperfine structure of different isotopes using narrow band lasers. This method puts stringent condition on the laser band width and the atomic beam parameters especially when the isotope shifts are small and the hyperfine spectra are overlapping. In polarization based isotope selective photoionization method, odd isotopes with non-zero nuclear spin are selectively excited while the even isotopes with zero nuclear spin are prohibited from excitation by judiciously choosing a proper angular momentum sequence of the energy levels involved in the excitation ladder and the laser polarizations. However, this method is applicable to elements having states with low total angular momentum (J-values) such as Zr, Gd, Yb, Sm etc.

This chapter describes polarization-based isotope-selective photoionization of odd isotopes of Sm I by using two-color three-photon photoionization spectroscopy. Atomic samarium (Sm I) has seven naturally abundant isotopes ^{144}Sm (3.1%), ^{147}Sm (15%), ^{148}Sm (11.3%), ^{149}Sm (13.8%), ^{150}Sm (7.4%), ^{152}Sm (26.6%) and ^{154}Sm (22.6%). Isotope-selectivity of more than 40 between the odd and even isotopes ($^{149}\text{Sm}/^{152}\text{Sm}$) of atomic Sm has been experimentally demonstrated by judiciously selecting proper angular momentum sequence of the levels involved in the excitation scheme and laser polarizations. This is the first experimental demonstration of isotope-selective photoionization of the odd isotopes of samarium using polarized laser beams. Since the technique has the advantage that the isotopic selectivity is not affected by the spectral broadening of the excitation lasers, it is highly useful for the separation of odd and even isotopes exhibiting overlapping spectra owing to small isotope shifts and broad hyperfine structures. The method described above has the unique advantage that it does not demand a high spectroscopic resolution and thus has the benefit of using broad band lasers and thermally distributed atomic beams. The chapter also describes

in detail the effect of different states of polarization of the excitation lasers and the relative polarization angle between them on the isotope selectivity.

Chapter 6 presents the conclusions including the summary of the work carried out in the present studies and the scope for future work.

References:

1. A. K. Pulhani, "*Laser Spectroscopic Investigations of Lanthanides and Actinides*", Ph. D. Dissertation, Mumbai University, India (2011).
2. P. G. Wilkinson, "A high resolution spectrograph for vacuum ultra violet, *Journal of molecular spectroscopy*", 1, 268 (1957).
3. M. L. Shah, "*Laser Spectroscopic Techniques and Related Instrumentation for Studies on Lanthanides and Actinides*", Ph. D. Dissertation, Homi Bhabha National Institute, India (2016).
4. V. S. Letokhov, "*Laser photoionization spectroscopy*", (Academic Press. INC, 1987).
5. W. Demtröder, "*Laser spectroscopy basis principles*", 5th edition (Springer-Verlag Berlin Heidelberg, 2014).
6. L. J. Radziemski, "*Laser spectroscopy and its applications*", (Marcel Dekker INC, 1987).
7. B. M. Suri, "*High-resolution spectroscopy*", (Springer India, 2015).
8. Robert D Cowan, "*The theory of atomic structure and spectra*", (Univ of California Press, 1981).



LIST OF FIGURES

Fig. 1.1: a) Single-colour two-photon and b) single-colour three-photon ionisation path ways. The dotted line represents a virtual level.	19
Fig. 1.2: a) Two-colour two-photon and b) Two-colour three-photon ionisation path ways.	19
Fig. 1.3: a) Three-colour three-photon process ending in continuum b) Three-colour three-photon ending in an autoionisation state c) Two-colour three-photon reaching a Rydberg level close to continuum.	20
Fig. 2.1: Schematic representation of the experimental set-up. DL_1 , DL_2 , DL_3 : tunable dye lasers, ODL: optical delay line, EDG: electronic delay generator, FC: fibre coupler, WM: wavelength meter, TOFMS: time-of-flight mass spectrometer, MCP: micro-channel plate detector, AMP: pre-amplifier, DSO: digital storage oscilloscope, PD: photo diode, BD: beam dump, M: mirror, BS: beam splitter, PC: personal computer.....	33
Fig. 2.2: Laser systems used in photoionization experiments	34
Fig. 2.3: Simplified energy level diagram of Nd:YAG laser[63]	36
Fig. 2.4: Energy level diagram for a dye molecule [64]	38
Fig. 2.5: Absorption and fluorescence spectrum of Rhodamine 6G dissolved in ethanol [3].	39
Fig. 2.6: Schematic of time of flight mass spectrometer	42
Fig. 2.7: (a) Schematic of the collimated atomic beam source (b) Atomic velocity components	47
Fig. 2.8: Hollow cathode discharge lamp.....	49
Fig. 2.9: Fabry-Perot etalon fringes	50
Fig. 2.10: Signal output of the photo diode.....	51

Fig. 3.1: Schematic representation of the experimental set-up for two-colour photoionization spectroscopy. DL_1 , DL_2 : tunable dye lasers, HCDC: U- Ne hollow cathode discharge lamp, FP: Fabry-Perot etalon, TOFMS: time-of-flight mass spectrometer, MCP: micro-channel plate detector, AMP: pre-amplifier, BCA: boxcar averager, DSO: digital storage oscilloscope, PD: photo diode, BD: beam dump, M: mirror, BS: beam splitter, ODL: optical delay line, FC: fiber coupler, WM: wavelength meter, PC: personal computer.....	65
Fig. 3.2: Schematic of photoionization pathways. (1) Scheme A (2) Scheme B.....	66
Fig. 3.3: A part of the two-colour photoionization spectrum of Sm I obtained using scheme A (a): Fabry-Perot fringes (b): Single-colour optogalvanic spectrum (c): Two-colour photoionization spectrum. Peaks labeled with star indicate actual two-colour resonances and are identified with the corresponding upper level energies. (d): Single-colour photoionization spectrum. Traces (a)-(c) were measured simultaneously.....	68
Fig. 3.4: Transitions between the magnetic sublevels of Sm I in scheme A for $J = 1 \rightarrow 0 \rightarrow 0$ transition in case of an (a) even isotope (b) odd isotope. Allowed and forbidden transitions are indicated by solid and dotted lines respectively.	70
Fig. 3.5: A typical single-colour TOF mass spectrum of Sm I when λ_1 is tuned to the first step transition of scheme A. The mass spectrum does not reflect the natural abundance of different isotopes because it depends on where exactly the laser wavelength is fixed in between the resonances of ^{144}Sm and ^{154}Sm isotopes.....	72
Fig. 3.6: Typical mass resolved two-colour photoionization spectrum of Sm I observed using scheme A. The resonance at 15518.3 cm^{-1} shows a positive isotope shift whereas the resonance at 15523.4 cm^{-1} shows a negative isotope shift. The resonances are also labelled with the corresponding upper level energies.....	74

Fig. 3.7: Typical mass resolved two-colour photoionization spectrum of Sm I for the isotopes ^{154}Sm , ^{149}Sm and ^{144}Sm	78
Fig. 3.8: Manifestation of odd-even staggering effect in the two colour spectra.	80
Fig. 4.1: Schematic representation of the experimental set-up for three-colour pump-probe spectroscopy. DL_1 , DL_2 , DL_3 : tunable dye lasers, ODL: optical delay line, EDG: electronic delay generator, A: Aperture, FC: fibre coupler, WM: wavelength meter, TOFMS: time-of-flight mass spectrometer, MCP: micro-channel plate detector, AMP: pre-amplifier, DSO: digital storage oscilloscope, PD: photo diode, BD: beam dump, M: mirror, BS: beam splitter, PC: personal computer.	93
Fig. 4.2: Schematic of photoionization schemes. (a) Scheme A (b) Scheme B, (c) pump and probe laser pulse sequencing for pump-probe scheme.	96
Fig. 4.3: Typical decay curve of the high-lying energy level at 34774.2 cm^{-1} along with the exponential fit.	98
Fig. 4.4: Decay curve of the first excited energy level at 18075.51 cm^{-1} along with the exponential fit.	99
Fig. 5.1: Excitation Scheme	107
Fig. 5.2: Transitions between magnetic sublevels of Sm I for parallel linear polarizations of the excitation lasers. (a) even isotope (b) odd isotope for the chosen scheme. Forbidden transition is labelled with a cross.	109
Fig. 5.3: Transitions between magnetic sublevels of Sm I in case of an even isotope when λ_1 is circularly polarized and λ_2 is linearly polarized.....	110
Fig. 5.4: Two-color photoionization mass spectra (a) when both λ_1 and λ_2 lasers have parallel linear polarization and (b) when λ_1 is circularly polarized and λ_2 is linearly polarized.....	112

Fig. 5.5: Mass-resolved two-color photoionization spectra of Sm I. (1) Two-color photoionization spectra for the odd isotope (^{149}Sm) (2) Two-color photoionization spectra for the even isotope (^{152}Sm) and (3) Fabry-Perot etalon fringes	113
Fig. 5.6: Population alignments along the excitation ladder in case of an even isotope with cross polarizations of the excitation lasers	115
Fig. 5.7: Dependence of the ratio of the photoionization signal for the even isotope to that of the odd isotope ($^{152}\text{Sm}/^{149}\text{Sm}$) on relative polarization angle (θ) between the two dye lasers	118

LIST OF TABLES

<i>Table 1.1: Ground state of atomic Samarium</i>	22
<i>Table 3.1: High-lying even-parity levels of Sm I</i>	71
<i>Table 3.2: Isotope shifts of the high-lying levels of Sm I in the energy region 33136-33960 cm⁻¹</i>	76
<i>Table 3.3: Isotope shifts of the high-lying levels of SmI in the energy range 35750-35450 cm⁻¹</i>	82
<i>Table 4.1: Measured radiative lifetimes of high-lying even-parity levels of atomic samarium</i>	101
<i>Table 4.2: Measured radiative lifetime of the first excited level of atomic samarium</i>	102



Chapter: 1

Introduction

Chapter 1

1.1 Introduction to spectroscopy

Spectroscopy is the branch of science which deals with the interaction of electromagnetic radiation with matter. Each atom or molecule absorbs or emits radiation which is characteristic of that species. Hence, atomic or molecular spectra can be used to detect, identify and quantify information about the matter under consideration. Basic research in spectroscopy is essential to solve primary problems related to the fundamentals of science as well as to invent novel spectroscopic techniques useful for various scientific and technological applications. Spectroscopy has made significant impact in many areas of science including laser physics, analytical chemistry, environmental science, medicine, astrophysics etc.

Most of the practical applications of spectroscopy in science and technology require the measurement of absorbed or emitted radiation or detection of ions/electrons. The major limitation in practical applications is imposed by the attainable detection sensitivity of atoms, molecules, ions or photons with a reasonable signal to noise ratio. Furthermore, many applications require a sufficiently high spectral and spatial resolution. Many a times, the demand for high sensitivity and high spectral resolution cannot be fulfilled simultaneously and an optimum compromise has to be opted out depending on the requirements. The recent developments of various types of lasers and the detection systems have pushed both the attainable resolution and sensitivity to significant limits of reaching sub-Doppler spectral resolution and single atom detection [1].

1.1.1 Atomic Spectroscopy

Atomic spectroscopy involves the interaction of light with atoms in gas phase. The electromagnetic spectrum covers a wide range of wavelengths, including gamma ray, X-ray, ultraviolet, visible, infrared, microwave, and radio frequency regions. Atomic spectrometry, is relatively limited to regions of the spectrum between 180 and 900 nm (ultraviolet, visible, and near infrared). These wavelengths are involved in electronic transitions of valence electrons.

In atomic spectroscopic experiments, the spectra, i.e. the light absorbed or emitted by the atom is recorded. A lot of information about the absorbing species can be derived from the recorded spectra. The wavelengths corresponding to the spectral lines are utilised in identifying the energy levels. The spectral line intensities are useful to extract the information about transition probabilities. The width of the spectral line carries information about the collision processes, velocity distribution of atoms in the sample and the inter-atomic potentials. Similarly, the information about the magnetic and electric moments of an atom can be obtained from the Zeeman and Stark splitting of spectral lines in external magnetic and electric fields respectively. Also, from the isotope shift and hyperfine structure of the atom it is possible to extract information about the interaction between the electron cloud and the nucleus. Accurate measurements of isotope shift can give information about the change in the nuclear charge radius among different isotopes. A detailed analysis of the hyperfine structure of the atoms allows the determination of the nuclear spin, magnetic dipole and electric quadrupole moments [2,3,4].

1.1.2 Conventional Spectroscopic methods and its limitations

Conventionally, absorption or emission techniques were utilized for studying atomic spectra. The traditional atomic sources used in absorption/emission experiments are hollow cathode discharge lamps, electrode-less discharges, flames and plasmas. The conventional techniques employing these sources were not suited for studying the high-lying atomic levels due to the following limitations: 1) the low spectral intensity associated with the conventional light sources 2) the absorption cross section decreases as one move up the excitation ladder making the detection of the high-lying levels difficult and 3) inaccessibility of an excited state with the same parity as that of the ground state using single-photon excitation due to selection rules. Further, if the spectra lie in the vacuum ultra violet region, then complex vacuum ultraviolet spectrometers have to be used for detection. Spectroscopic investigations utilizing traditional spectroscopic sources put stringent conditions on the resolution of the spectrometer as these sources contain atoms, ions and multi-atomic species in diverse states. The resolution and sensitivity that can be achieved in the conventional spectroscopic methods will be limited by the attainable dispersion of monochromators and the brightness of the radiation sources. Also the complexity in assigning the atomic states increases, as in these sources many excited states can decay to various low-lying states. Furthermore, only a very minute fraction of the atoms in these discharge are in the high-lying states. The atoms from these states decay to a large number of low lying states, resulting in a very few photons emitted per allowed transition leading to poor detection sensitivity. Hence it is tedious to get complete spectroscopic information using conventional techniques [5, 6]. Despite these, a large number of spectroscopic data has been generated using conventional spectroscopic techniques.

1.1.3 Laser Spectroscopy

Laser spectroscopy differentiates itself from the classical spectroscopy in many ways. Contrary to the radiation sources with broad emission spectra used in conventional spectroscopy, tunable lasers offer efficient spectroscopic light sources in the spectral range from UV to far IR with exceptionally narrow bandwidths and spectral power densities that may exceed those of incoherent light sources by many orders of magnitude. Employing such a tunable monochromatic source, a spectrum can be recorded by measuring light intensity (fluorescence/ transmission) or photoion yield as a function of the wavelength of the tunable source by wavelength scanning. It may be reasonable to evoke comparative advantages of laser spectroscopy over that of the classical, even though the latter has made significant contributions to its credit. In classical spectroscopy, the spectral resolution attainable is limited by the dispersing spectrometers, where as in case of laser spectroscopy, using tunable lasers with narrow line widths, high spectral resolutions can be attained. If the laser spectral line width $\Delta\nu_L$ is smaller than the absorption line width $\Delta\nu_a$, then the spectral resolution will be limited by the width of the absorption lines which is decided by the dominating broadening mechanism. While it is possible to achieve extremely high spectral resolution with CW single mode lasers, ultrafast dynamic effects can be explored using femto and attosecond lasers [7]. Another important feature of laser spectroscopy compared to classical spectroscopy is that it is possible to transfer selectively a significant atomic population in an excited state comparable to the absorbing ground state. This allows one to perform the absorption, fluorescence or photoionization spectroscopy of the excited states and to upgrade the existing spectroscopic techniques which were till then restricted to the electronic ground states.

Depending on whether the resolution is limited by the Doppler width of the absorbing transition or not, laser spectroscopic techniques can be classified into two groups viz. Doppler limited and Doppler-free. Doppler-free spectroscopic techniques circumvent the limit set on the resolution by the Doppler broadening and hence allow performing high resolution spectroscopy. Saturation absorption spectroscopy, polarization spectroscopy and two-photon spectroscopy are some examples of Doppler-free spectroscopic techniques which can be employed in high resolution measurements like isotope shift, hyperfine structure etc [8].

1.1.3.1 Absorption spectroscopy with lasers

The sensitivity and resolution of the absorption techniques have significantly enhanced due to the introduction of lasers to absorption spectroscopy. This is mainly due to the orders of magnitude enhancement in the attainable resolution and brightness associated with the laser sources compared to the conventional light sources coupled with dispersion elements. In laser absorption spectroscopy, the attainable resolution is not limited by the instrumental line width, but can be the natural line width of the transition under consideration. Also the enhanced photon flux associated with laser sources has improved the signal to noise ratio in the absorption spectra.

The amount of information which can be extracted from the absorption spectra depends on the attainable spectral resolution, time resolution and detection sensitivity. High detection sensitivity can be achieved by increasing the path length, choosing a transition with higher cross section or by increasing the signal to noise ratio. Large path lengths can be achieved by performing intra cavity absorption, i.e. by keeping the sample inside a laser cavity or by performing cavity ring down spectroscopy, i.e. by keeping the sample inside a highly reflective external cavity.

1.1.3.2 Laser induced Fluorescence

Laser induced fluorescence (LIF) spectroscopy is a very sensitive and potent means of detecting atoms or molecules, measuring their concentrations, determining the energy level population distributions and the level lifetimes etc. In LIF measurements the atoms/molecules are excited from the ground electronic state to the excited state by the absorption of laser. The excited atoms/molecules can decay back to various low-lying states by spontaneous emission of photons. The intensity of the spontaneous emission i.e. the fluorescence is directly proportional to the number density of the excited state species. The fluorescence signal is collected and given to a wavelength selective element and the output from this device is detected by photomultiplier or other light sensitive devices. The electrical signal from the detector is then given to the signal processing unit. In many cases fluorescence spectroscopy is used as a very sensitive species detection technique.

Contrary to absorption technique, where the absorption is measured over a large background noise, the fluorescence can be detected at very small background noise, which results in high detection sensitivity. Also the high intensity of the exciting laser radiation facilitates the observation of fluorescence signal even from weak transitions and at low atom densities. Using fluorescence technique it is possible to measure the radiative lifetimes of excited states of atoms employing pulsed lasers. This can be achieved by exciting the atomic species by a very short laser pulse and monitoring the resultant fluorescence emission at subsequent time delays. However, LIF is not suitable for studying discrete levels above the continuum (AI levels) due to the spontaneous ionisation of the atoms from these levels. Also, the method is not suitable for studying Rydberg levels due to the large radiative lifetimes of these levels resulting in weak fluorescence [9].

1.1.3.3 Ionisation Spectroscopy

Ionization spectroscopy monitors the absorption of photons on atomic transition, by detecting the ions or electrons produced by ionization of the excited state. The necessary ionization of the excited state may be performed by collisions, by an external electric field or by photons.

a) Collision-Induced Ionization

Laser excitation followed by collisional ionisation is one of the methods employed in ionisation spectroscopy. This ionisation method is used when the excited level is not too far from the ionization limit, the atom/molecule can be ionized by thermal collisions with electrons, buffer gas atoms, as well as with excited atoms or molecules of the same species.

b) Field Ionisation

Field ionization has proven to be a versatile and efficient tool for the detection of Rydberg atoms. In case of Rydberg atoms, the outer electron is very weakly bound to the atomic core so that even a relatively weak electric field can remove the electron from the atom. The electric field strength at which the ionisation happens depends on the state of the Rydberg atom. Pulsed electric field ionisation is a potent means of detecting and analysing the states of Rydberg atoms. If the high-lying state is at energy where the excited electron is unbound in the combined field produced by the core and the externally applied dc field, then the electron is free to move and the ion is produced. For a Rydberg state of effective principle quantum number n^* , the critical field for field ionisation is given by [5],

$$E_c = \frac{1}{16 n^{*4}} \text{ (atomic units)} = 3.21 \times 10^8 \frac{1}{n^{*4}} \frac{V}{cm} \quad (1.3)$$

c) Photoionization

In photoionization spectroscopy, the excited atomic species is ionised by absorption of another photon either from the same laser or from another laser or from an incoherent light source. The resultant photoions are extracted by applying an electric field and subsequently detected by a channeltron or a micro channel plate (MCP) detector. The method has the distinctive feature of exceptionally high sensitivity of detecting even single atom or molecule. The technique can also be combined with high spectral and temporal resolution. All these features make it an efficient tool for basic research and technological applications. Most importantly, photoionization method is a universal technique since it is applicable to any atom or molecule [8].

The tunable lasers used in photoionization experiments can be operated in either pulsed or continuous mode (cw). The cw lasers generally have narrow line widths \sim MHz or even lesser whereas the line widths of the pulsed lasers are typically \sim GHz. Thus for carrying out high resolution photoionization spectroscopic studies, cw lasers are used. The final width of the spectral line will be the convolution of the laser line width and the atomic absorption line width. The atomic line width is due to the several broadening mechanisms inside the vapour source. These mechanisms include natural broadening, Doppler broadening, collisional broadening, power broadening, transit time broadening etc.

1.1.3.3.1 Multi-step resonance photoionization and its importance to atomic spectroscopy

Most of the elements in the periodic table have their ionization potentials in the range of 2 - 9 eV. Modern tunable lasers, both CW and pulsed, can cover spectral region from 2 to 4 eV. Thus, employing two - or three - step resonant photo-excitation with a range of excitation/ionization schemes, most of the elements and isotopes can be efficiently and

selectively photoionized. In order to get maximum efficiency and better photon utilisation in a multi-step photoionization process, the transitions involved in the ladder should be chosen such that the photo excitation/ionisation cross sections should be high. Also for better atom utilisation, the radiative lifetimes of the states involved in the transition should be much more than the excitation laser pulse duration. This will reduce the loss of atoms due to radiative decay or other non-radiative energy transfer processes. Also for an isotope selective photoionization process, the isotope shift of the transitions involved in the scheme should be large. Hence the choice of an efficient and selective multi-step photoionization scheme demands developing a complete data set of the atomic parameters of the energy levels with the detailed spectroscopic characterisation.

Multi-step resonance photoionization spectroscopy is an unparalleled method by which it is possible to characterise almost all the atomic and molecular properties and its dynamics. Another important aspect of this method is that the ultimate sensitivity achievable using this can easily be combined with the high resolution associated with a collimated atomic beam source. The technique offers potentially high selectivity in multi-step photoionization schemes, which is given by the product of the selectivity at each stage.

Multi-step resonance ionisation spectroscopy in its simplest form requires only one tunable laser. When the laser is tuned to the resonant transition of the atom, it is excited to an upper level. If the laser photon energy $E_p \geq IP/2$, where IP is the ionisation potential of the atom, then a second photon from the same laser can ionise the excited atom. More advanced is the two-colour photoionization, with two tunable lasers, where the possibility exists of isotope selective excitation at each step. The first laser is tuned to a selected transition while the second laser can be tuned to wavelength regions of interest. If the ionization energy is larger than $h\nu_1 + h\nu_2$, then two or more photons of the second laser are required for

ionization. In such cases, two-colour excitation is clearly superior to the multi-photon ionization with a single laser, because both lasers can be tuned in resonance with the two successive transitions and a resonant two step excitation of a high-lying atomic state is possible. The most versatile is the three-colour resonance ionisation using three tunable lasers, with the possibility of isotope selective excitation at all the three steps involved in the excitation ladder. If the photon energy $h\nu_1 + h\nu_2 + h\nu_3$ is greater than the ionisation potential, then a three-colour three-photon ionisation with high efficiency and selectivity can be achieved by choosing a narrow autoionising level as the final step of excitation.

As discussed above, multi-step photoionization spectroscopy is based on resonant multi-step excitation and subsequent ionization of excited atoms. Since the ionization potentials of lanthanides are ~ 6 eV, typically three visible photons are required for ionization. These photons can be of the same wavelength, which corresponds to single-colour photoionization, which again can be classified into two categories viz. single-colour two photon photoionization or single-colour three-photon photoionization depending on the number of photons involved in the ionisation process as shown in Fig. 1.1 (a & b). Alternatively, the photons involved in the ionisation process can be of different wavelengths, which give rise to two-colour or three-colour photoionization processes. Figs. 1.2 & 1.3 represents the prominent multi-step photoionization path ways in single-colour, two-colour and three-color photoionization processes.

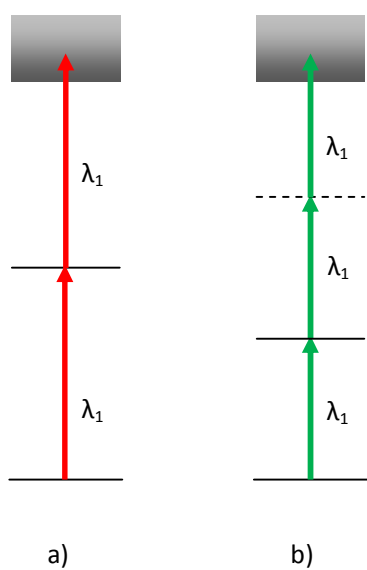


Fig. 1.1: a) Single-colour two-photon and b) single-colour three-photon ionisation path ways. The dotted line represents a virtual level.

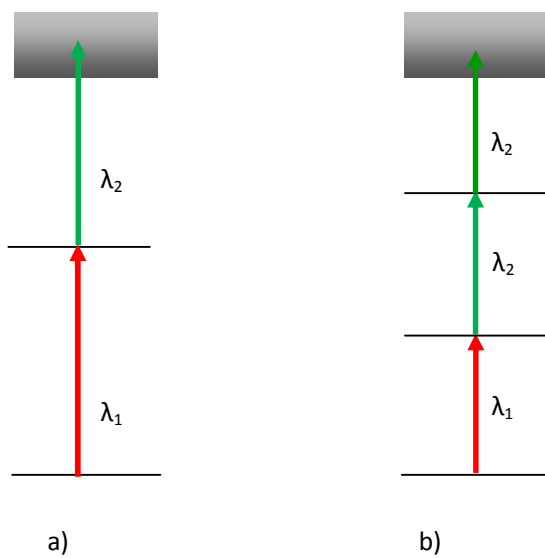


Fig. 1.2: a) Two-colour two-photon and b) Two-colour three-photon ionisation path ways.

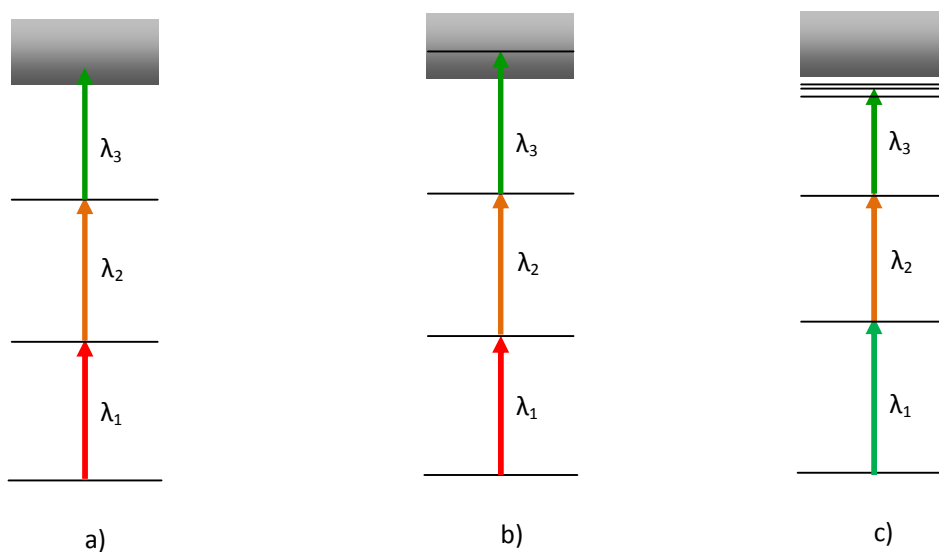


Fig. 1.3: a) Three-colour three-photon process ending in continuum b) Three-colour three-photon ending in an autoionisation state c) Two-colour three-photon reaching a Rydberg level close to continuum.

One of the important applications of multi-step photoionization to atomic spectroscopy is in the identification and assignment of high-lying and autoionising levels of complex atoms that cannot be accessed using the standard methods. The technique can be augmented with time - resolution and polarisation features to further simplify the complex atomic spectra. The method employs multiple lasers of specific wavelengths to map out the relevant regions of the spectrum. The autoionising Rydberg spectrum recorded using multi-step photoionization can be utilised for the determination of accurate ionisation potential of atomic systems. Narrow and strong autoionisation resonances are characteristics of heavy atoms with several optically active electrons. Multi-step resonance photoionization spectroscopy can provide accurate information about the position and strength of these transitions which are important in applications like laser isotope separation, trace elemental

analysis etc. The technique has been successfully implemented for measuring the cross sections of bound-bound and bound-free transitions. Time-resolved multi-photon ionisation method can be used to determine the absolute value of the oscillator strength by determining the lifetime and the emission branching ratio to the relevant low-lying state [10]. Owing to the high sensitivity of the multi-step photoionization technique, it is also used for spectroscopic investigations of short-lived radio isotopes as well [11].

Multi step resonance photoionization in combination with mass spectrometry is a versatile tool for trace analysis, in particular for achieving highest elemental and isotopic selectivity. Resonant excitation and ionization of atoms with lasers provides the highest intrinsic isobaric selectivity through the uniqueness of optical atomic transitions. Subsequent mass spectrometry on the photoions generated further enhances the isotopic selectivity [12].

In this thesis, this technique is exploited for the determination of new highly excited energy levels of atomic samarium, a representative of lanthanide series. The technique has been further exploited for the determination of the total angular momenta, isotope shifts and radiative lifetimes of the high-lying levels. Most of these studies employed either multi-step two-color three-photon or three-color three-photon resonance ionization mass spectrometry (RIMS) utilising a time of flight mass spectrometer [13].

1.2 Atomic Spectroscopy of samarium: A literature review

Samarium is one of the representatives of lanthanide series with atomic number ($Z=62$) and the ground state electronic configuration is $[\text{Xe}] 4f^6 6s^2$. The ground state is a septet $^7F_{0,6}$ with energy levels as given in the Table 1.1. This was first reported by Albertson et.al [14] who have assigned energies of 175 energy levels using the lines from the arc

emission spectra. In a subsequent work, the same group has identified 910 new energy states of samarium which accounted for all the unidentified lines in the previous work and also in this work they approximately determined the ionisation potential of samarium [15].

Table 1.1.: *Ground state of atomic Samarium*

Configuration	Term	Energy Level(cm ⁻¹)
4f ⁶ 6s ²	⁷ F ₀	0.00
	⁷ F ₁	292.58
	⁷ F ₂	811.92
	⁷ F ₃	1489.55
	⁷ F ₄	2273.09
	⁷ F ₅	3125.46
	⁷ F ₆	4020.66

Before the invention of lasers, a large number of atomic spectroscopic studies both experimental and theoretical have been carried out on atomic samarium by various groups [14-31]. Extensive studies on the energy levels of samarium have been carried out by Albertson et.al. [14, 15] and King et.al. [16] as early as 1935. Most of the spectroscopic data obtained in the earlier work were based on classical emission or absorption spectroscopy carried out in arc, spark, hollow cathode discharges, electrode-less discharge lamps, furnaces etc. Martin et.al [31] in 1978 did the compilation of the energy levels for all rare earths known till then as a part of the program on evaluation and compilation of atomic energy levels, spectral wavelengths and classifications initiated by the National Bureau of Standards. However, the information obtained from these studies was incomplete due to the limited capacity of the techniques employed in these studies. Hence the subsequent spectroscopic

works employing lasers were focused on exploring the high-lying and autoionising energy levels and the relevant atomic parameters.

Subsequent to the development of tunable lasers, a variety of laser based spectroscopic techniques have been emerged for determination of atomic parameters [32-56]. Worden et.al [32] have reported the ionization potential of Sm I to be $45519 \pm 8 \text{ cm}^{-1}$ (5.6437 eV) using laser spectroscopy. They have employed step-wise laser excitation and ionisation method to find the Rydberg series and the ionisation thresholds of ten lanthanides. Accurate ionisation limits were derived from the experimentally observed photoionization thresholds. Later on Hu Sufen et.al.[34] have identified and measured high-lying and autoionising levels of atomic samarium in the energy range $45322 - 47092 \text{ cm}^{-1}$ using multi-step photoionization technique. Subsequently Jia et.al [35] have studied the high-lying even-parity energy levels of atomic samarium in the energy range $35779 - 37054 \text{ cm}^{-1}$ by employing resonantly enhanced Doppler-free two-photon spectroscopy in hollow cathode discharge lamp. In this work the J-values of these energy levels have been partially determined by spectrally resolving the laser induced fluorescence from the laser excited energy levels with a monochromator.

Jayasekharan et.al [36] have employed two-colour three-photon photoionization method to find eighty six even parity high-lying states of atomic Sm in the energy region $32950 - 36000 \text{ cm}^{-1}$. They have determined the absolute energy level values with an accuracy of $\pm 0.3 \text{ cm}^{-1}$. The total angular momentum values of most of the levels were determined uniquely. The observations were further extended by the same group to the energy range $34850 - 45300 \text{ cm}^{-1}$, and identified 571 new even parity energy levels. They used the method of accessing the same level using multiple excitation routes to determine the angular momentum of the energy levels [37]. Jayasekharan et.al. [38] have also studied the even

parity Rydberg levels with angular momentum $J=1$ by using two-colour photoionization spectroscopy. They found that the bound and the autoionising Rydberg levels converge to three different ionic states of samarium viz. $4f^6(^7F)6s[{}^8F_{1/2}]$, $4f^6(^7F)6s[{}^8F_{3/2}]$ and $4f^6(^7F)6s[{}^8F_{5/2}]$. Apart from the identification of Rydberg levels, the work also resulted in the determination of 80 new autoionizing levels with a unique total angular momentum of $J=1$. Analysis of the Rydberg levels lead to a more precise determination of the first ionisation potential of atomic samarium to be $45519.64 \pm 1.39 \text{ cm}^{-1}$.

Subsequently, Park et.al [39] have investigated more than fifty autoionisation states of Sm I by three step excitation in the energy range $48000 - 51200 \text{ cm}^{-1}$. Gonomai et.al.[40, 41] have found fifteen new even parity high-lying levels of Sm I along with their angular momentum values in the energy range $34713- 40527 \text{ cm}^{-1}$ using single-colour three-photon ionization. Kajurai and Ogawa et.al [42] determined the even parity autoionisation states and their probable J values using laser optogalvanic spectroscopy in a Sm hollow cathode lamp. They found 357 new autoionisation states in the energy region $45520 - 49188 \text{ cm}^{-1}$. T. Wakui et.al. [43] carried out high resolution laser spectroscopy of rare earths in a well collimated atomic beam using a tunable diode laser and determined the hyperfine structure and the isotope shift of eight transitions. Schmitt et.al [45] determined the ionization energy of ${}^{154}\text{Sm}$ employing high-resolution three-step resonance ionization mass spectrometry. Pulhani et.al [46] reported the observation of new high-lying even-parity excited levels of samarium in the energy region $34814 \text{ cm}^{-1} - 35111 \text{ cm}^{-1}$ using two-color laser-induced fluorescence spectroscopy in an atomic beam set-up. In a subsequent work the same group has determined the total angular momentum of seven high-lying levels in the energy region $34800 - 36200 \text{ cm}^{-1}$ employing the same technique [47]. Zhao et.al. [48] have studied the high-lying even parity levels in the energy regions $37588 - 39927 \text{ cm}^{-1}$ and $41061 - 42478 \text{ cm}^{-1}$ by

employing two-colour photoionization spectroscopy. Qin et.al.[49] have studied the autoionising states of atomic samarium in the energy range $57900 - 61030 \text{ cm}^{-1}$. They have classified these states into autoionising series converging to four different ionisation limits. The level energies and widths of these autoionising states have been determined by fitting Lorentzian profiles to the line shapes. The configuration interaction among these autoionisation states is also discussed in this work. The same group in a subsequent study has identified and characterised fifty seven new autoionising levels of atomic samarium in the energy range $60700 - 66500 \text{ cm}^{-1}$ [50] using a three step excitation scheme. Li et.al. [51] and Zhao et.al. [52] have studied the even parity high-lying states of atomic samarium using two-colour three step excitation and photoionization method. They have accessed the high-lying levels using three different excitation routes. Using this method they have identified many even parity high-lying states and assigned a unique total angular momentum to most of the identified states by comparing the three spectra obtained with different excitation routes. Gomonai et.al. [53] have studied the even-parity highly excited states of samarium in the energy range $34104 - 39155 \text{ cm}^{-1}$ using single-colour three-photon resonance ionisation spectroscopy. The energies and the total angular momenta of 342 states have been determined using this method. Lawler et.al [54] determined the transition probabilities of 299 lines in the first spectrum of samarium utilising the emission branching fraction measurements data from a Fourier transform spectrometer and the radiative lifetimes from laser induced fluorescence measurements. Shah et.al.[55] have investigated the even parity high-lying energy levels in the energy region $36510 - 36875 \text{ cm}^{-1}$ by simultaneously observing the two-colour three-photon photoionization and two-colour laser induced fluorescence signals. They have also studied the dependence of these signals on the second-step laser power. In a subsequent work the same group has measured the second step transition probability and the photoionization cross section by utilising the two-colour three-photon photoionization and the two-colour

fluorescence signals from a single experiment [56]. Even though voluminous work has been carried out previously on atomic samarium, the spectroscopic information available in literature especially about the high-lying levels is far from complete.

1.3 Motivation for the present work

Spectroscopic studies of lanthanides are of fundamental importance in improving the understanding of basic atomic physics as well as in applied research because of its scientific and technological applications such as laser isotope separation, trace elemental analysis, development of metal halide high intensity discharge lamps with rare earth emitting admixtures etc. [57,58]. Sm ($Z= 62$) being one of the representatives of lanthanide series has a rich and complex spectrum due to its less than half filled 4f-shell. Due to the presence of many electrons in the outer d and f shells, Sm is known for a large number of strong transitions in the visible region with strong oscillator strengths. Due to its rich radiative properties, Sm has been one of the major dopants for optical amplifications such as laser amplifiers and communication devices along with other lanthanides like neodymium and erbium. Samarium is also used in magnets and in some metal alloys. It is often blended with cobalt for a stronger alloy which resists demagnetization. Optical properties of samarium doped materials are of great interest in the field of photonics. Even though a lot of laser spectroscopic work has been previously carried out on samarium for the measurement of atomic parameters, the spectroscopic information available in literature especially about the high-lying levels is far from complete. Isotopic data on high-lying levels is a vital information required for determining isotopic selectivity in a multi-step excitation scheme [59]. Moreover, the stable isotopes of Sm I lie in a region where great changes in the nuclear

shapes occur [60]. Thus there is a continuing interest in the investigation of the spectroscopic properties of atomic Sm I.

Atomic samarium (Sm I) has seven naturally abundant isotopes ^{144}Sm (3.1%), ^{147}Sm (15%), ^{148}Sm (11.3%), ^{149}Sm (13.8%), ^{150}Sm (7.4%), ^{152}Sm (26.6%) and ^{154}Sm (22.6%). Among these, ^{149}Sm , with high thermal neutron absorption cross-section (40140 barns), is a promising candidate as burnable poison in nuclear reactors [61]. The use of natural samarium as a burnable poison was discarded previously because of the large residual negative reactivity worth of samarium isotopes and their daughter products at the end of life of the fuel. Recently, Renier et al [62] have investigated the potential benefits of using enriched samaria (Sm_2O_3) as a burnable poison in the fuel pellets of PWRs and shown that the use of Sm enriched in ^{149}Sm has greatly reduced this residual absorber problem. In this thesis, a polarisation based isotope selective photoionization of the odd isotopes of atomic samarium (^{149}Sm & ^{147}Sm) using broad band lasers has been demonstrated for the first time.

The present Ph.D thesis deals with the application of multi-step resonance ionization spectroscopic techniques for the measurement of various atomic parameters of samarium, a representative of lanthanide series. The work described in the subsequent chapters involves the determination atomic parameters like energy levels, total angular momenta, isotope shifts and radiative lifetimes of the high-lying energy levels of atomic samarium using multi-step resonance ionization spectroscopy. Most of these atomic parameters find application in many areas of science such as atomic physics, laser physics, plasma physics, laser chemistry, atmospheric science, astrophysics etc. It also describes in detail a novel isotope selective photoionization technique based on polarisation selection rule for efficient isotope-selective photoionization of odd isotopes of samarium using broad band

lasers. The thesis has been structured into six chapters, elaborating the work carried out in the above mentioned areas. The chapter-wise description of the work is given below:

Chapter 2 deals with the experimental set-up employed for the photoionization studies described in this thesis. It includes a detailed description of the Nd-YAG pumped dye laser systems used for photoionization studies, time of-flight mass spectrometer, its working principle, hollow cathode discharge lamp used for coarse wavelength calibration of the photoionization spectra, Fabry-Perot etalon and photo diode unit used for fine wavelength calibration, signal detection and processing systems utilized in these experiments.

Chapter 3 deals with the measurement of energy level values, total angular momenta and isotope shifts of the high-lying levels of samarium using two-colour photoionization spectroscopy. Two-colour three-photon resonance photoionization spectra of atomic Sm are investigated in the energy region $33136 - 33960 \text{ cm}^{-1}$ and $35450 - 35750 \text{ cm}^{-1}$. The work resulted in the identification of more than twenty energy levels in these regions. The energy values of the newly identified energy levels have been assigned with an accuracy of $\pm 0.3 \text{ cm}^{-1}$. Based on the excitation scheme used, most of the new levels have been identified with a unique total angular momentum (J). In addition, by performing mass-resolved photoionization spectroscopy, the isotope shift of twenty eight high-lying levels of Sm I was measured. The details of this work will be presented in this chapter.

Chapter 4 deals with the radiative lifetime measurements of the even-parity high-lying levels of atomic samarium by delayed photoionization measurements using pump-probe spectroscopy. This chapter lists the radiative lifetimes of the even-parity high-lying levels of atomic samarium in the energy range $34000 - 34815 \text{ cm}^{-1}$ measured for the first time. The measurements were carried out by detecting time resolved delayed three-colour photoionization signal by pump-probe technique in an atomic beam coupled with a time-of-

flight mass spectrometer. The measured values are in the range of 35 to 349 ns. Accuracy of the measurements was validated by measuring the lifetime of the first excited level used in the excitation scheme by employing two-colour pump-probe photoionization spectroscopy and comparing the measured value with that reported in the literature. The details of the measurement technique will be presented in the chapter.

Chapter 5 describes the experimental demonstration of a polarization based isotope selective photoionization technique for selective photoionization of odd isotopes of samarium using broad band lasers. Isotope-selectivity of more than 40 between the odd and even isotopes ($^{149}\text{Sm} / ^{152}\text{Sm}$) of atomic Sm has been experimentally demonstrated by judiciously selecting proper angular momentum sequence of the levels involved in the excitation scheme and laser polarizations. This is the first experimental demonstration of isotope-selective photoionization of the odd isotopes of samarium using polarized laser beams. Since the technique has the advantage that the isotopic selectivity is not affected by the spectral broadening of the excitation lasers, it is highly useful for the separation of odd and even isotopes exhibiting overlapping spectra owing to small isotope shifts and broad hyperfine structures. The chapter also describes in detail the effect of different states of polarization of the excitation lasers and the relative polarization angle between them on the isotope selectivity.

Chapter 6 presents the conclusions including the summary of the work carried out in the present studies and the scope for future work.

Chapter: 2

Experimental Set-up

Chapter 2

2.1 Introduction

This chapter describes the experimental set-up (Fig. 2.1) employed for the photoionization studies described in this thesis. It includes a detailed description of the Nd:YAG and dye laser systems used for photoionization studies, time-of-flight mass spectrometer, its working principle and its advantages over other conventional type mass spectrometers, hollow cathode discharge lamp used for coarse wavelength calibration of the photoionization spectra, Fabry-Perot etalon and photo diode unit used for fine wavelength calibration and other signal detection and processing systems utilized in the experiments.

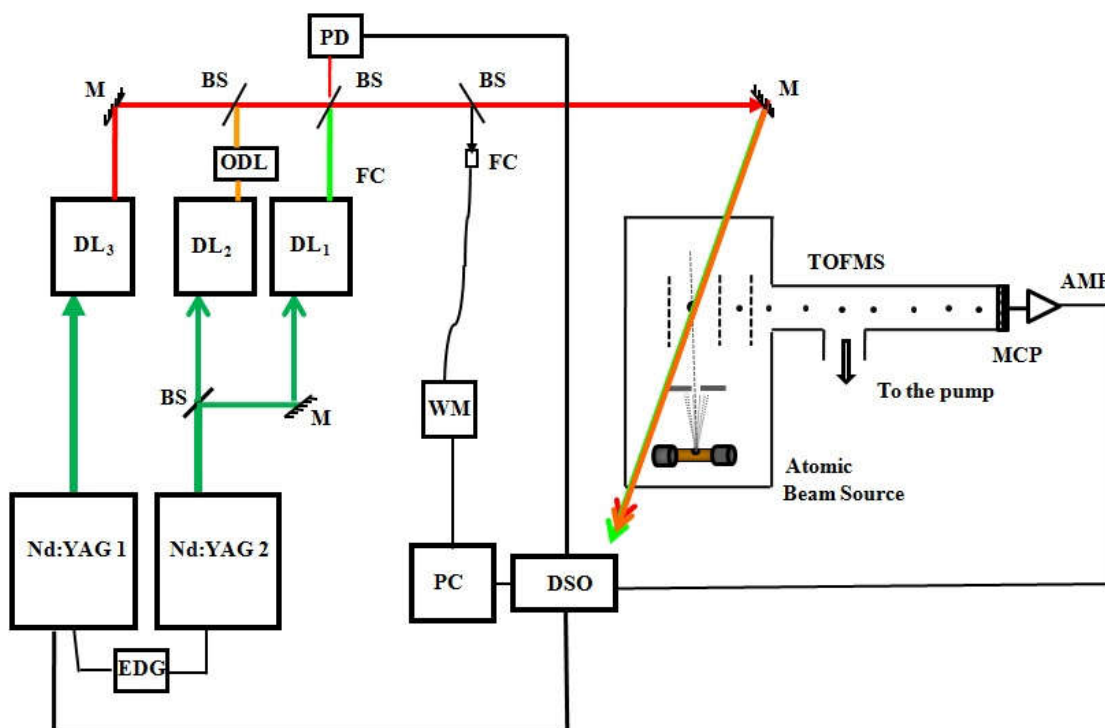


Fig. 2.1: Schematic representation of the experimental set-up. DL_1 , DL_2 , DL_3 : tunable dye lasers, ODL: optical delay line, EDG: electronic delay generator, FC: fibre coupler, WM: wavelength meter, TOFMS: time-of-flight mass spectrometer, MCP: micro-channel plate detector, AMP: pre-amplifier, DSO: digital storage oscilloscope, PD: photo diode, BS: beam splitter, PC: personal computer.

2.2 Different Laser systems employed in the multi-step photoionization set-up

The multi-step photoionization experimental set-up consists of two Q-switched Nd:YAG lasers (Model No: YG 981, Quantel, France) and three dye lasers (Model No. TDL 90, make: Quantel, France) with a pulse repetition rate of 20 Hz and temporal duration of ~ 6 ns. The second harmonic output of the Nd:YAG laser (@ 532 nm) is used for pumping the dye lasers employed in the multi-step excitation and ionization process. The typical pulse energy of the second harmonic output from the Nd:YAG laser is ~ 350 mJ and that of the dye laser is ~ 20 mJ. The output of all the lasers have vertical linear polarisation with purity better than 99%. A photograph of the laser systems used in the photoionization spectroscopic studies carried out in this thesis is shown in Fig. 2.2.



Fig. 2.2: Laser systems used in photoionization experiments

2.2.1 Nd:YAG Laser

Neodymium lasers are most popular type of four-level solid-state lasers using rare earth ions. The host medium in Nd:YAG laser is a YAG crystal (acronym for yttrium aluminium garnet $Y_3Al_5O_{12}$), in which some of the Y^{3+} ions are replaced by Nd^{3+} ions. The typical doping levels in Nd:YAG are ~ 1 atomic percentage. Undoped host materials are generally transparent. After doping these host material becomes pale purple because of the Nd^{3+} absorption band in the red region.

The simplified energy level diagram for the Nd:YAG laser is shown in Fig.2.3. The energy levels of this ion in almost any crystalline lattice are essentially the same. Level notation is based on L-S coupling scheme and the term value for each level has the form $^{2S+1}L_J$, where S is the total spin quantum number, J is the total angular momentum quantum number and L is the orbital quantum number. Each level is $(2J+1)$ fold degenerate corresponding to the magnetic quantum number m_J . Due to the Stark effect in the crystal field, the levels with same $|m_J|$ values are degenerate. Hence each $^{2S+1}L_J$ level split into $(2J+1)/2$ doubly degenerate sub levels.

The main two absorption bands of Nd:YAG corresponds to 730 nm and 800 nm for flash lamp pumping. These bands are coupled by fast non-radiative decay to the $^4F_{3/2}$ lower level. The lasing action occurs between the levels $^4F_{3/2}$ to $^4I_{11/2}$. This level has got higher lifetime ($\tau = 230 \mu s$), since this transition is a dipole forbidden transition in an isolated ion (the selection rule for an electric dipole transition being $\Delta J = 0$ or ± 1). But in this case, the transition becomes weakly allowed due to crystal field interaction. Due to the large lifetime of the level, the level $^4F_{3/2}$ accumulates a large fraction of the excited population, making it a suitable candidate as upper level for laser action.

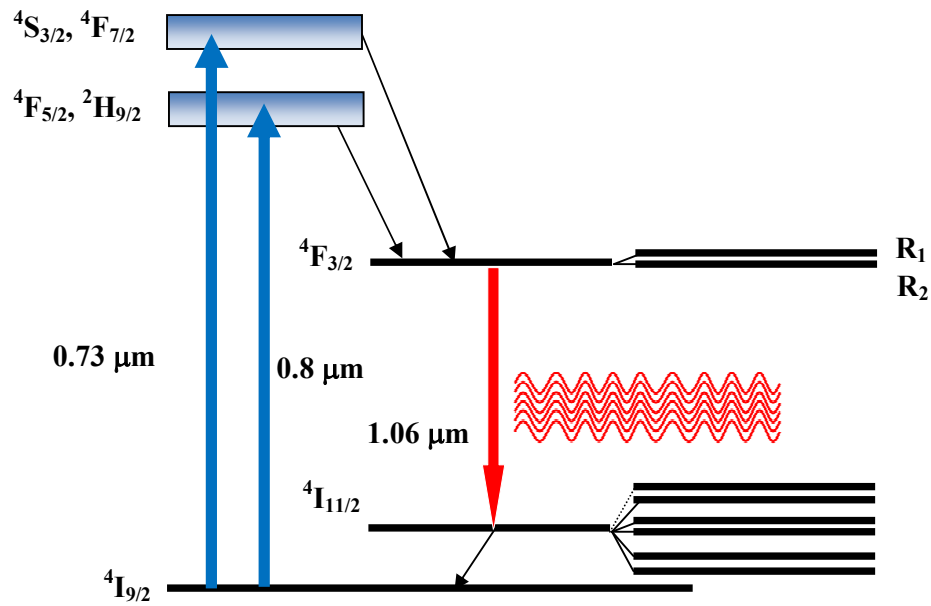


Fig. 2.3: Simplified energy level diagram of Nd:YAG laser[63]

In principle, several lasing transitions are possible between the upper ${}^4F_{3/2}$ level and the low-lying I levels; of which ${}^4F_{3/2} \rightarrow {}^4I_{11/2}$ is the strongest one. The lower lasing level is coupled by a fast non-radiative decay (hundreds of picoseconds) to the ground level (${}^4I_{9/2}$) establishing a fast thermal equilibrium with the ground state. Thus Nd:YAG laser operation corresponds to a four level scheme. Since ${}^4F_{3/2}$ level is split into two sublevels (R_1 and R_2) and the lower lasing level is split into six sublevels, the laser action usually takes place between the R_2 level and the ${}^4I_{11/2}$ sublevel, due to the high stimulated emission cross section for this transition. This transition occurs in the near infrared wavelength at $1.06 \mu\text{m}$, which is the most popularly used fundamental wavelength of Nd:YAG laser. The laser action is homogeneously broadened at room temperature. The corresponding line width is approximately $\Delta\nu \cong 4.2 \text{ cm}^{-1}$. The long lifetime of the upper level also makes it suitable for Q-switched operation. Nd:YAG laser can operate in either continuous wave (cw) or pulsed mode and can be pumped by a lamp or a semiconductor laser[63].

2.2.2 Dye Laser

Dye lasers have played a prominent role in the multi-step photoionization spectroscopy of atoms and molecules. In these types of lasers, an organic dye dissolved in a suitable solvent such as ethyl alcohol, methyl alcohol, benzene, acetone, water etc. is used as the active medium. The dyes which are most efficient are classified into eight groups: xanthenes, polymethines, oxaines, coumarins, anthracenes, acridines, azines and phthaloziamins. Most widely used dye is the Rhodamine 6G dye (Xanthene dye) which emits in the yellow-red region. For emission in the blue-green region coumarin dyes are used. Dye lasers are capable of giving laser output from 0.3 to 1.3 μm using different dyes. Using harmonic generation the accessible spectral region can be extended into the far infra red to the vacuum ultra violet.

The typical energy level diagram of a dye in solution is given in Fig.2.4. Each electronic level comprises of several vibrational levels and each vibrational level is associated with several rotational levels. The vibrational level separation is $\sim 1400 - 1700 \text{ cm}^{-1}$ where as the rotational level separation is of the order of 150 cm^{-1} . Because of the collisional broadening in liquids, the rotational levels which are very close will give rise to a continuum states of levels between the vibrational levels.

The dye molecules are characterised by singlet as well as triplet states. In the singlet state the spin of the active electron and the remainder of the molecule are anti-parallel and in the triplet state the spins are parallel. The singlet to triplet transition in which a spin flip occurs is forbidden by the selection rule ($\Delta S=0$).

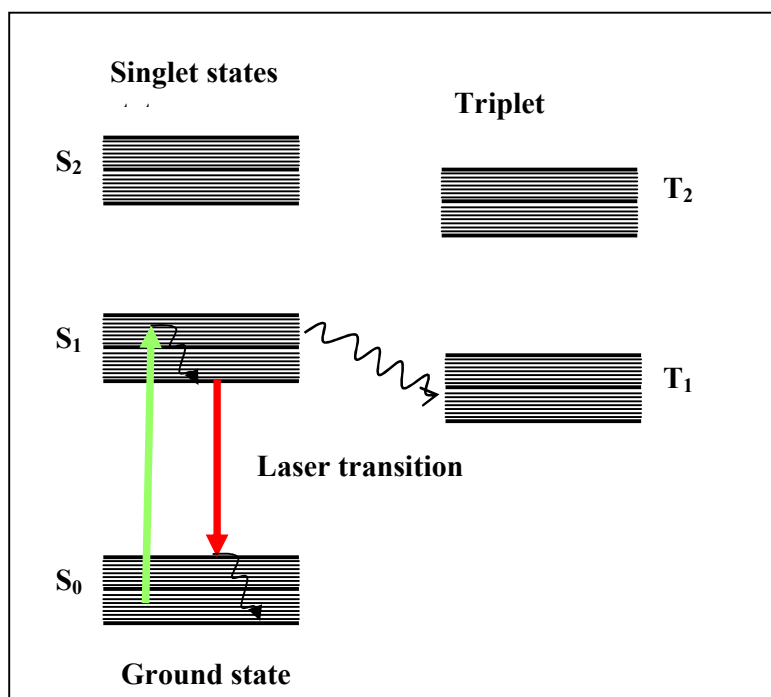


Fig. 2.4: Energy level diagram for a dye molecule [64]

Optical pumping raises the molecule from the lowest vibronic level of the electronic ground state S_0 to one of the upper vibronic level of the excited state S_1 . This excitation is followed by a rapid relaxation by non-radiative process with a time scale of the order of few picoseconds to the lower vibronic level of the excited state S_1 . Lasing occurs between this state and one of the upper vibronic levels of the state S_0 . Another non-radiative decay from this level takes the molecule from this state to the ground level.

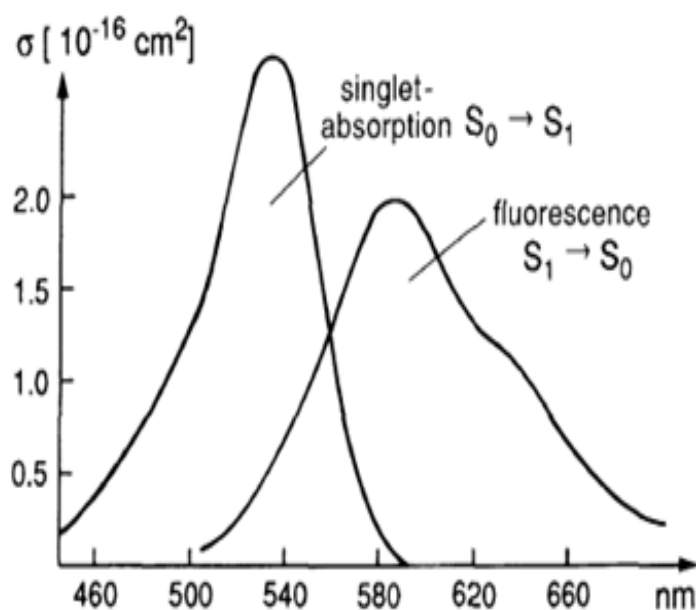


Fig. 2.5: Absorption and fluorescence spectrum of Rhodamine 6G dissolved in ethanol [3].

The presence of the triplet levels pose a to hurdle to lasing action as the molecules in the singlet state S_1 can decay to the triplet state T_1 via collision. This is known as intersystem crossing. If the lifetime of the state T_1 is larger than the intersystem crossing time, then the molecules will get accumulated in the state T_1 . Hence inter system crossing will reduce the number of molecules available in the upper lasing level reducing the gain. This can be reduced by adding oxygen to the dye solution as it acts as a triplet state lifetime quenching additive.

The radiative lifetime of the level S_1 is ~ 100 ns, hence most of the molecules decay from this level by fluorescence contributing to the laser action at fluorescence wavelength. The dye solution is transparent at these wavelengths as the emission band is shifted from the absorption band. A typical absorption and fluorescence spectrum of Rhodamine 6G dissolved

in ethanol is shown in Fig. 2.5 [3]. Since the levels involved in the pumping process are different from that involved in the lasing action, dye laser system is essentially a four level laser system. Dye molecules have got very high absorption cross-section, hence these lasers have very high gain compared to the solid state lasers. Because of the fast relaxation time of the dye molecules, it requires a very intense and fast pumping mechanism to maintain population inversion in the medium. The large amount of thermal energy deposited in the dye solution can cause a variation in the refractive index in the cell resulting in losses in the cavity. These effects can be overcome by rapidly circulating the dye solution through the cuvette [64].

Pulsed laser action can be obtained by pumping the dye by using very fast flash lamps or by short pulses from other pulsed lasers like Nd:YAG laser, N₂ laser etc. For wavelength tuning, a spectral selective element is introduced into the cavity. The dye laser system used in the present studies uses a grazing incidence grating (GIG) configuration in the oscillator cavity for wavelength tuning.

2.3 Time-of-flight mass spectrometer

The multi-step photoionization studies reported in this thesis are carried out in an atomic beam source using a time-of-flight mass spectrometer (TOFMS) as the ion detection system. The basic working principle of a TOFMS is described in this section.

A time-of-flight mass spectrometer separates ions of different mass to charge ratio (m/q) based on the difference in the transit time through a drift tube. The simplest TOFMS consists of an ion source and a collector situated at the opposite ends of an evacuated tube. The ions formed in the laser-atom interaction zone are accelerated out of the source towards the collector by either one or a series of constant electric fields. Pulsed or continuous

fields can be used for acceleration. In either case, the velocity of the ions in the field-free region is a function of their q/m values. Hence the arrival of ions of different q/m values can be registered in time by a detector placed at the end of a drift tube. If only singly charged ions were present, then the group of ions having the lightest mass will reach the detector first followed by the groups with successively heavier masses. Thus it is possible to get entire mass spectrum for each ionising pulse in every few micro seconds. Hence it is possible to determine the relative intensities more accurately, even in the presence of unpredictable variations in the source conditions, provided the variation affects different masses in a similar manner. Another advantage of using TOFMS is that its accuracy depends on the electronic circuits and not on the highly uniform magnetic fields and the extremely precise mechanical alignments like in other kinds of mass spectrometers such as magnetic sector mass spectrometer, quadrupole mass spectrometer etc.

The time-of-flight mass spectrometer (TOFMS) used in these studies is a Wiley-McLaren type [65] mass spectrometer. The schematic of the TOFMS is given in the Fig.2.6. It consists of a high temperature oven kept in a high vacuum chamber for producing the atomic vapours of the element under consideration, a series of electrodes for extracting and accelerating the photoions and a drift tube. The potential of the first grid provides the electric field in the extraction region in which the ions are formed and the potential applied to the second grid decides the ion energy in the drift tube.

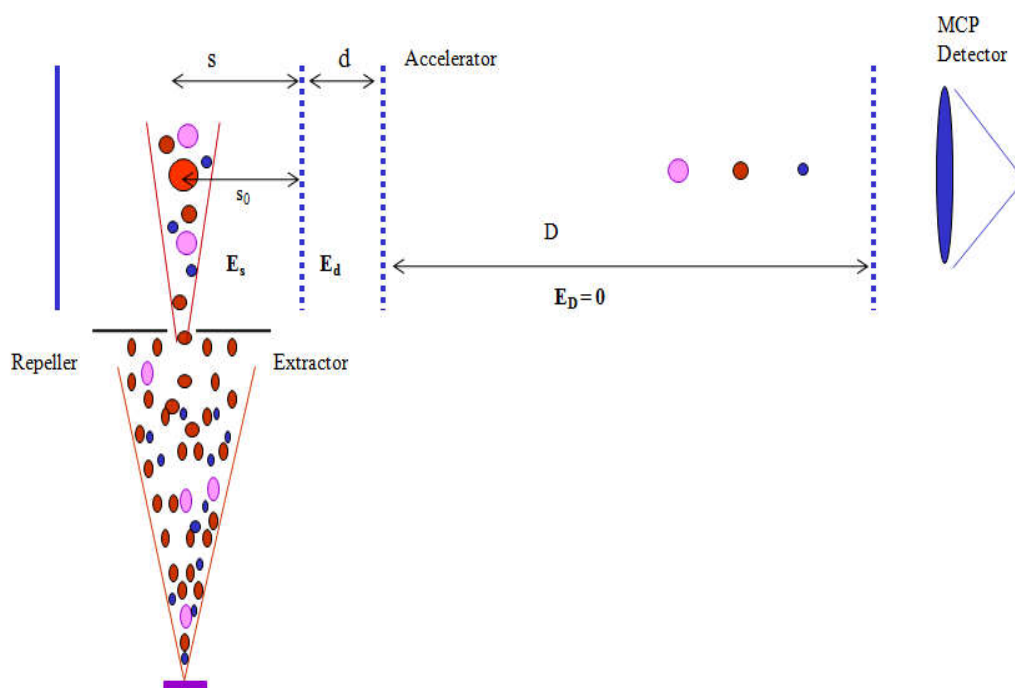


Fig. 2.6: Schematic of time of flight mass spectrometer

In Fig. 2.6 E_s is the electric field in the extraction region, E_d is the electric field in the acceleration region and the region D (drift region) is electric field free. The double field source used in this type of mass spectrometer has the advantage of higher resolution due to the presence of the additional parameters d and E_d/E_s which are not available in a single field source.

2.3.1 Flight time of TOFMS

The total energy gained by an ion with initial energy U_0 is given by,

$$U = U_0 + qsE_s + qdE_d \quad (2.1)$$

The time of flight is given by,

$$T(U_0,s) = T_1 + T_2 + T_D, \quad (2.2)$$

where T_1 , T_2 and T_D are the time taken by the ion to reach the extraction grid, acceleration grid and the detector respectively.

$$T_1 \propto \frac{\sqrt{m}}{qE_s} \left[(U_0 + qsE_s)^{\frac{1}{2}} \pm (U_0)^{\frac{1}{2}} \right] \quad (2.3)$$

$$T_2 \propto \frac{\sqrt{m}}{qE_d} \left[(U_0)^{\frac{1}{2}} - (U_0 + qsE_s)^{\frac{1}{2}} \right] \quad (2.4)$$

$$T_D \propto \sqrt{m} \frac{D}{U^{\frac{1}{2}}} \quad (2.5)$$

The plus and minus signs correspond to the initial velocities directed away from and towards the collector respectively.

Since $T_D \gg (T_1 + T_2)$, the total flight time $T \approx T_D$.

$$T_D \propto \sqrt{m} \quad (2.6)$$

2.3.2 Resolution of TOFMS

Resolution is the largest mass M , for which the adjacent masses are essentially completely separated. This corresponds to the mass M for which the time spread for the ions of the same mass equals the time interval for the adjacent masses.

Hence the mass resolution of the spectrometer,

$$\frac{m}{\Delta m} = \frac{T}{2\Delta T} \quad (2.7)$$

In typical experimental conditions, $T \sim 25\mu\text{s}$ and $\Delta T \sim 25\text{ns}$, resulting in a mass resolution of 500. The resolution of a time of flight mass spectrometer is limited by the following three factors: a) The longitudinal extension of the region where the ions are formed i.e. the laser beam diameter b) the initial longitudinal velocity distribution of the ions and c) the time interval during which the ionisation takes place. i.e. the laser pulse duration. The typical temporal width of the photoionization signal ~ 25 nano seconds where as the FWHM of temporal duration of the laser pulse is ~ 6 ns. Hence the major contribution to the temporal width of the signal is coming from the longitudinal spatial distribution and the velocity distribution of ions.

2.3.2.1 Space resolution of TOFMS

The ability of a TOFMS to resolve masses in spite of its initial space distribution is called space resolution. It can be improved by minimising the spread (Δs) in the initial space distribution of ions from its mean position (s_0). Another method to improve space resolution is by space focussing which gives each ion a velocity dependent on its original position as well as on q/m so that $\Delta T_{\Delta s}$ can be minimised. Space focussing depends on the fact that an ion

initially away from the end plate acquires less energy and hence it is eventually overtaken by the ion which is closer to the end plate (and thus having larger s value). Hence, at a certain drift length D , the first derivative of the time of flight with respect to the coordinate s_0 , where the ions start vanishes, i.e. the fastest ions will catch up with the slowest ones. The position at which the ions with their initial s positions were $s = s_0 \pm \delta/2$ pass each other is given by[65],

$$D = 2s_0 k_0^{3/2} \left(1 - \frac{1}{k_0 + k_0^{1/2}} \frac{d}{s_0} \right) \quad (2.8)$$

,where

$$k_0 = 1 + \frac{dE_d}{s_0 E_s} \quad (2.9)$$

Hence space focussing can be achieved in a double field system by adjusting E_d/E_s values, since all other parameters d , s_0 and D are fixed.

2.3.2.2 Energy resolution of TOFMS

There can be a temporal spread in the TOF mass spectrum due to the initial kinetic energy distribution of the ions. Suppose if two ions are formed at the same s position but with oppositely directed same initial velocities there will be a time spread (ΔT_θ) for ions of same mass also. This decides the energy resolution of the TOFMS. One method to improve energy resolution is by increasing the ratio of the ions total energy to its initial energy. Alternatively, energy resolution can be improved by employing a reflectron type TOFMS in which an ‘ion-mirror’ is used to compensate for the kinetic energy distribution along the flight direction. The ions with higher initial kinetic energy penetrate farther and spend more time in the reflectron. Using appropriate potentials and geometries, the shorter time that the high energy

ion spends in the flight tube can be compensated with the increased time spend in the reflecting mirror [66].

2.4 Atomic Vapour Source

A resistively heated atomic vapour source coupled with TOFMS was used for producing atomic vapours of samarium. The oven was made of rolled tantalum sheet of thickness 25 microns. To reduce the Doppler width of the atomic beam source, the Sm vapour effusing out of the oven orifice of 1mm diameter was further apertured by using a fixed aperture of diameter, $b = 3\text{mm}$ at a distance of, $d = 15\text{mm}$ from the oven orifice.

A schematic of the atomic beam source is shown in Fig. 2.7.

The reduced Doppler width is given by,

$$\Delta v_{red} = \sin\theta \Delta v_D \quad (2.10)$$

$$\text{,where } \Delta v_D(\text{Hz}) = 7.16 \times 10^{-7} v_0(\text{Hz}) \sqrt{\frac{T(\text{K})}{M(\text{amu})}} \quad (2.11)$$

is the Doppler width at equilibrium temperature T , M atomic mass in amu and v_0 is the line centre of absorption line profile. The reduced Doppler width of the atomic absorption line in the interaction zone is $\sim 100\text{MHz}$ and the typical number density of Sm in the interaction zone is calculated to be $\sim 10^9\text{atoms/cm}^3$.

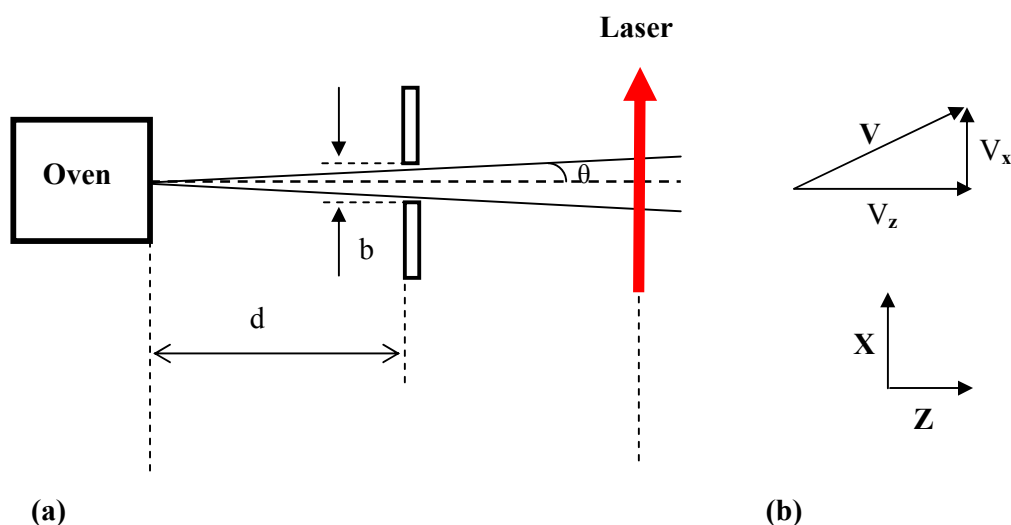


Fig. 2.7: (a) Schematic of the collimated atomic beam source (b) Atomic velocity components

2.5 Experimental set-up for spectral calibration

The coarse calibration of the photoinisation spectra is done by using the opto-galvanic signal from a uranium-hollow cathode discharge lamp and the fine calibration of the spectra is carried out by using a Fabry Perot etalon along with a photo diode set up. The detailed working principle of the system is described in the following section.

2.5.1 Coarse calibration with Opto-galvanic signal

The coarse calibration of the spectra was carried out by detecting the opto-galvanic signal from a uranium-hollow cathode discharge lamp. The detection mechanism is based on the ‘Opto-galvanic effect’, i.e., by detecting the change in the discharge impedance when atoms in a discharge are photo-excited or ionised using resonant photons from an external light

source. It is a very simple and inexpensive detection technique for spectroscopic investigation of atoms, ions, molecules and radicals. This method has proven to be a powerful and convenient spectroscopic technique to investigate all kinds of matter in vapour phase, in discharge plasmas and flames over a wide spectral range from UV through visible to IR. Unlike absorption and emission spectroscopic techniques, the method does not require a monochromator or any other optical detectors. Also the method does not require background filtering and has got a moderate signal to noise (S/N) [67].

When the laser is tuned in resonance to an atomic or molecular transition of the species present in the discharge, the electrical properties of the discharge changes due to the following two mechanisms: (a) A variation in the electron-ion production due to excitation to a level close to continuum (b) a variation in the electron and gas temperatures due to super elastic collisions with laser excited atoms. Either process can dominate the opto-galvanic signal depending on the discharge conditions.

Opto-galvanic spectroscopy is intrinsically more sensitive than absorption, since absorption is based on recording a small variation superimposed on a large background signal, where as the former is based on a signal on zero background. When compared to fluorescence, OG offers the advantage of being not affected by the background signal either due to the discharge luminosity or by the scattered excitation light intensity. This is of significance while detecting fluorescence at the same wavelength as that of the absorbed radiation.

Opto-galvanic technique provides an accurate and economical way to calibrate the spectra recorded in an experiment. In the experiments carried out in this thesis, a hollow cathode discharge lamp, shown in Fig. 2.8, made of uranium, an element with a rich transition spectrum was utilised for the coarse calibration of the spectra. Palmer *et al.*[68]

have previously published an atlas, which reports the Fourier-transform spectrum emitted from a U-Ne hollow cathode discharge lamp, with an accuracy of 0.005 cm^{-1} , in the region between 348 nm to 908 nm. The OG spectrum recorded was compared with the emission lines reported in the atlas for the coarse calibration of the experimental data [69]. The interference fringes produced by a Fabry - Perot etalon were detected by a fast photo diode described in sections 2.5.2 and 2.5.3. The Fabry-Perot fringes were recorded simultaneously along with the photoionization spectra. The fine calibration of the photoionization spectra was carried by using these fringes along with the OG signal. An additional cross check on the wavelength calibration was carried out by using the wavelength meter High Finesse Angstrom WS/6 DL (refer section 2.6.4).



Fig. 2.8: *Hollow cathode discharge lamp*

2.5.2 Fine calibration using Fabry-Perot Etalon

The fine calibration of the photoionization spectra is carried out by using a Fabry-Perot etalon along with a photo diode set up. Etalons are two glass plates separated by a spacer and the inner surfaces of the two plates coated with partially reflecting layers. With this interferometer, frequency markings are obtained by transmitted light after multiple reflections between the glass plates. Here the multiple reflections take place in the thin film between the glass plates. The condition for maximum intensity is given by,

$2\mu t \cos\theta = n\lambda$, where $n = 0,1,2,3,\dots$, ' μ ' is the refractive index of the spacer and ' t ' is its thickness i.e. the separation between the two reflecting surfaces. On scanning the incident wavelength, transmission peaks separated by the free spectral range (FSR) of the etalon will be produced. A typical FP fringes obtained on scanning the photoionizing laser wavelength is shown in Fig. 2.9.

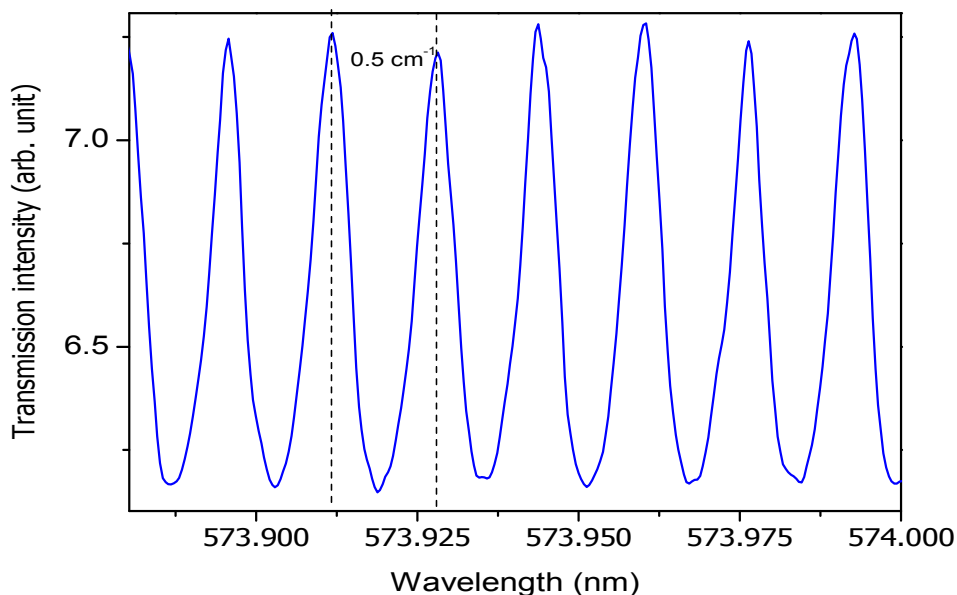


Fig. 2.9: Fabry-Perot etalon fringes

2.5.3 Photo diode

A photo diode is a reverse biased PN junction diode which converts light energy into electrical current. When photons of suitable energy is incident on the P-N junction through an optically transparent window, the electrons from the valance band jump to the conduction band, creating electron-hole pairs resulting in a current flow in the circuit. In PIN type junction diodes, an intrinsic semiconductor layer is introduced between the PN junction to increase the width of the depletion region which results in a lower capacitance and correspondingly a smaller rise time. In the experimental set-up employed in this thesis, a PIN type photo diode was used to monitor the output of the transmission signal of the Fabry-Perot etalon which was used as a fine frequency marker for calibration of photoionization spectra. It is also employed for checking the temporal delays between the laser pulses. Fig. 2.10 shows a typical temporal profile of the dye laser pulse.

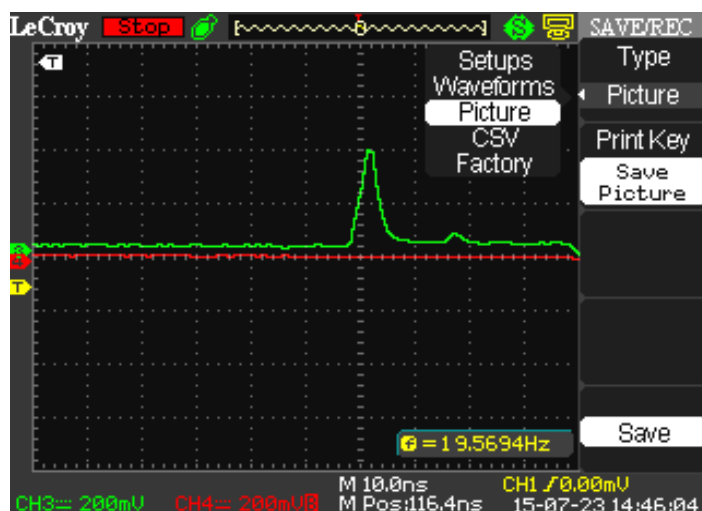


Fig. 2.10: Signal output of the photo diode

2.6 Signal detection and measurement systems

2.6.1 Micro Channel Plate (MCP) Detectors

A micro channel plate detector is used for the detection of the photoionization signal. The signal is amplified using a pre-amplifier and then processed using a boxcar averager unit to improve the signal to noise ratio. The working principle of MCP is briefly described below.

MCP's are used to detect single particles of electrons, ions or photons by the multiplication of electrons via secondary emission. It consists of an array of 10^4 - 10^7 miniature electron multipliers oriented parallel to one another. Typical channel diameters are in the range of 10 -100 μm and the length to diameter (L/D) ratios is in the range of 40 to 100. Channel axes are typically normal or biased at a small angle to the MCP input surface. Each channel can be considered to be a continuous dynode structure. Parallel electrical contact to each channel is provided by a metallic coating on the front and the rear surface of the MCP, which serves as the input and the output electrodes respectively. The total resistance between the electrodes is of the order of 1000 mega ohms. Such micro channel plates used in single or in cascade can provide an electron multiplication factors $\sim 10^4$ - 10^7 coupled with an ultra high time resolution (<100 ps). The spatial resolution of the MCP's is limited only by the channel dimensions and the spacing. Typical MCP's have a channel diameter of ~ 12 μm with a centre to centre spacing of 15 μm . [70]. In the experimental set-up mentioned in this thesis, a Chevron type MCP (Make : El-Mul) with a gain of 10^6 at an operating voltage of 1800 V is used.

2.6.2 Pre-amplifier

The output of the micro channel plate detector was amplified with the help of a charge sensitive fast pre-amplifier with a gain of 100 and a band width of 100 MHz before it is fed to a boxcar averager (BCA) for processing. The photoionization signal after amplification by the pre-amplifier is typically in the range of 5 to 300mV.

2.6.3 Boxcar averager

A boxcar averager is used to improve the signal to noise ratio of the photoionization spectrum. It relies on the incoherent nature of the noise component to increase the S/N ratio of a repetitive input signal. The basic principle behind the working of boxcar is briefly described here:

An input signal can be considered as the sum of true signal $V_s(t)$, which is repetitive in nature with a period Γ plus a random noise $V_N(t)$.

$$i.e., V_s(t) = V_s(t + \Gamma) = V_s(t + m\Gamma), \quad (2.12)$$

where m is an integer. However for the noise $V_N(t)$, there is no correlation between $V_N(t)$ and $V_N(t + m\Gamma)$. In boxcar averager the input waveform $V_{in}(t)$ is applied to an integrating circuit with time constant T from $t = t_0$ to $t = t_0 + \tau$ set by the gate. The normalised output of the integrating circuit is given by

$$V_{out}(t) = \frac{1}{\tau} \frac{1}{T} \int_{t_0}^{t_0 + \tau} (V_s(t) + V_N(t)) dt \quad (2.13)$$

The integration is repeated for N pulses separated by the time period Γ . The average output voltage $V_{avg}(t)$ is given by,

$$V_{avg}(t) = \frac{1}{N} \frac{1}{\tau T} \sum_{m=0}^N \left[\int_{t_0}^{t_0+\tau} (V_s(t) + V_N(t)) dt \right] \quad (2.14)$$

For the repetitive signal $V_s(t)$, the integral is constant for all samples m at given gate delay t_0 and width τ , i.e.

$$\int_{t_0}^{t_0+\tau} V_s(t) dt = \overline{V}_s(t_0, \tau) = \text{constant} \quad (2.15)$$

Hence,

$$V_{avg}(t) = \frac{1}{\tau T} \overline{V}_s(t_0, \tau) + \frac{1}{N} \frac{1}{\tau T} \sum_{m=0}^N \left[\int_{t_0}^{t_0+\tau} V_N(t) dt \right] \quad (2.16)$$

Because of the random nature of the noise, the second integral is distributed according to Gaussian function and the sum of N such Gaussian gives a value which varies statistically with an expectation value proportional to \sqrt{N}

$$V_{avg}(t) = \frac{1}{\tau T} \overline{V}_s(t_0, \tau) + \frac{1}{\sqrt{N}} \frac{1}{\tau T} \overline{V}_N(\tau) \quad (2.17)$$

From this equation it is clear that if $V_s(t)$ is repetitive in nature, averaging over N samples will improve the S/N ratio by a factor of \sqrt{N} [71].

2.6.4 Wavelength meter

The laser wavelength was accurately measured during the experiment with the help of a Fizeau interferometer based wavelength meter (WS 06, High Finesse, Germany), which has an resolution of 600 MHz and a measuring range from 420 – 1100 nm. The coarse wavelength measurements were carried out by an inbuilt prism or grating spectrometer and the fine wavelengths were determined with the help of Fizeau interferometers. Wavelength measurements were carried out by comparing the interference fringes obtained from the different interferometers with a standard stored interferogram of a known wavelength. The

measured wavelengths are stored in a computer using a data acquisition system. These wavelength readings are also utilised to cross check the photoionization spectra calibrated using Fabri-Perot etalon fringes and the opto-galvanic signals.

2.6.5 Laser power meter

The power meter consists of a power sensor (Model 30A-BB-18 and 3A – P, Ophir Optronics, Israel) and a display unit (Model: VEGA). The working of the power meter is based on measuring the increase in the sensor temperature on absorbing the incident radiation by using a series of bimetallic junctions (thermopiles). Thermopiles generate electrical voltage corresponding to the change in the radial and axial temperature. Since only temperature difference is measured, the measurement is independent of the ambient conditions. It has got sensitivity in the range of 2 mW to 20 W.

Chapter: 3

Determination of high-lying energy levels, total angular momenta and isotope shifts by two-colour resonance ionization mass spectrometry

Chapter 3

3.1 Introduction

Spectroscopic studies of rare earths are of fundamental importance in improving the understanding of basic atomic physics as well as in applied research because of its scientific and technological applications such as laser isotope separation, trace analysis, development of metal halide high intensity discharge lamps with rare earth emitting admixtures etc. [57,58]. Sm being one of the representatives of lanthanide series has a rich and complex spectrum due to its less than half filled 4f-shell. Isotopic data on high-lying levels is vital information required for determining isotopic selectivity in a multi-step excitation scheme [59]. Moreover, the stable isotopes of Sm I lie in a region where great changes in the nuclear shapes occur [60]. Thus there is a continuing interest in the investigation of isotope shift and hyperfine structure of Sm I [35, 72, 73, 74, 44]. In this context, most of the work reported in the literature is pertaining to the low-lying energy levels whose electronic configuration is expected to be pure. In heavier atoms such as Sm, with many electrons in the outer electronic shell, the electronic configuration of high-lying levels is generally mixed, therefore the measurements of isotope shifts and hyperfine structures of these levels were not of much interest to the researchers who were mainly interested in the of shape and size of the nucleus. The isotope shifts and hyperfine structures of high-lying levels are of great interest for those who are interested in isotope-selective photoionization employing multi-step routes.

3.2 Origin of isotope shift

An atomic spectral line is characteristic of the element producing the spectrum. However, the energy of a spectral line does slightly depend on the different isotopes of the same element. This is known as isotope shift. Broadly there are two different types of effects that contribute to the total isotope shift: (1) mass shift and (2) the field shift (volume shift). The mass shift, which is due to the reduced mass effect, is prominent in lighter elements and the field shift, which is due to the nuclear volume effect, is prominent in heavier elements.

3.2.1 Mass Shift

The mass dependent isotope shift of the atom is due to the change in the kinetic energy of the atom due to the difference in the masses of different isotopes of the atom.

The total energy of the atom is the sum of the kinetic and potential energies. The total kinetic energy E_k of an n electron system is given by,

$$E_k = \sum_{i=1}^n \frac{p_i^2}{2m} + \frac{P^2}{2M} \quad (3.1)$$

,where p_i are the momenta of the electrons, P is the momentum of the nucleus, M and m are the masses of the nucleus and the electrons respectively. In the centre of mass frame the resultant momentum is zero. i.e,

$$P = -\sum_{i=1}^n p_i \quad (3.2)$$

$$E_k = \sum_{i=1}^n \frac{p_i^2}{2m} + \frac{\left(-\sum p_i\right)^2}{2M} \quad (3.3)$$

$$E_k = \sum_{i=1}^n \frac{p_i^2}{2m} + \frac{p_i^2}{2M} + \frac{1}{M} \sum_{i<j} p_i \cdot p_j \quad (3.4)$$

$$E_k = \sum_{i=1}^n \frac{p_i^2}{2\mu} + \frac{1}{M} \sum_{i<j} p_i \cdot p_j \quad (3.5)$$

where, $\mu = \frac{mM}{m+M}$ is the reduced mass of the electron-nucleus system.

The contribution to the isotope shift from the first term in Eqn. (3.5) is known as the normal mass shift (NMS). It gives the shift in the energy due to the change in the reduced mass of n independent electrons. However the electrons are not really independent and the correlated motion of the electrons cause an additional coupling term in the expression for the total kinetic energy. In a multi-electron atom, the additional coupling term due to the momentum correlation between the orbiting electrons, in general produces different shifts for different energy levels. The contribution to the isotope shift from the momentum correlation term (second term in Eqn. (3.5)) is called the specific mass shift (SMS). It is very difficult to accurately calculate SMS for heavier elements. The usual convention is to treat the isotope shift positive if the transition frequency corresponding to the heavier isotope is on the higher side. NMS is always positive while SMS can be either positive or negative depending on the correlation between the electrons.

3.2.2 Field shift

The field shift arises due to the change in the potential energy which is dependent on the nuclear volume. In elements with high atomic number (Z), the field shift is expected to be large. If the nucleus is assumed to be a point charge which occupies no volume, then the coulomb field due to the nucleus follows the inverse square law. However, the nucleus does have a finite volume and hence the inverse square law does not hold good at distances very close to the nucleus. It is modified according to the nuclear charge distribution and there is a corresponding change in the energy levels of the atoms in the modified electric field. The field shift is given by,

$$\delta E = \pi \Delta |\Psi_0|^2 \frac{a_0^3}{Z} f(Z) \delta \langle r^2 \rangle \quad (3.6)$$

, where $\Delta |\Psi_0|^2$ is the change in the electron density at the nucleus, a_0 is the Bohr radius, $f(Z)$ is a function of Z and $\delta \langle r^2 \rangle$ is the change in the mean square radius of the nucleus.

In heavy elements, which have larger nuclear volume, a small change in the volume between two isotopes can cause relatively large field shifts. This effect is appreciable only for orbitals that represent an appreciable electron density at the nucleus, *i.e.* s-electrons and to some extent p-electrons. The volume isotope shift (field shift) tends to be same for all levels of same configuration. Hence measured isotope shifts are of considerable help in assigning experimental energy levels to specific configurations. The contribution of the volume shift increases with increasing nuclear size, where as the contribution from the mass shift decreased with increasing atomic mass. The observed shift in lighter elements is primarily due to the mass shift where as in heavier elements they tend to be primarily due to the volume effect. It is difficult to infer the absolute isotope shift from the measured wave number data.

Generally, relative level shifts are given with the isotope shift of the ground level arbitrarily chosen as zero [13,75,76] .

In case of nuclei having odd number of protons or neutrons, due to the interaction of the nuclear spin with the total angular momentum, there will be hyperfine splitting of the energy levels leading to hyperfine structure of the spectral lines. Hence in such cases, isotope shift is measured as the frequency separation between the line corresponding to the even isotope and the centre of gravity of the line corresponding to the odd isotope.

3.3 Present work on the measurements of atomic parameters

This chapter deals with the measurement of energy values, total angular momenta and isotope shifts of the high-lying levels of samarium using two-colour photoionization spectroscopy. Two-colour three-photon resonance photoionization spectra of atomic Sm are investigated in the energy regions $33136 - 33960 \text{ cm}^{-1}$ and $35450 - 35750 \text{ cm}^{-1}$. The work resulted in the identification of more than twenty energy levels in these regions. The energy values of the newly identified energy levels have been assigned with an accuracy of $\pm 0.3 \text{ cm}^{-1}$. Based on the excitation scheme used, most of the new levels have been identified with a unique total angular momentum (J). In addition, by performing mass-resolved photoionization spectroscopy, the isotope shifts of twenty eight high-lying levels of Sm I were measured. The details of this work will be presented in this chapter.

3.3.1 Experimental details

The functional block diagram of the experimental arrangement is shown in Fig. 3.1. A frequency doubled Nd: YAG laser at 532 nm is used to pump two dye lasers DL₁ and DL₂ to provide tunable output at wavelengths λ_1 and λ_2 respectively. The typical line width of DL₁ laser is $\sim 0.20 \text{ cm}^{-1}$ and that of DL₂ laser is $\sim 0.13 \text{ cm}^{-1}$. Both lasers have pulse duration ~ 6 ns and typical pulse energies of $\sim 1 \text{ mJ/pulse}$. The DL₂ is temporally delayed by 8 ns (i.e. more than the dye laser pulse width) using an optical delay line in order to ensure sequential absorption of photons. Rh6G and DCM dyes are used in DL₁ and DL₂ lasers to produce laser photons at desired wavelengths λ_1 and λ_2 respectively. Spatially overlapped DL₁ and DL₂ lasers are then send through a samarium atomic beam formed in a high vacuum atomic beam generator that is coupled to a linear time-of-flight mass spectrometer (TOFMS). The typical fluence in the interaction zone is $\sim 200 \mu\text{J}/\text{cm}^2$ for DL₁ and that of DL₂ is variable in the range of 200 to $500 \mu\text{J}/\text{cm}^2$. Both lasers used for excitation and ionization have parallel linear polarization. Atomic vapour of Sm is produced by resistively heating few hundred mg of Sm metal to $\sim 800 \text{ }^\circ\text{K}$ in a high vacuum chamber maintained at a pressure of $\sim 10^{-6}$ mbar. The Sm vapour effusing out of the oven orifice of 1mm diameter is further apertured by using a fixed aperture of diameter 3mm at a distance of 15mm from the oven orifice. The typical number density of Sm in the interaction zone is $\sim 10^9 \text{ atoms}/\text{cm}^3$. The reduced Doppler width of the atomic absorption line in the interaction zone is $\sim 100 \text{ MHz}$. The photoions generated in the interaction region are extracted by a dc electric field of strength 150V/cm and then introduced into the flight tube of the TOFMS. After travelling a field free flight region of 90 cm, the photoions are detected by a micro-channel plate (MCP) detector. The detector output signal is amplified using a pre-amplifier (gain ~ 100 and a band width $\sim 100 \text{ MHz}$) before it is fed to a boxcar averager (BCA) for processing. The output of the boxcar averager is then

3.3.2 Measurements of high-lying energy levels and the angular momenta

Even-parity high-lying levels of Sm I in the energy region $33136\text{--}33960\text{ cm}^{-1}$ were investigated by employing two-colour three-photon photoionization spectroscopy using two different excitation schemes as shown in Fig.3.2.

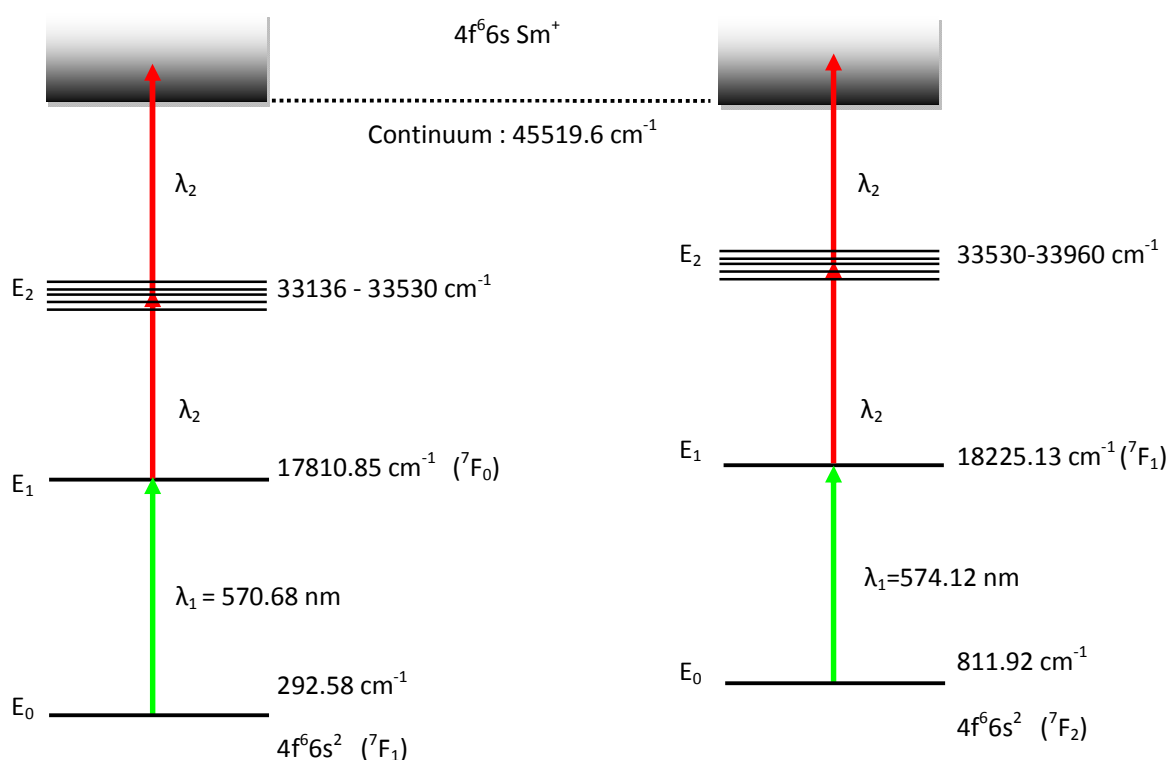


Fig. 3.2: Schematic of photoionization pathways. (1) Scheme A (2) Scheme B.

The wavelength of the first step laser is tuned in resonance to the following transitions of Sm I:



Where, the first excited levels 17810.85 cm^{-1} and 18225.13 cm^{-1} are admixtures of two pure configurations $4f^6 6s 6p$ and $4f^5 5d 6s^2$ with the former as the leading configuration [77]. The wavelength of the second laser is scanned in the DCM dye range (635.5-652.5 nm) to access the high-lying energy levels in the energy region $33136 - 33960 \text{ cm}^{-1}$. The tuning of DL₁ wavelength to the Sm I first step resonance is done by observing the single-colour photoionization signal. The wavelength of DL₁ is monitored using wavelength meter (High Finesse WS6). The calibration of the wavelength meter is pre-verified by simultaneously recording known single-colour optical galvanic spectrum from a U-Ne HCDL along with Fabry-Perot etalon fringes. The accuracy of the wavelength meter is better than $\pm 0.02 \text{ cm}^{-1}$. In order to improve signal to noise ratio in the two-colour spectrum, DL₁ power is attenuated using neutral density filters such that the single-colour photoionization signal completely disappears. Subsequently DL₂ laser is scanned. When the second step laser photon energy matches with $E_2 - E_1$, where E_1 and E_2 are the energies of the first and the second intermediate states, then most of the Sm atoms are ionized by $\lambda_1 + 2\lambda_2$ process via the resonant intermediate level, resulting in the photoionization signal. The two-colour photoionization spectra is a composite one, containing single- and two-colour three-photon features like $3\lambda_2$ and $\lambda_1 + 2\lambda_2$. In order to discriminate the single-colour features, the photoionization spectra are also recorded by blocking λ_1 laser. A part of the two-colour three-photon photoionization

spectra of Sm I recorded along with the Fabry-Perot etalon fringes and the optogalvanic signal used for wavelength calibration (using scheme A) are shown in Fig.3.3.

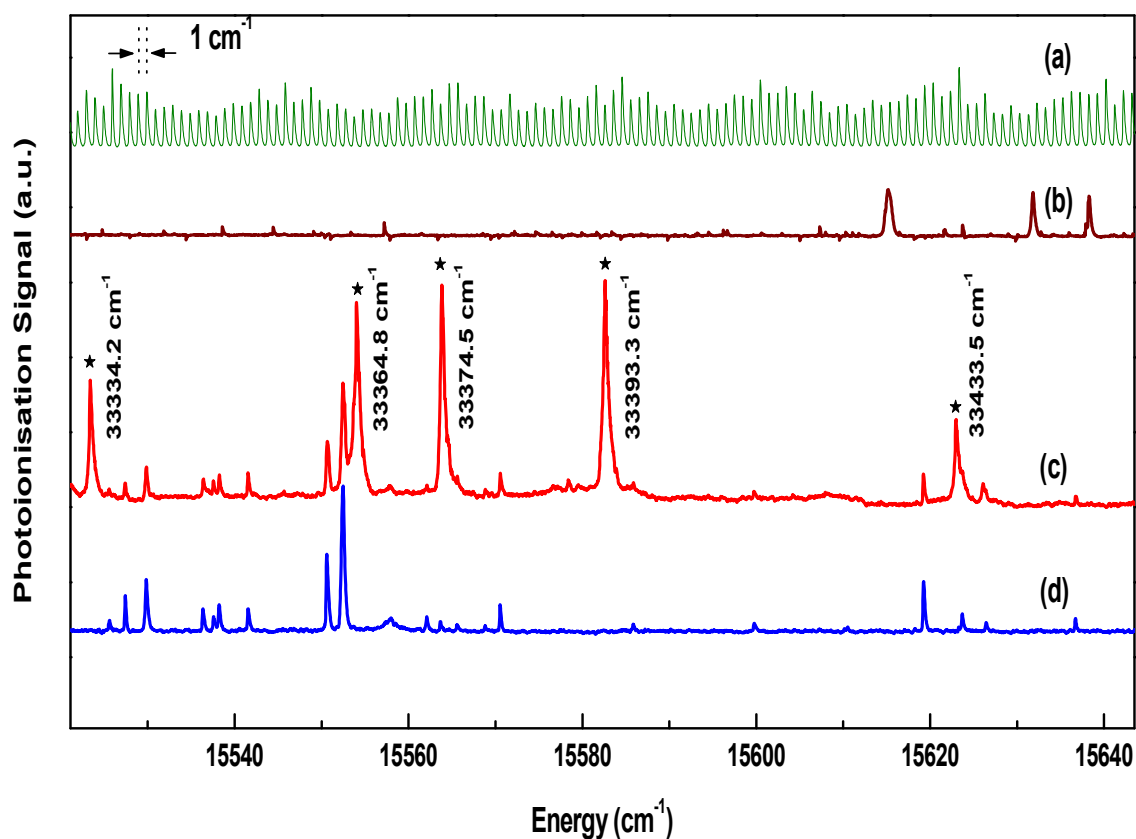


Fig. 3.3: A part of the two-colour photoionization spectrum of Sm I obtained using scheme A (a): Fabry-Perot fringes (b): Single-colour optogalvanic spectrum (c): Two-colour photoionization spectrum. Peaks labeled with star indicate actual two-colour resonances and are identified with the corresponding upper level energies. (d): Single-colour photoionization spectrum. Traces (a)-(c) were measured simultaneously.

The analysis of the two-colour spectra resulted in the identification of twenty nine high-lying levels in the range 33136 cm^{-1} - 33960 cm^{-1} . By recording the spectra repeatedly, the uncertainty in the measurement of resonances is reduced to $\pm 0.3 \text{ cm}^{-1}$. Out of the twenty nine resonances observed, twenty one are new levels and the energy values for the remaining eight

levels are in good agreement (within $\pm 0.5 \text{ cm}^{-1}$) with the values previously reported by Jayasekharan *et al.* [36].

The J-value assignment of the high-lying levels is done by using the J-momentum selection rule $\Delta J = 0, \pm 1$ where $\Delta J = 0$ is not allowed for $J = 0 \leftrightarrow 0$ transitions. However, in case of odd isotope due to the non-zero nuclear spin I ($I=7/2$) there is hyperfine interaction between J and I , therefore F (the total angular quantum number) is the good quantum number in place of J . Thus in case of an odd isotope, as shown in Fig.3.4, transitions between magnetic sublevels satisfying $\Delta m_F = 0$ for $\Delta F = 0, \pm 1$ are allowed and hence excitation to a high-lying level with $J=0$ is possible [78, 79]. So in order to rule out any ambiguity that can arise in the assignment of J value of the new levels due to the hyperfine interaction of the odd isotopes in scheme A, the boxcar averager gate is kept on the even isotope (^{154}Sm) in the mass spectrum, while recording the two-colour photoionization spectrum.

The measured energy values will deviate slightly from the value averaged over all naturally occurring Sm I isotopes. But considering the measured isotope shifts between the two extreme isotopes (^{144}Sm - ^{154}Sm), the deviation is expected to be well within the uncertainty in the measurement of $\pm 0.3 \text{ cm}^{-1}$. Since in scheme A, the high-lying levels are accessed from the intermediate state with total angular momentum $J = 0$, by electric dipole selection rule, all levels accessed using this scheme are assigned with a unique total angular momentum of $J = 1$. In scheme B, since the intermediate level is of $J = 1$, the levels accessed by using this scheme will have possible J values of 0, 1 or 2. Table- 3.1 summarizes the resulting energy levels, where the information about the level energy, the angular momentum and the relative intensities are given. To classify the relative intensities of various transitions the symbols W, M and S are used. They represent the relative intensity regions 0-0.3, 0.3-0.7 and 0.7-1 respectively.

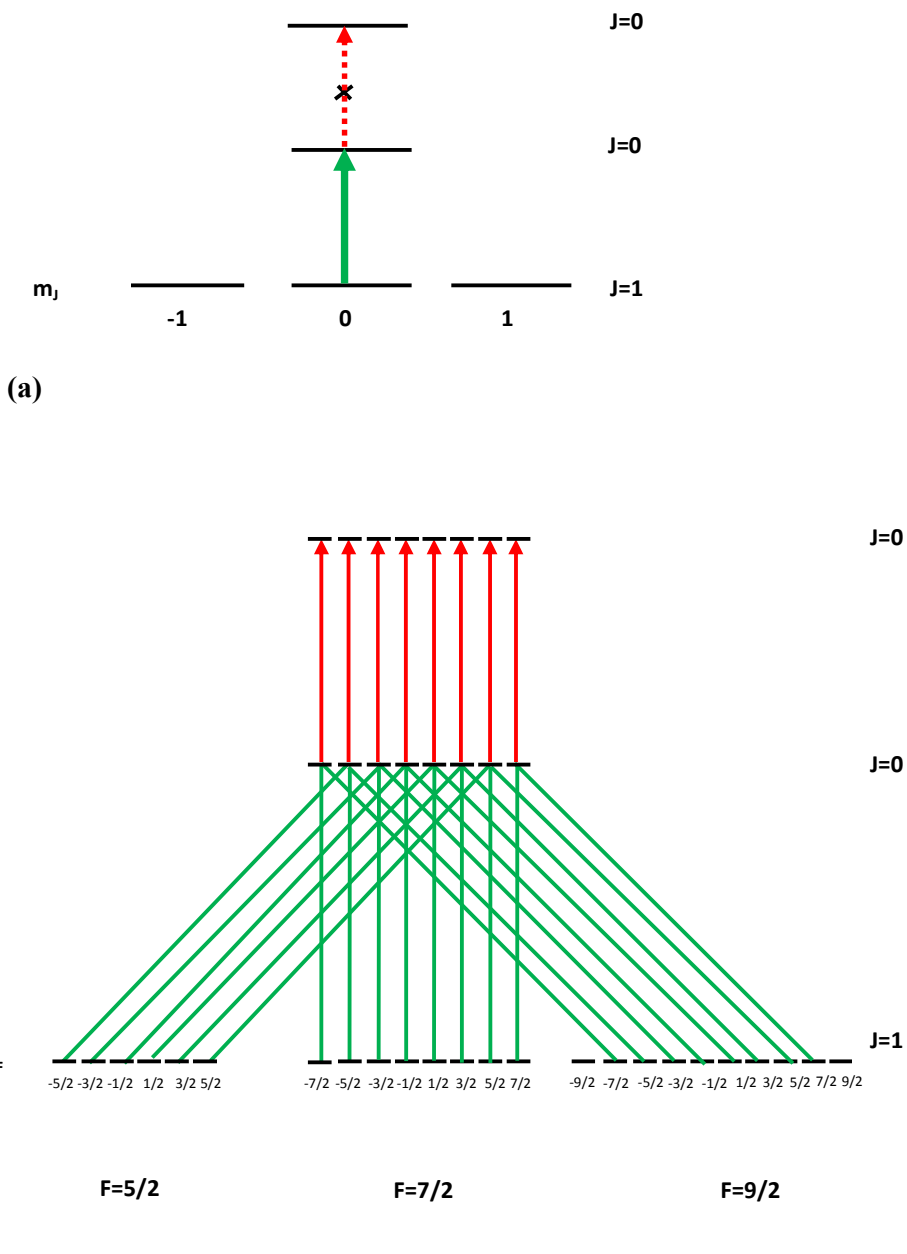


Fig. 3.4: Transitions between the magnetic sublevels of Sm I in scheme A for $J = 1 \rightarrow 0 \rightarrow 0$ transition in case of an (a) even isotope (b) odd isotope. Allowed and forbidden transitions are indicated by solid and dotted lines respectively.

Table 3.1: High-lying even-parity levels of Sm I

Energy Levels (cm^{-1})	Scheme	J - value	J - value (Reported in Literature)	Observed Ion Signal Intensity
33144.1	A	1		W
33157.8	A	1		W
33198.3	A	1		M
33223.7	A	1		M
33240.9	A	1		S
33325.6	A	1		M
33329.1	A	1		M
33334.2	A	1		M
33364.8	A	1		S
33374.5	A	1		S
33393.3	A	1		S
33433.5	A	1		M
33462.9	A	1		S
33502.0	A	1		S
33522.1	A	1		M
33526.2	A	1		W
33541.2	B	0,1,2		M
33585.2 ^a	B	0,1,2	2 ^a	S
33588.1	B	0,1,2		S
33645.6 ^a	B	0,1,2	1 ^a	M
33739.2	B	0,1,2		S
33747.9 ^a	B	0,1,2	2 ^a	M
33801.4	B	0,1,2		W
33833.5 ^a	B	0,1,2	2 ^a	S
33849.7 ^a	B	0,1,2	2 ^a	W
33893.9 ^a	B	0,1,2	2 ^a	W
33912.6	B	0,1,2		M
33956.0 ^a	B	0,1,2	2 ^a	S
33957.5 ^a	B	0,1,2	2 ^a	S

S: Strong; M: Medium; W :Weak

^a: Jayasekharan et al., [36].

3.3.3 Determination of Isotope Shift

3.3.3.1 Measurements in the energy region 33136 cm^{-1} - 33960 cm^{-1}

Sm I has seven naturally abundant isotopes ^{144}Sm , ^{147}Sm , ^{148}Sm , ^{149}Sm , ^{150}Sm , ^{152}Sm and ^{154}Sm with an abundance of 3.1, 15, 11.3, 13.8, 7.4, 26.6 and 22.6 percentages respectively. For measuring the isotope shifts (IS) of the intermediate levels, the wavelength of the first step laser is fixed in between the resonances of ^{144}Sm and ^{154}Sm isotopes and the wavelength of the second laser is scanned.

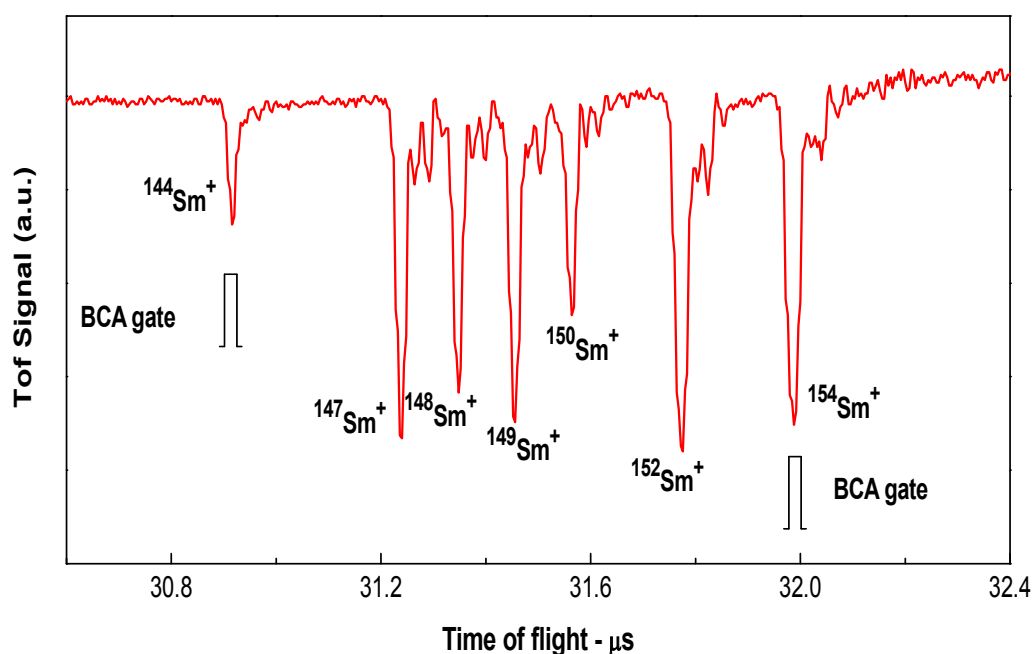


Fig. 3.5: A typical single-colour TOF mass spectrum of Sm I when λ_1 is tuned to the first step transition of scheme A. The mass spectrum does not reflect the natural abundance of different isotopes because it depends on where exactly the laser wavelength is fixed in between the resonances of ^{144}Sm and ^{154}Sm isotopes.

A typical single-colour non-selective photoionization mass spectrum of Sm I from the time of flight mass spectrometer when λ_1 is tuned to the atomic resonance 292.58 cm^{-1} ($J=1$) \rightarrow 17810.85 cm^{-1} ($J=0$) ($\lambda_1 \sim 570.68 \text{ nm}$) is shown in Fig. 3.5. The TOF mass spectrum does

not reflect the natural abundance of different isotopes because it depends on where exactly the laser wavelength is fixed in between the resonances of ^{144}Sm and ^{154}Sm isotopes. For measuring the isotope shift of the high-lying levels in the energy range 33136 cm^{-1} - 33960 cm^{-1} , the first step laser is tuned successively to the transitions corresponding to scheme A and scheme B (refer §3.3.2) and the second laser is scanned. The transition isotope shift between ^{144}Sm and ^{154}Sm reported in literature for the first step transitions $292.58\text{ cm}^{-1} \rightarrow 17810.85\text{ cm}^{-1}$ and $811.92\text{ cm}^{-1} \rightarrow 18225.13\text{ cm}^{-1}$ are -210 mK and $+31\text{ mK}$ respectively ($1\text{ mK} = 10^{-3}\text{ cm}^{-1}$) [77]. The criteria for choosing these transitions is that, the first step laser with a band width of 0.2 cm^{-1} can almost cover the isotope shift and excite all the isotopic components. The mass selective two-colour photoionization spectra of the naturally abundant isotopes ^{154}Sm and ^{144}Sm is recorded simultaneously by fixing the gates of the two boxcar averagers on the respective mass peaks in the TOF mass spectrum as shown in Fig.3.5 and scanning the wavelength of the second step laser.

Isotope shift measurements for the intermediate levels are performed for over sixteen levels in the energy region 33136 cm^{-1} - 33960 cm^{-1} . Fig.3.6 shows a part of the mass resolved two-colour photoionization spectrum recorded simultaneously by keeping gate positions of the boxcar averagers on ^{144}Sm and ^{154}Sm mass peaks using scheme A. From such spectra, the energy interval between the ^{144}Sm and the corresponding ^{154}Sm peaks were measured.

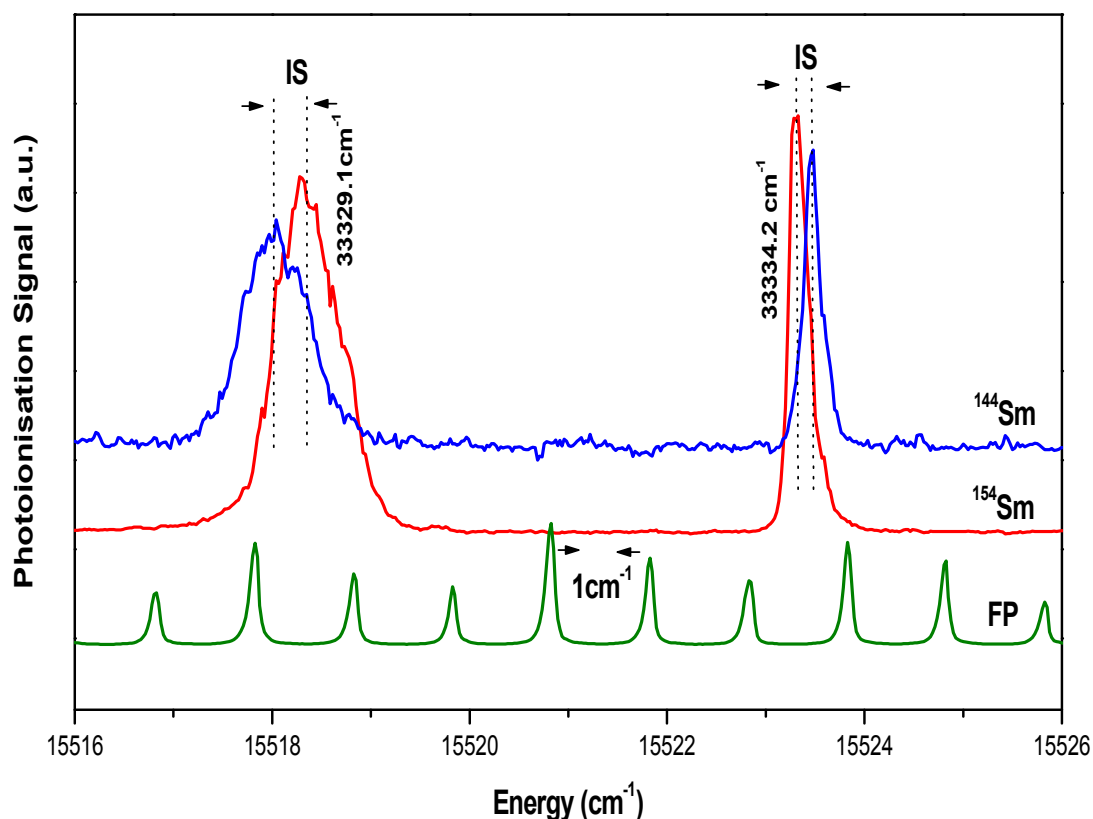


Fig. 3.6: Typical mass resolved two-colour photoionization spectrum of Sm I observed using scheme A. The resonance at 15518.3 cm^{-1} shows a positive isotope shift whereas the resonance at 15523.4 cm^{-1} shows a negative isotope shift. The resonances are also labelled with the corresponding upper level energies.

Conventionally, the isotope shift is positive if ^{154}Sm line lies on the higher wave number side. It is evident from Fig.3.6 that the resonance at 15518.3 cm^{-1} shows a positive isotope shift whereas the resonance at 15523.4 cm^{-1} shows a negative isotope shift. It is known that the isotope shift is the sum of both mass and field shifts, but for heavier elements the major contribution comes from the field shifts and is typically negative. In our measurements all the transitions exhibited negative isotope shift with the exception of resonance at 15518.3 cm^{-1} . One of the possible reasons for the observed negative isotope shifts for most of the transitions could be the configurations belonging to the levels involved

in the transition may possess more s-character, where the electron density at the nucleus is maximum, resulting in large field shifts. Out of the twenty nine resonances observed, the isotope shift could be measured for sixteen transitions only because for weak transitions the ion signal for ^{144}Sm could not be measured due to its low abundance and for some transitions the measured isotope shift values were very small and were comparable with the uncertainty involved in the measurements and therefore not reported.

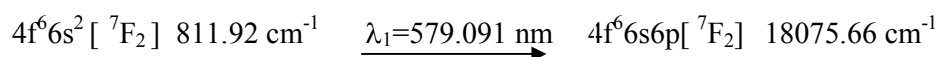
The level isotope shifts values of high-lying levels are obtained by adding the measured second step transition isotope shifts to that of the first step transition reported in literature and are summarized in Table-3.2. These level isotope shifts values reported are relative to the initial state E_0 , assuming the isotope shift for this level to be zero. The data represents averages of typically four measurements. The maximum deviations of the individual values from the average is ± 30 mK.

Table 3.2: Isotope shifts of the high-lying levels of Sm I in the energy region 33136-33960 cm^{-1}

E_0 (cm^{-1})	First Step Transition Isotope Shift $\delta_1(^{154}Sm - ^{144}Sm)$ (mK)	Energy Levels (cm^{-1})	Measured Second Step Transition Isotope Shift $\delta_2(^{154}Sm - ^{144}Sm)$ (mK)	Level Isotope Shift IS ($^{154}Sm - ^{144}Sm$) = ($\delta_1 + \delta_2$) (1mK = $10^{-3} cm^{-1}$)
292.58	-210	33198.3	- 106	- 316
292.58	-210	33240.9	- 265	- 475
292.58	-210	33329.1	+357	+147
292.58	-210	33334.2	- 144	- 354
292.58	-210	33374.5	- 190	- 400
292.58	-210	33393.3	- 233	- 443
292.58	-210	33433.5	- 180	- 390
292.58	-210	33462.9	- 238	- 448
292.58	-210	33502.0	- 85	- 295
811.92	+31	33541.2	- 232	- 201
811.92	+31	33585.2	- 331	- 300
811.92	+31	33588.1	- 269	- 238
811.92	+31	33747.9	- 291	- 260
811.92	+31	33912.6	- 334	- 303
811.92	+31	33956.0	- 504	- 473
811.92	+31	33957.5	- 433	- 402

3.3.3.2 Measurements in the energy region 35750 - 35450 cm⁻¹

This section describes the isotope shift measurement of the high-lying levels for the pairs of isotopes, ¹⁵⁴Sm - ¹⁴⁴Sm and ¹⁴⁹Sm - ¹⁴⁴Sm in the energy region 35750-35450 cm⁻¹ by performing two-colour three-photon resonance ionization spectroscopy. The experimental set-up used is similar to the one used in our previous section. The wavelength of the first-step laser is tuned in resonance to the following samarium transition:



The wavelength of the second laser is scanned in the Rh 6G dye range (562-576 nm) to access the high-lying energy levels in the energy region 35750 - 35450 cm⁻¹. Total twelve two-colour resonances were observed in this energy region. All the observed high-lying levels and their angular momenta are previously reported in literature [37].

As described in the previous section, for measuring the isotope shifts (IS) of the intermediate levels, the wavelength of the first step laser is fixed in between the resonances of ¹⁴⁴Sm and ¹⁵⁴Sm isotopes and the wavelength of the second laser is scanned. The transition isotope shift (¹⁵⁴Sm - ¹⁴⁴Sm) and (¹⁴⁹Sm - ¹⁴⁴Sm) for 292.58 → 18075.66 cm⁻¹ transition reported in literature is + 312 mK and +119 mK respectively (1mK = 10⁻³ cm⁻¹) [77]. The level isotope of 292.58 cm⁻¹ level is fraction of a mK and hence the transition isotope shift is taken as the level isotope shift. Since the second step level isotope shifts measured in the previous case (§3.3.3.1) were found to be mostly negative, in the present case, the first step is selected with a relatively large positive isotope shift in order to get large second step transition isotope shift. Because of the comparatively large transition isotope shift observed in the present scheme, it was possible to record the mass selective two-colour photoionization spectra of the naturally abundant isotopes ¹⁵⁴Sm, ¹⁴⁹Sm and ¹⁴⁴Sm simultaneously by fixing

the gates of the two boxcar averagers on the respective mass peaks in the TOF mass spectrum and scanning the wavelength of the second step laser. In order to discriminate the single-colour features, all the resonances appeared in the two-colour spectra were verified by blocking λ_1 laser.

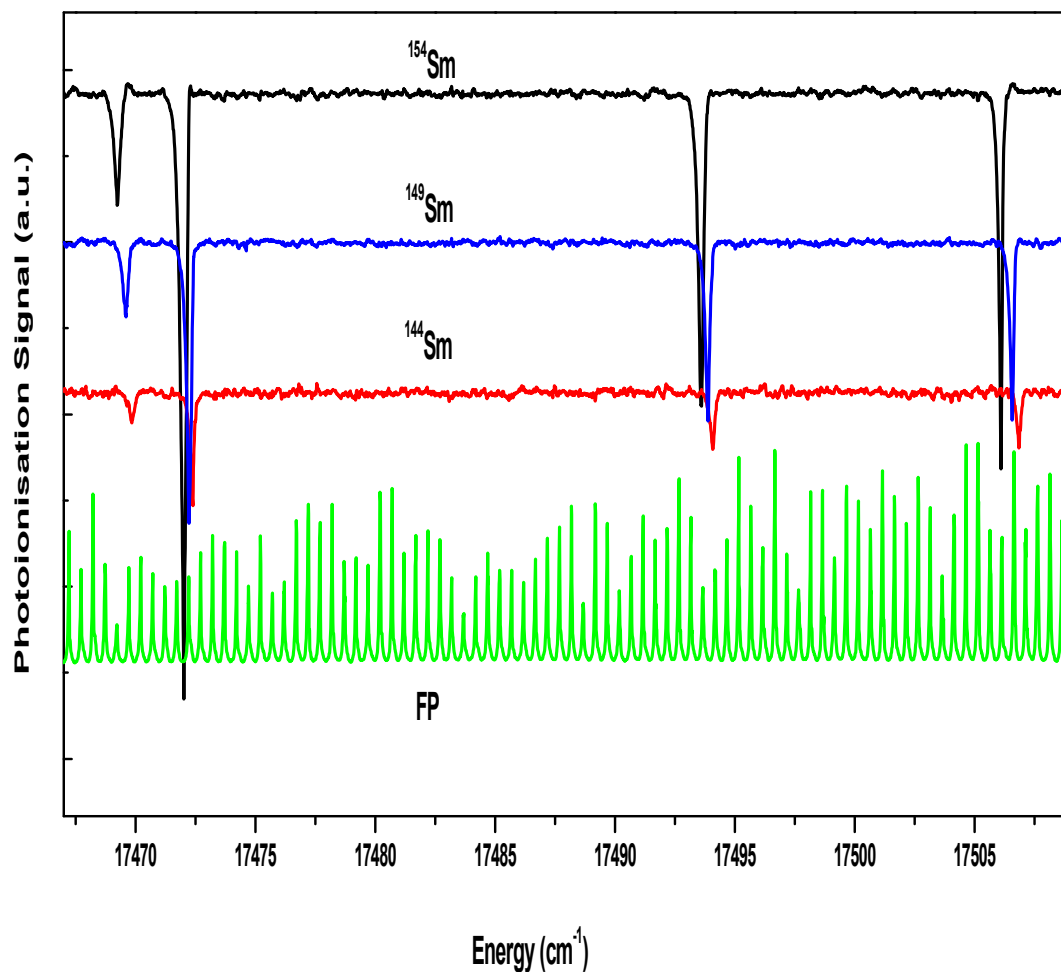


Fig. 3.7: Typical mass resolved two-colour photoionization spectrum of Sm I for the isotopes ^{154}Sm , ^{149}Sm and ^{144}Sm

Isotope shift measurement for the intermediate levels is carried for all the twelve levels in the energy region 35750 cm^{-1} - 35450 cm^{-1} . Fig.3.7 shows a part of the mass resolved

two-colour photoionization spectrum recorded simultaneously by keeping gate positions of the boxcar averagers on ^{144}Sm , ^{149}Sm and ^{154}Sm mass peaks. From such spectra, the energy interval between the ^{144}Sm and ^{154}Sm peaks and ^{144}Sm and ^{149}Sm peaks were measured. The measured level isotope shifts are listed in Table-3.3. The data represent averages of typically four measurements. The maximum deviations of the individual values from the average is ± 30 mK.

3.3.3.2.1 Odd-Even Staggering Effect

The observed mass resolved two-colour photoionization spectra of the isotopes ^{154}Sm and ^{144}Sm and ^{149}Sm exhibited odd-even staggering in their relative positions as can be clearly seen in Fig.3.8. The odd-even staggering i.e. the centre of gravity of the spectral components of an isotope with odd number of neutrons (in this case ^{149}Sm) was found to lie closer to the line of the adjacent lighter even N- isotope (^{144}Sm) than to the line of the adjacent heavier even N-isotope (^{154}Sm). This is interpreted as a field shift (FS) effect. $\text{FS} \propto \delta\langle r^2 \rangle$, where $\delta\langle r^2 \rangle$ is the change in the mean square radius of the nuclear charge distribution. It is previously reported by King et.al. that the change in the mean square radius of the nuclear charge distribution is found to be smaller when a neutron is added to an even N- isotope than to an odd N- isotope [75].

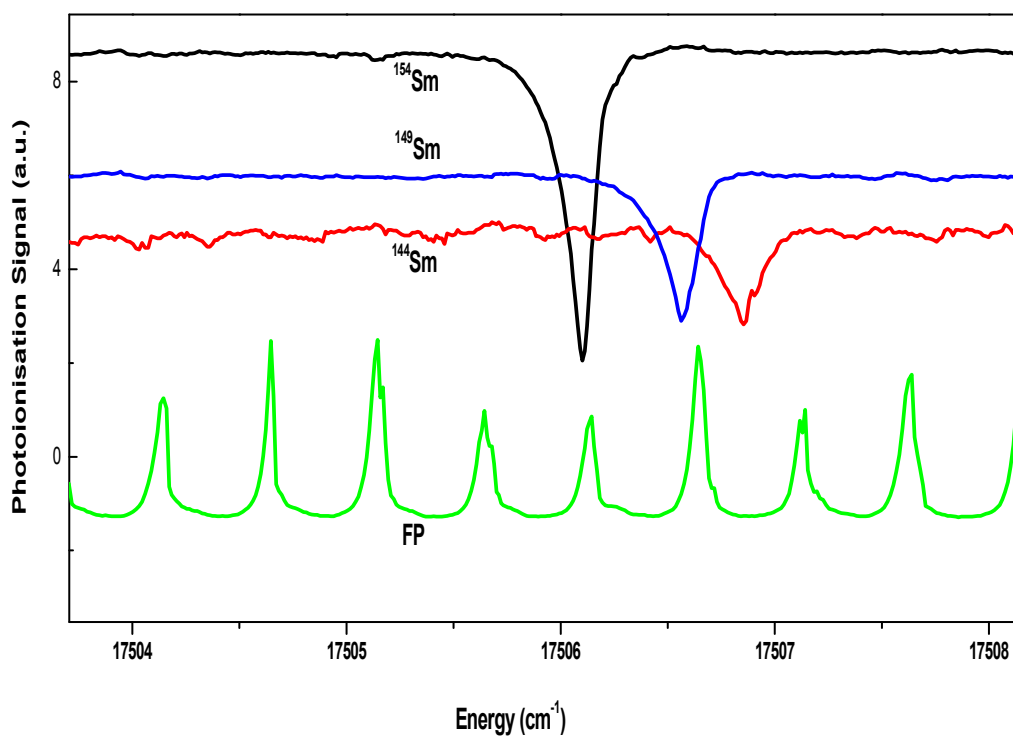


Fig. 3.8: Manifestation of odd-even staggering effect in the two colour spectra.

Systematic and statistical errors in the measurements were reduced carefully in order to ensure the accuracy of the experimental data. For instance, the minimum scan step size of 0.001nm contributes to a systematic uncertainty of ± 15 mK in defining the peak position. Statistical errors in the measurements were reduced by taking the average value after repeatedly recording the spectra.

3.4 Conclusions

Two-colour three-photon resonance photoionization spectra of atomic Sm were investigated in two different energy regions 33136 - 33960 cm^{-1} and 35750 - 35450 cm^{-1} . Analysis of the photoionization spectra recorded in the range 33136 - 33960 cm^{-1} resulted in the identification of twenty one new and confirmation of eight previously reported energy levels in this region. These energy levels have been assigned with an accuracy of $\pm 0.3 \text{ cm}^{-1}$. Based on the excitation scheme used, most of the new levels have been identified with a unique total angular momentum. By performing mass resolved photoionization spectroscopy, the isotope shift ($^{154}\text{Sm} - ^{144}\text{Sm}$) of sixteen high-lying levels in the energy range 33136-33960 cm^{-1} were measured. Analysis of the two-colour spectra recorded in the region 35750-35450 cm^{-1} resulted in the identification of twelve even-parity energy levels which are previously reported in literature. In addition, the mass resolved photoionization spectra recorded in the energy range 35750-35450 cm^{-1} resulted in the determination of the isotope shifts between the pairs of isotopes, $^{154}\text{Sm} - ^{144}\text{Sm}$ and $^{149}\text{Sm} - ^{144}\text{Sm}$, for twelve even- parity high-lying energy levels.

Table 3.3: Isotope shifts of the high-lying levels of SmI in the energy range 35750-35450 cm^{-1}

Second Step transition (cm^{-1})	Energy Levels ^a $E_2(cm^{-1})$	J ^a	Measured Second Step Transition Isotope Shift δ_2 ($^{154}Sm - ^{144}Sm$) (mK)	Measured Level IS($^{154}Sm - ^{144}Sm$) ($\delta_1 + \delta_2$) (mK)	Measured Second Step Transition Isotope Shift δ_2 ($^{149}Sm - ^{144}Sm$) (mK)	Measured Level IS($^{149}Sm - ^{144}Sm$) ($\delta_1 + \delta_2$) (mK)
17671.2	35746.9	2	- 571	-259	- 205	-86
17666.4	35742.0	1	- 622	-310	- 240	-121
17624.6	35700.3	1	-420	-108	-286	-167
17603.9	35679.6	3	- 458	-146	- 138	-19
17576.2	35651.8	1	- 559	-247	- 169	-50
17518.4	35594.0	2	- 539	-227	- 238	-119
17506.1	35581.7	3	- 745	-433	- 332	-213
17493.5	35569.2	2	- 466	-154	- 183	-64
17471.9	35547.6	2	- 397	-85	- 181	-62
17469.1	35544.8	1	- 608	-296	- 255	-136
17411.6	35487.3	2	- 505	-193	- 174	-55
17385.3	35460.9	2	- 616	-304	- 238	-119

^a: Jayasekharan et al., [37].

Chapter 4:

Radiative lifetimes of even-parity high-lying levels of SmI by delayed photoionization measurements

Chapter 4

4.1 Introduction

Accurate measurements of radiative properties such as radiative lifetimes, branching ratios and absolute transition probabilities of an atomic system are important from technological viewpoint as well as from scientific requirements. Transition probabilities of lanthanides, in particular, are of great interest in astrophysics where it is used to determine the composition of chemically peculiar stars which show overabundance of lanthanides when compared to the solar system composition [80]. In applied research such as laser isotope separation, trace elemental analysis etc. transition probabilities play a vital role in the selection of efficient photoionization wavelength schemes [54, 80, 81, 82]. It is known that radiative lifetime when combined with branching ratio can provide the most reliable means to determine the absolute atomic transition probability [83, 84]. This requirement for accurate transition probabilities has stimulated a variety of radiative lifetime measurements of lanthanides in general and samarium in particular. In addition, the rare-earths because of their favourable radiative properties have become important additives in commercial metal-halide high intensity discharge lamps and hence radiative data on energy levels of these elements is important information needed in lighting technology [54].

4.2 Radiative lifetimes of excited atoms

Consider an assembly of atoms in which $N_k(0)$ atoms per unit volume are excited to the level $|k\rangle$ at $t = 0$. In general these atoms can decay by spontaneous emission to any of the low lying levels $|i\rangle$. In the absence of collisional depopulation/ repopulation etc., the population density of the level changes at a rate given by,

$$-\frac{dN_k}{dt} = \frac{N_k}{\tau_k} \quad (4.1)$$

,where τ_k is the radiative lifetime of the level $|k\rangle$. Hence the time dependent population of the excited level is given by,

$$N_k(t) = N_k(0) \exp\left(-\frac{t}{\tau_k}\right), \quad (4.2)$$

with the radiative lifetime τ_k given by,

$$\tau_k = \frac{1}{\sum_i' A_{ki'}} \quad (4.3)$$

,where $A_{ki'}$ represents the transition probability from the level $|k\rangle$ to any of the degenerate levels of $|i\rangle$ and the prime on the summation indicates that the summation is over for all the levels below the level $|k\rangle$. In case of the lowest excited levels of many atoms, there will be only one term in the summation of the above equation, hence the measurement of the radiative lifetime will directly give the transition probability [85].

4.3 Measurement Techniques

Measurement of radiative lifetimes of excited atomic levels are performed either directly by observing exponential decay of the level population or indirectly through the measurement of lifetime dependent change of properties (phase, polarization etc.) of the emitted radiation. The basic measurement procedure can be divided into two steps: excitation of atoms by absorption of light photon or collision with electrons and observation of emitted light/fluorescence or delayed photoions after the excitation. In all the measurements, laser frequencies are tuned to the centre frequency of the absorbing transitions. In case of fluorescence detection, fluorescence terminating to initial level i.e. resonance fluorescence are avoided to improve the signal to noise ratio.

4.3.1 Techniques based on observation of exponential decay curve

In these techniques, the decay of excited level population as a function of time is observed and the resultant decay curve is fitted to extract the lifetime values [3].

4.3.1.1 Single-pulse excitation method

The atoms are excited by a short laser pulse. The trailing edge of the laser pulse should be short compared to the radiative lifetime of the excited level. The decay of the excited level results into time dependent fluorescence which can be detected by a fast photomultiplier tube or by a transient recorder. Another method is by using a boxcar integrator, where the signal is passed through a gate which opens only during a selected time interval Δt . After each successive laser pulses, the delay between the trigger and the gate is increased by $\Delta t/n$. After n excitation cycles, the time window T will be covered. The temporal step size of increasing delay depends on the lifetime and desired number of data points. The experimental decay curve is fitted with exponential decay formula to extract the lifetime values. The advantage of this method is that for sufficiently intense fluorescence one need only a single excitation pulse, although averaging over many excitation cycles are performed to improve the signal to noise ratio. This technique of single-pulse excitation is very suitable for low repetition rate pulsed lasers such as Nd:YAG or excimer laser pumped dye lasers. In many experimental conditions, fluorescence may be extremely weak either due to very low vapour density or due to weak fluorescence; in that case alternate techniques are required.

4.3.1.2 Delayed coincidence method

Delayed coincidence method also uses short laser pulses as in the previous method for the excitation of selected levels. However, the pulse energy is kept so low that the detection probability P_D of a fluorescence photon per laser excitation pulse remains small ($P_D \leq 0.1$). During the time interval between t and $(t + dt)$ after the laser excitation, the probability of fluorescence detection is $P_D(t)dt$. The mean number of fluorescence photon (n_{FL}) detected within this time interval dt for N excitation cycles ($N \gg 1$) is

$$n_{FL}(t)dt = NP_D(t)dt \quad (4.4)$$

In this method, a part of the exciting laser pulse is sent to a fast photo diode, the output of this fast photo diode at time $t = t_0$ starts a time to amplitude converter (TAC). TAC generates a fast rising voltage ramp $U(t)$ whose amplitude is proportional to $(t-t_0)$. The fluorescence photons are detected by a photomultiplier with a large amplification factor, which generates an output pulse that triggers a fast discriminator. The normalised output of the discriminator stops the TAC at time t . Hence the amplitude $U(t)$ of the TAC is proportional to the delay between the excitation pulse and the fluorescence photon emission. These pulses are stored in a multi-channel analyzer. The number of events per channel gives the number of fluorescence photons emitted at the corresponding delay time. In this method is suitable for measuring lifetimes with high repetition rate lasers especially mode-locked lasers.

4.3.1.3 Beam foil method

This technique is most suitable for measuring lifetimes of ions of different charge state. Here a time measurement is reduced to a distance and velocity measurement. In this technique, mass selected accelerated ion beam is passed through thin carbon foil in high

vacuum environment. Interaction of the primary ions with the foil causes further ionization and excitation. Excited ions emit light from many excited levels. Because of the high velocity of the beam, the particles move a considerable distance before decaying. The emitted light (the emission line of interest is chosen using a monochromator) in a direction perpendicular to the direction of motion, by means of a photomultiplier at different positions and a decay curve is measured as a function of the distance between the foil and the point of observation. For a given acceleration voltage, velocity of the ion is known and thus distance can be easily converted into time.

4.3.1.4 Fast beam method

As in previous method the fast beam method also measures distance and velocity for lifetime measurement. This method is used for measuring the radiative lifetimes of neutral atoms as well as ions very accurately. In this method, accelerated ions after mass selection by a magnet are excited at $x = 0$ by a CW laser beam and the resultant LIF is monitored as a function of distance between the laser excitation position and photo detector. Since the velocity of the ions is known from the acceleration voltages, the time is determined from the measured x positions.

4.3.1.5 Pump-probe method

For measuring very short lifetimes which demand a time resolution better than 10^{-10} s, this technique is the best choice since most of the available detectors (except streak camera) cannot offer time resolution better than 100 ps.

In this method, the atoms/molecules under investigation are excited by a short laser pulse and the probe laser with a variable time delay probes the time evolution of the

population density of the level with respect to the pump level. The method has the advantage that the time resolution is limited by the pulse width T of the pump and the probe lasers, but not by the time constants of the detectors.

This technique can be directly adopted in a resonance ionization spectroscopy facility to carry out lifetime measurements. In this technique, probe laser ionizes the excited atoms and the ions formed are subsequently detected by ion detector (micro-channel plate, channeltron etc.). Since in this technique, the photoionization takes place at different time delays, it is also known as delayed photoionization technique. The work described in this chapter describes the utilisation of this method to determine the radiative lifetimes of the even parity high-lying levels of atomic samarium. The details of which are described in § 4.4.

4.3.2 Techniques not based on observing exponential decay curve

4.3.2.1 Phase shift method

In this method intensity of the laser (well below the saturation intensity) is sinusoidally modulated and intensity dependent LIF is monitored. The phase shift between the fluorescence light and the incident light is measured using a phase comparator. This phase shift depends on the modulation frequency and the lifetime. For a given modulation frequency, the radiative lifetime can be determined from the measured phase shift.

4.3.2.2 Hanle effect Method

In this method, polarized light is used to excite the atom and resonance fluorescence is passed through analyzer and detected by a photo-multiplier tube. If a magnetic field is applied in a direction perpendicular to the laser polarisation, then the excited atom will precess about the

magnetic field and hence the resultant radiation field distribution will also precess with the excited atom. A plot of the fluorescence intensity as a function of magnetic field is recorded. From the half width of this curve, lifetime values can be extracted provided the Lande-g factor is known.

4.4 Present work on radiative lifetime measurements

The ground term of Sm I is $4f^6 6s^2 ({}^7F_J)$ with seven fine structure levels, identified by $J = 0 - 6$ corresponding to energy levels at $0 \text{ cm}^{-1} ({}^7F_0)$, $292.58 \text{ cm}^{-1} ({}^7F_1)$, $811.92 \text{ cm}^{-1} ({}^7F_2)$, $1489.55 \text{ cm}^{-1} ({}^7F_3)$, $2273.09 \text{ cm}^{-1} ({}^7F_4)$, $3125.46 \text{ cm}^{-1} ({}^7F_5)$ and $4020.66 \text{ cm}^{-1} ({}^7F_6)$. At the operating temperature of $800 \text{ }^\circ\text{K}$ of atomic beam source, the percentage population in the septet ground state (${}^7F_{J=0-6}$) is calculated to be 21.67, 38.42, 25.16, 10.41, 3.27, 0.86 and 0.20 respectively [48]. Spectroscopic studies of Sm have the added experimental advantage that due to the thermally populated septet ground state (${}^7F_{J=0-6}$), various low-lying levels in the energy region $16000 \text{ cm}^{-1} - 20000 \text{ cm}^{-1}$ with wide range of J values can be easily accessed using tunable dye lasers with Rhodamine dyes.

In the early work on lifetime determination, Corliss *et.al* deduced some results from the available arc emission data [86]. Subsequently, many spectroscopic studies on radiative lifetime measurements of atomic samarium were carried out using various spectroscopic techniques such as Hanle effect method, delayed coincidence method, beam foil technique, laser induced fluorescence etc. [87, 80]. Recently, Wei Zhang et al. measured the radiative lifetimes of a large number of excited levels of atomic samarium belonging to the series $J = 0,1,2,3$ and $J = 4,5,6,7$ in the energy range $18,985$ to $34,189 \text{ cm}^{-1}$ using time-resolved laser-induced fluorescence technique in an atomic beam produced by laser ablation [88, 89]. Shah *et.al* reported the measurements of radiative lifetimes, branching fractions and absolute

transition probabilities in atomic samarium using laser-induced fluorescence [90]. More recently, Den Hartog *et.al* carried out an extensive work on the measurement of radiative lifetimes of 120 odd-parity levels of neutral samarium, in the energy range from 17190 to 33507 cm^{-1} , using the technique of time-resolved laser-induced fluorescence [80]. Sahoo *et.al* demonstrated the measurements of radiative lifetime by simultaneously detecting laser-induced fluorescence and laser-induced photoionization signals using pump-probe technique [91]. Even though radiative lifetimes of high-lying levels of Sm I covering up to 34800 cm^{-1} have been measured extensively, but due to single resonant excitation, the levels accessed in these studies are mostly limited to odd-parity high-lying levels. Consequently, the information available in literature on the lifetimes of the even-parity high-lying levels in the energy region above 30000 cm^{-1} is scanty.

4.4.1 Experimental Method

The functional block diagram of the experimental arrangement used for measurement of radiative lifetimes is shown in Fig.4.1. It consists of a high temperature Sm atomic vapour source coupled to a time-of-flight mass spectrometer (TOFMS), three pulsed tunable dye lasers pumped by the second harmonic of two Nd: YAG lasers, a photo diode, a wavelength meter, an electronic delay generator (EDG), a digital storage oscilloscope (DSO) and a computer for signal recording. As shown in figure, the dye lasers DL₁ and DL₂ are pumped by the same laser and DL₃ is pumped independently by another laser.

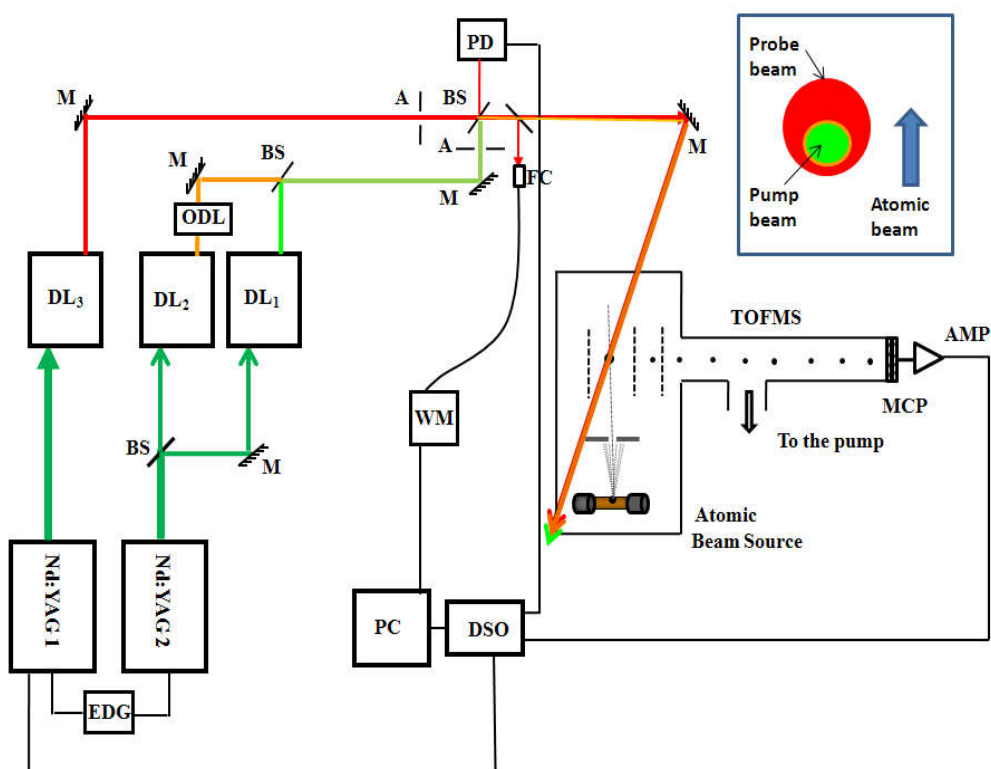


Fig. 4.1: Schematic representation of the experimental set-up for three-colour pump-probe spectroscopy. DL_1 , DL_2 , DL_3 : tunable dye lasers, ODL: optical delay line, EDG: electronic delay generator, A: Aperture, FC: fibre coupler, WM: wavelength meter, TOFMS: time-of-flight mass spectrometer, MCP: micro-channel plate detector, AMP: pre-amplifier, DSO: digital storage oscilloscope, PD: photo diode, BD: beam dump, M: mirror, BS: beam splitter, PC: personal computer.

An electronic delay generator is used to control the relative delay between the pump and the ionising probe laser pulses to an accuracy of ± 1 ns. An optical delay line (ODL) is used to ensure sequential absorption of DL_1 and DL_2 pulses. The pulse duration of all the dye lasers used in these studies is ~ 6 ns. Rh6G and DCM dyes are used in the dye lasers to produce laser photons at desired wavelengths. The typical fluence in the interaction zone is $\sim 200 \mu\text{J}/\text{cm}^2$ for DL_1 and DL_2 lasers and that of DL_3 is variable in the range of 500 to $2000 \mu\text{J}/\text{cm}^2$. By introducing two variable apertures in the path of the pump and the probe

beams uniform part of the laser beams was selected. The beam diameters of the pump and probe lasers in the interaction zone are independently adjusted to be 2 mm and 4 mm respectively. The probe laser beam was shifted away from the centre of the pump laser beam in the direction of the atomic beam to ensure that the excited atoms are not lost before getting ionized due to the atomic beam flow velocity at large time delays. Spatially overlapped dye laser beams interact with an effusive atomic beam of samarium formed in a high vacuum atomic beam generator that is coupled to a linear time-of-flight mass spectrometer in a perpendicular configuration.

Atomic vapour of Sm is produced by resistively heating few hundred mg of Sm metal in a high temperature oven at ~ 800 °K in a vacuum chamber maintained at a pressure of $\sim 10^{-7}$ mbar. The Sm vapour effusing out of the oven orifice of 1mm diameter is further apertured by using a fixed aperture of diameter 3 mm at a distance of 15 mm from the oven orifice. At the operating temperature of 800 K, the typical number density of Sm in the interaction zone is estimated to be $\sim 10^9$ atoms/cm³. The reduced Doppler width of the atomic absorption line in the interaction zone is ~ 100 MHz. The photoions generated in the interaction region are extracted by a dc electric field of strength 150 V/cm and then introduced into the flight tube of the TOFMS. After travelling a field free flight region of 130 cm, the photoions are detected by a micro-channel plate (MCP) detector. The detector output signal is amplified using a pre-amplifier (gain ~ 100 and a band width ~ 100 MHz). The amplified output signal is recorded using a digital storage oscilloscope (DSO). The Q-switch output from the first Nd: YAG laser is used for triggering the DSO.

Two different excitation schemes were employed in this experiment, schemes A & B schematically shown in Fig. 4.2, to access the high-lying levels of interest. The resonant first laser (DL₁) excites the population from the initial state (E_0) to an intermediate state (E_1) from which it is further excited to a high-lying even-parity level (E_2) by a temporally synchronized

second resonant laser (DL₂). The population in this level can reach the continuum either by absorbing a photon from DL₁ or DL₂. This process gives rise to a two-colour three-photon ($\lambda_1+\lambda_2+\lambda_1$, $\lambda_1+\lambda_2+\lambda_2$) photoionization background signal synchronous with DL₂ pulse. The magnitude of this two-colour photoionization signal is minimised by attenuating the intensities of DL₁ and DL₂ lasers. The atoms excited to the high-lying level of interest by the pump lasers are subsequently non-resonantly ionized using a probe laser (DL₃) with a variable time delay. The delayed three-colour photoionization signal ($\lambda_1 + \lambda_2 + \lambda_3$) produced is temporally synchronous with the DL₃ pulse. A well resolved time-of-flight mass spectrum similar to the one observed in our previous work [92] was obtained. To measure the lifetime of the excited level, the delay between the pump and the probe lasers is varied in finite steps and the delayed three-colour photoionization signal of ¹⁵⁴Sm is monitored on a digital storage oscilloscope. Each data point is obtained after averaging over 64 laser pulses to improve the signal to noise ratio.

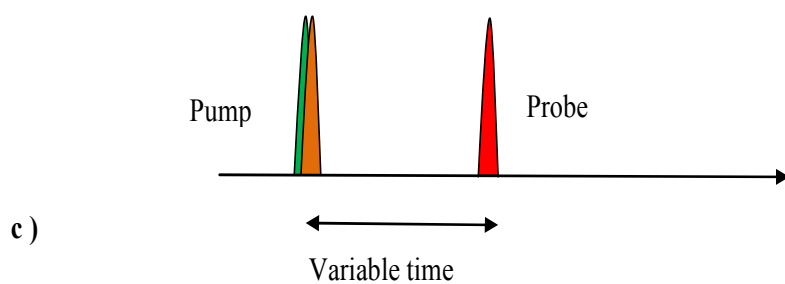
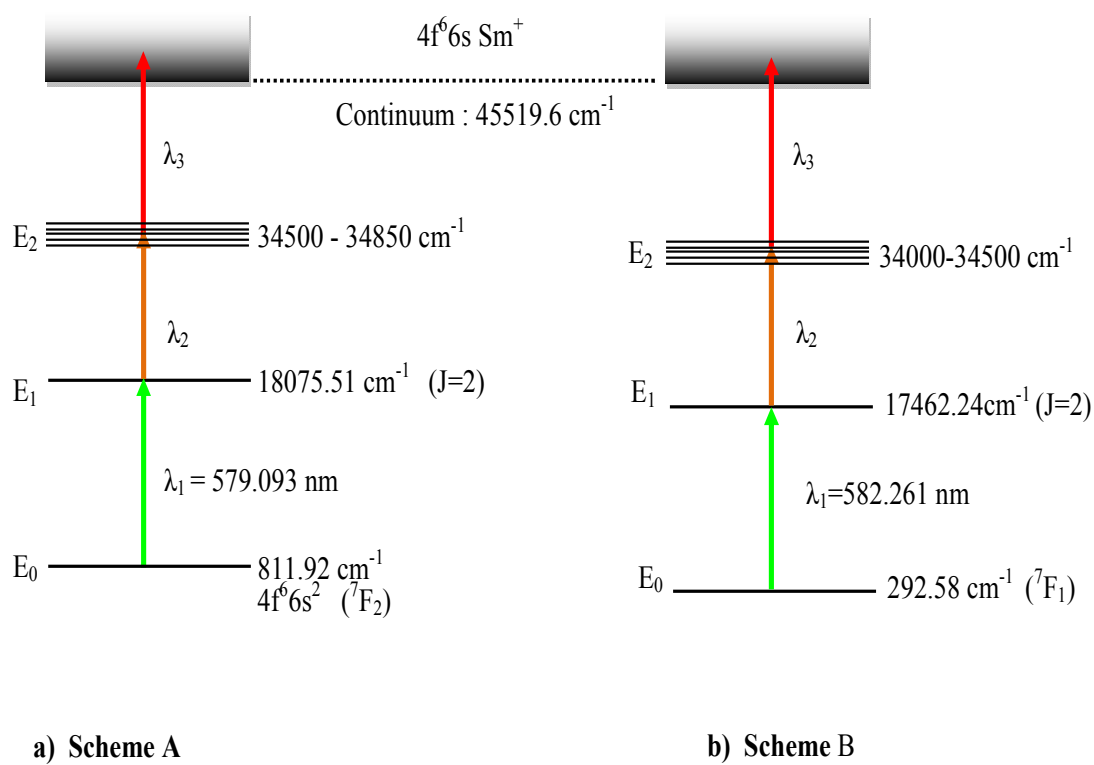


Fig. 4.2: Schematic of photoionization schemes. (a) Scheme A (b) Scheme B, (c) pump and probe laser pulse sequencing for pump-probe scheme.

To validate the results, the lifetime of the first excited level at 18075.51cm^{-1} , used in the excitation (Scheme A), was measured by employing single-colour photo-excitation followed by time-resolved photoionization using a second laser (DL₃) via $\lambda_1 + 2\lambda_3$ photoionization process and compared the measured value with the data available in the literature.

4.4.2 Results and Discussion

For measuring the lifetimes of the even-parity high-lying levels, two-colour photo-excitation followed by time-resolved photoionization is employed. The delayed third-step dye laser, DL₃, probes only the population of the second excited level was ensured by the disappearance of the photoionization signal on blocking DL₂ laser. The three-colour photoionization signal observed at different delays was fitted using the exponential decay formula, $S(t) = S(0) \exp(-t/\tau)$, where $S(t)$ is the three-colour delayed photoionization signal at delay time t , $S(0)$ is the three-colour photoionization signal at zero delay and τ is the radiative lifetime of the level concerned. Fig. 4.3 shows a typical decay curve of the even-parity high-lying level at 34774.2 cm^{-1} with exponential fit. To avoid optical pumping effect during the laser pulse, the lifetime data having time delay more than 12 ns were considered for fitting. Table.4.1 lists the measured lifetimes of the even-parity high-lying levels along with the excitation wavelengths employed. There is no data available in literature on the radiative lifetimes of the even-parity high-lying levels of atomic samarium in this energy range, hence these results are new.

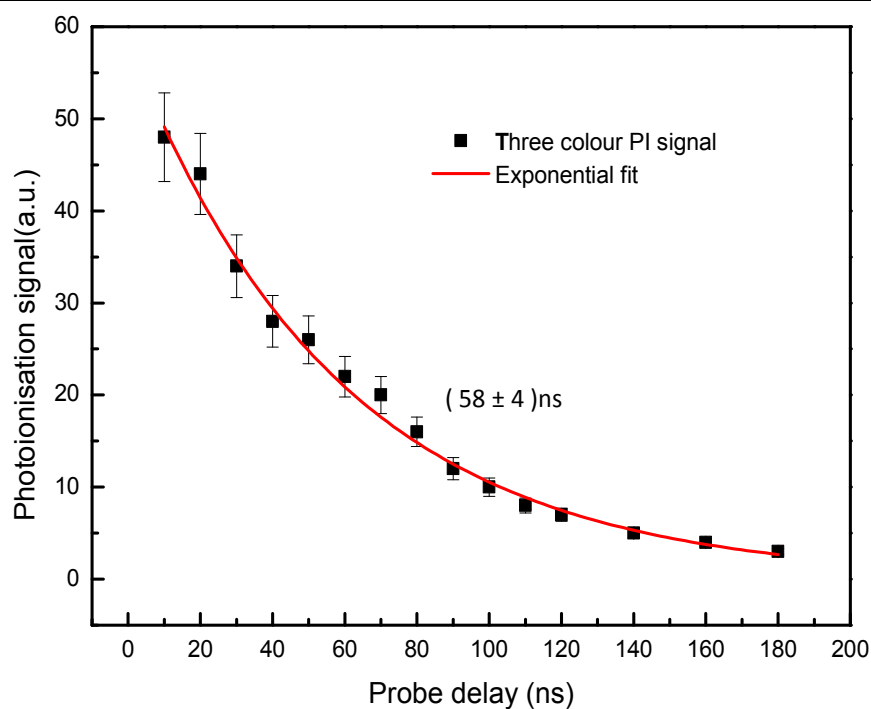


Fig. 4.3: Typical decay curve of the high-lying energy level at 34774.2 cm^{-1} along with the exponential fit.

These results have been validated by measuring the radiative lifetime of a first excited odd-parity level and comparing the value with the data previously reported in literature. Fig.4.4 shows the decay curve of the odd parity level at 18075.51 cm^{-1} along with the exponential fit. In these measurements, the two dye lasers DL_1 & DL_3 were used. The first dye laser DL_1 was tuned in resonance to the first step transition of Sm at wavelength 579.093 nm to populate the level of interest at 18075.51 cm^{-1} . The second dye laser DL_3 , which can be electronically delayed with respect to DL_1 , was used to probe the population via $\lambda_1 + 2\lambda_3$ photoionization process at various time delays. The measured lifetime value of the first excited level at 18075.51 cm^{-1} along with the corresponding values reported in literature are listed in Table 4.2. It is evident from the Table 4.2 that the measured value of radiative lifetime matches reasonably well with those reported in the literature.

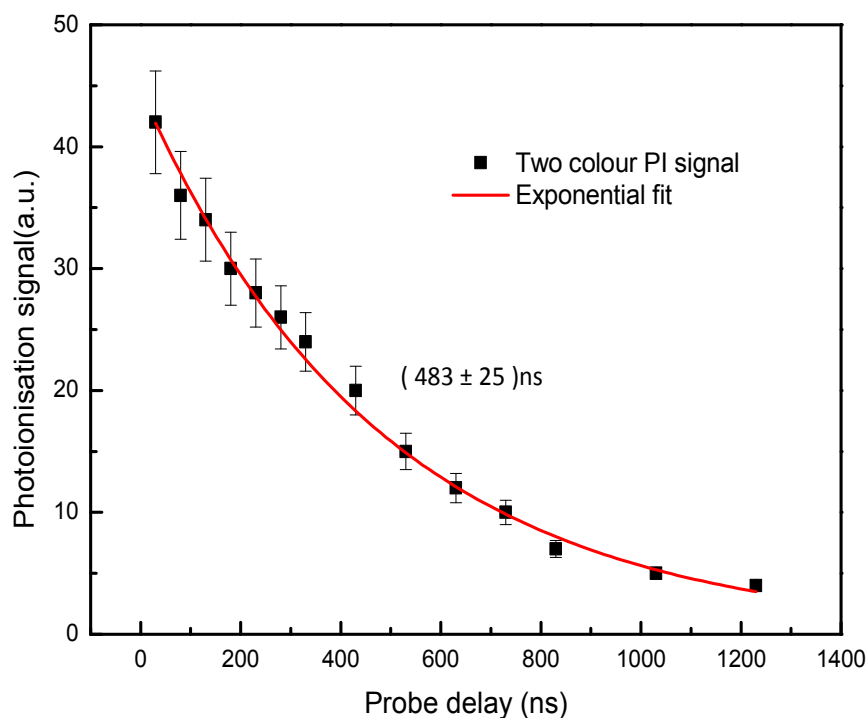


Fig. 4.4: Decay curve of the first excited energy level at 18075.51 cm^{-1} along with the exponential fit.

The errors listed in the tables 4.1 and 4.2 are based on the spread in the lifetime values obtained from different sets of measurements due to small changes in the oven temperatures/atomic number densities, laser intensities etc. The observed statistical error is ~ 5 to 10% of the average measured values. In addition to the statistical uncertainties, various effects such as atomic motion, radiation trapping, collisional depopulation and repopulation etc. may contribute to systematic uncertainties in the measurements. At large time delays, the excited atom can move out of the interaction zone before getting ionised and thus can effectively shorten the lifetime of the levels. To minimize this effect, the probe laser beam diameter was deliberately kept (4 mm) more compared to the pump laser diameter (2 mm) and also the pump laser beam spot is kept downstream of the atomic beam as shown in Fig. 4.1. In our experiment, the transit time of atoms through the interaction zone is about (~ 4)

μs and our measurements are limited to $1.5 \mu\text{s}$. Therefore, the systematic error in these measurements due to atomic motion is expected to be very small. Similarly, the effect of radiation trapping is not significant in the experiments as any measurable change in the lifetimes of the levels even at higher permissible oven temperatures were observed. Since the experiment is carried out in a high vacuum chamber evacuated to a pressure of 10^{-7} mbar, the systematic error in the lifetime measurements due to collisional depopulation effects can also be neglected. Hence the cumulative systematic error in the lifetime measurements due to all the effects discussed above is negligible in comparison to the statistical error. The lifetimes of two of the second excited levels, marked with asterisk in Table. 4.1, were also measured by using scheme B as well and the radiative lifetime values obtained by both the routes are in good agreement.

Table 4.1: Measured radiative lifetimes of high-lying even-parity levels of atomic samarium

Energy Level ^a E ₂ (cm ⁻¹)	J ^a	Scheme	Excitation Wavelength λ_2 (nm)	Measured Lifetime (ns)
34811.8	3	A	597.338	136 ± 7
34795.8	2	A	597.910	140 ± 8
34774.2	2	A	598.683	58 ± 4
34736.2	3	A	600.049	64 ± 4
34722.9	2	A	600.528	131 ± 7
34712.6	1	A	600.900	83 ± 6
34698.8	2	A	601.399	294 ± 15
34659.5*	3	A	602.824	96 ± 9
34590.1*	2	A	605.357	50 ± 3
34522.1	3	B	586.009	132 ± 9
34311.5	3	B	593.333	35 ± 3
34206.5	2	B	597.054	36 ± 3
34185.6	3	B	597.800	349 ± 25
34150.2	2	B	599.068	38 ± 3
34041.3	1,3	B	603.003	137 12

*Lifetime measured by both the schemes

^a Jayasekharan et al. 1996 [36]

Table 4.2: Measured radiative lifetime of the first excited level of atomic samarium

Energy Level (cm^{-1})	J	Configuration	Excitation Wavelength λ_2 (nm)	Measured Lifetime (ns)	Reported Value in literature (ns)
18075.51	2	$4f^5(6H^\circ)5d6s^2$	582.553	483 (± 25)	477(± 24) ^a , 471(± 49) ^b , 517(± 19) ^c , 480(± 20) ^d

^aDen Hartog et al. 2013 [80]^bShah *et al* 2010 [90]^cGao *et al* 1993 [93]^dHannaford and Lowe 1986 [94]

4.4.3 Conclusions

The radiative lifetimes of fifteen even-parity high-lying levels of atomic samarium in the energy range 34000-34815 cm^{-1} has been measured. The measurements were carried out by detecting time-resolved three-colour photoionization signal by pump-probe technique in an atomic beam coupled to a time-of-flight mass spectrometer. The results were validated by measuring the radiative lifetime of a first excited level using pump-probe method and comparing the value obtained with the data previously reported in literature.

Chapter 5:

Polarization-based isotope-selective two-color photoionization of atomic samarium using broad band lasers

Chapter 5

5.1 Introduction

Multi-step resonance ionization spectroscopy has played a key role in achieving high selectivity and yield in isotope selective photoionization processes. Generally, in laser isotope separation (LIS) process, isotope-selective photoionization of the target isotope is achieved by utilising the isotopic shift or the difference in the hyperfine structure of different isotopes using narrow band lasers. The selectivity that can be achieved using this method will be degraded significantly if the targeted isotope has an overlapping absorption spectrum with the undesired one. Hence, when the isotope shifts are small and the hyperfine spectra are overlapping, this method puts stringent conditions on the laser band widths and the atomic beam parameters. In such cases, there is an alternative method of isotope-selective photoionization based on atomic population alignment induced by polarized lasers. In this method, odd isotopes with non-zero nuclear spin are selectively excited while even isotopes with zero nuclear spin are prohibited from excitation by judiciously choosing a proper excitation sequence of angular momenta of the levels and the laser polarizations. Isotope separation method based on population alignment using polarized broad band lasers has been previously applied for separation of odd and even isotopes of Zr, Gd, and Yb where the isotope shifts are small and the hyperfine spectra are complex. Isotope separation of many of these elements is of great importance to nuclear industry [78,79, 95-100]. However, this method is applicable to elements having states with low total angular momentum (J-values).

As already mentioned, atomic samarium (Sm I) has seven naturally abundant isotopes ^{144}Sm (3.1%), ^{147}Sm (15%), ^{148}Sm (11.3%), ^{149}Sm (13.8%), ^{150}Sm (7.4%), ^{152}Sm (26.6%) and ^{154}Sm (22.6%). Among these, ^{149}Sm , with high thermal neutron absorption cross-section

(40140 barns), is a promising candidate as burnable poison in nuclear reactors [61]. The use of natural samarium as a burnable poison was discarded previously because of the large residual negative reactivity worth of samarium isotopes and their daughter products at the end of life of the fuel. Recently, Renier et al [62] have investigated the potential benefits of using enriched samaria (Sm_2O_3) as a burnable poison in the fuel pellets of PWRs and shown that the use of Sm enriched in ^{149}Sm has greatly reduced this residual absorber problem.

This chapter describes in detail, isotope-selective photoionization of atomic samarium (Sm I) using two-color resonance ionization polarization spectroscopy with broad band lasers. A two-color excitation scheme, $0 \text{ cm}^{-1} (J = 0) \rightarrow 15650.5 \text{ cm}^{-1} (J = 1) \rightarrow 33116.8 \text{ cm}^{-1} (J = 1) \rightarrow \text{Sm}^+$ for selective excitation of the odd isotopes of Sm I has been identified [101, 36]. Using this scheme, selective excitation of odd isotopes of Sm I (^{147}Sm and ^{149}Sm) with isotopic selectivity better than 40 has been demonstrated using broad band lasers. In addition, the effect of different polarization states of the excitation lasers and relative polarization angle between them on the selectivity has been studied. The method has the unique advantage that it does not demand a high spectroscopic resolution and thus has the benefit of using broad band lasers and thermally distributed atomic beams. These inherent characteristics make the method highly useful for the separation of odd isotopes with small isotope shifts and broad hyperfine structures.

5.2 Experimental scheme employed

The experimental set up is similar to the one described in § 3.3.1. The schematic excitation scheme used in these experiments is given in Fig.5.1.

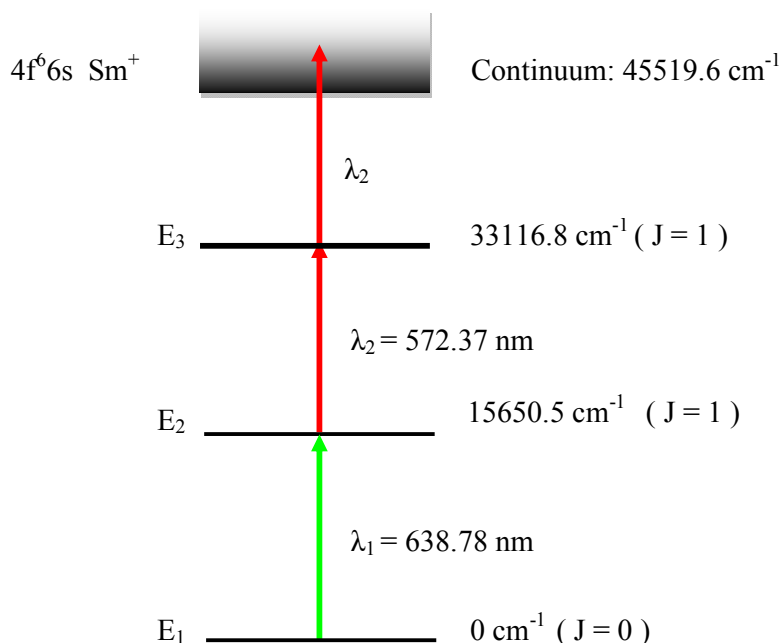


Fig. 5.1: Excitation Scheme

Photoionization experiments were performed by tuning the first dye laser (DL_1) to the known Sm I atomic transition $0 \text{ cm}^{-1}(J=0) \rightarrow 15650.5 \text{ cm}^{-1} (J=1)$. The excitation of the population from the level at $15650.5 \text{ cm}^{-1} (J=1)$ to the second excited level at $33116.8 \text{ cm}^{-1} (J=1)$ and further ionization to the continuum is done by using the second dye laser (DL_2) via a resonant $\lambda_1 + 2\lambda_2$ process. DCM and Rh6G dyes are used in DL_1 and DL_2 lasers to produce laser photons at desired wavelengths λ_1 and λ_2 respectively. Spatially overlapped DL_1 and DL_2 lasers are then sent through a samarium atomic beam formed in the high vacuum atomic beam generator that is coupled to the TOFMS.

In these experiments, two different polarizations for the excitation lasers were used: case

(a) when both lasers have parallel linear polarization ($\hat{e}_1 \parallel \hat{e}_2$) and case (b) when λ_1 is circularly polarized while λ_2 is linearly polarized.

5.3 Principle behind the process

The basic principle behind Sm isotope separation technique based on polarization selection rules is schematically shown in Fig.5.2 (a & b). The figures illustrate the possible excitation routes for even and odd isotopes from the ground state of Sm I for parallel linear polarizations the excitation lasers. The symbols J and M_J denote the total angular momentum quantum number and the magnetic quantum number respectively. As shown in the Fig. 5.2(a), each energy state of an even isotope has $2J+1$ degenerate magnetic sublevels. The dipole transitions for the linearly polarized (π) radiations are allowed between magnetic sublevels of same M_J except for the forbidden transition $\Delta J = 0, \Delta M_J = 0$ and $M_J : 0 \leftrightarrow 0$. Thus the second step transition ($J = 1, M_J = 0 \rightarrow J = 1, M_J = 0$) is forbidden for an even isotope and hence the population remains trapped in the first excited state, $E_1 (J=1)$ when both the excitation lasers have parallel linear polarization. In the case of an odd isotope, due to nonzero nuclear spin ($I = 7/2$) there is hyperfine interaction between J and I and hence F becomes the good quantum number instead of J resulting in hyperfine structure for the energy state. For example, the excited state ($J = 1$) splits into three ($F= 5/2, F=7/2$ and $F= 9/2$) hyperfine energy levels. Each hyperfine state has $2F+1$ degenerate magnetic sublevels M_F as shown in Fig. 5.2(b). Transitions between the magnetic sublevels satisfying $\Delta M_F = 0$ for $\Delta F = 0, \pm 1$ are then allowed in this case with the exception of the transition $\Delta F = 0, \Delta M_F = 0$ and $M_F = 0 \leftrightarrow 0$.

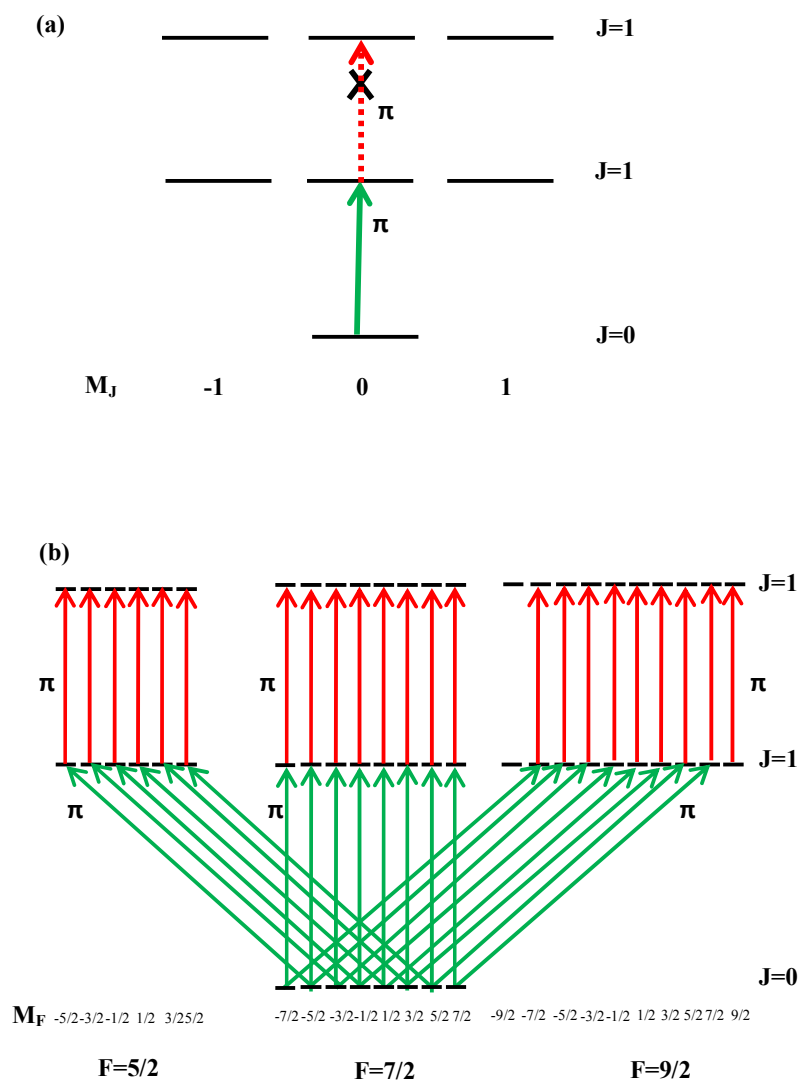


Fig. 5.2: Transitions between magnetic sublevels of Sm I for parallel linear polarizations of the excitation lasers. (a) even isotope (b) odd isotope for the chosen scheme. Forbidden transition is labelled with a cross.

Thus, there are possible excitation pathways to the excited level E_2 ($J=1$) in the case of an odd isotope. Conversely, if any one of the excitation lasers is circularly polarized, due to the M_J selection rule of $\Delta M_J = \pm 1$ for circularly polarized light; the yield of the even isotope will be non-zero. For example, Fig. 5.3 illustrates the transitions between magnetic sublevels of even isotopes in case when the first step laser is circularly polarised and the second laser is linearly polarised. Hence, isotope-selective excitation of the odd isotopes is possible when appropriate combinations of J-values and laser polarizations are used.

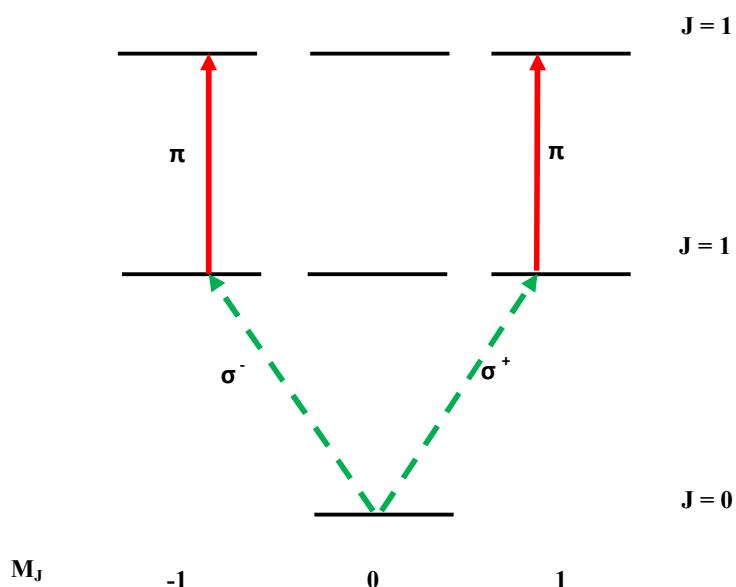


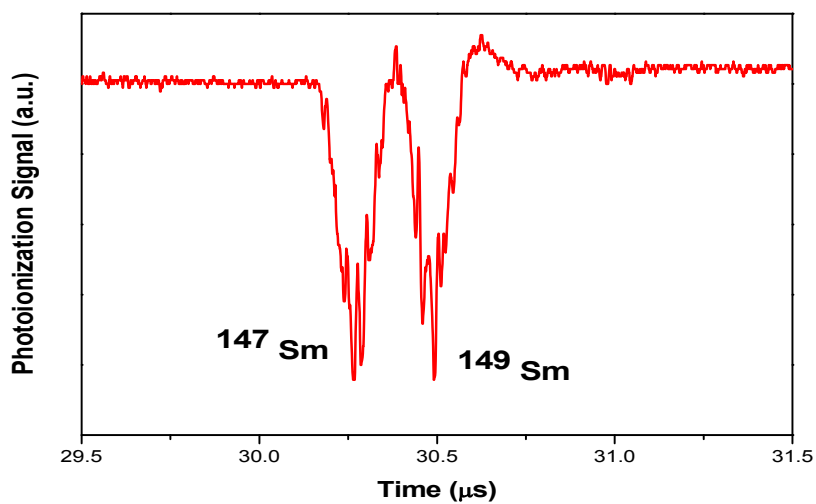
Fig. 5.3: *Transitions between magnetic sublevels of Sm I in case of an even isotope when λ_1 is circularly polarized and λ_2 is linearly polarized*

5.4 Results and discussion

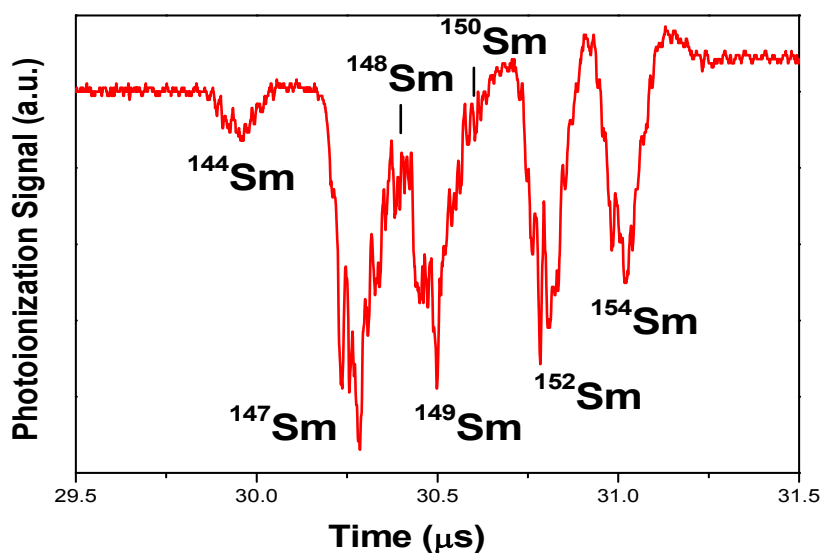
Two-color photoionization spectroscopy of Sm I is performed for two different cases of polarizations of the excitation lasers while keeping all other experimental parameters unchanged. The TOF-mass spectra of the photoions produced when a) both λ_1 and λ_2 lasers

have parallel linear polarization and b) λ_1 is circularly polarized and λ_2 is linearly polarized are shown in Fig.5.4 (a & b) respectively. In case (a), selective ionization of the two odd isotopes of Sm (^{147}Sm and ^{149}Sm) could be seen very clearly, whereas, in case (b), non-selective photoionization is observed as shown in Fig. 5.4 (b). The observed isotopic ratio ($^{149}\text{Sm}/^{152}\text{Sm}$) measured in case (a) is ~ 40 and in case (b) it is ~ 1 . It may be noted that the mass spectrum observed in Fig. 5.4 (b) does not reflect the natural abundance since it depends on where exactly the peak centre of the first step laser is fixed in between the resonance of ^{144}Sm and ^{154}Sm isotopes and also on the polarization characteristics of the excitation lasers. Thus, using parallel linearly polarized lasers, for the chosen two-color photoionization scheme of Sm I, the isotopic selectivity, which is defined in these studies as the ratio of the observed abundance of $^{149}\text{Sm}/^{152}\text{Sm}$ in case (a) to case (b), of ~ 40 is achieved. It may be added that when compared with the natural abundance ratio of $^{149}\text{Sm}/^{152}\text{Sm}$ of 0.52 the selectivity obtained in case (a) will be approximately 77.

To corroborate it further, the mass-resolved two-color photoionization spectrum of odd and even isotopes were recorded with polarizations of $\hat{e}_1 \parallel \hat{e}_2$, by keeping the boxcar averager gates on the mass peaks corresponding to the odd and even isotopes (^{149}Sm and ^{152}Sm). In this experiment, λ_1 was tuned to the Sm I atomic resonance $0\text{ cm}^{-1}(J=0) \rightarrow 15650.5\text{ cm}^{-1}(J=1)$ and λ_2 was scanned from 570 to 573 nm. The mass-resolved two-color photoionization spectrum observed is shown in Fig.5.5. The resonance at 572.37 nm corresponds to the high-lying level at $33116.8\text{ cm}^{-1}(J=1)$, previously reported in the literature [36] and the second resonance at 570.60 nm corresponds to a new level at 33170.9 cm^{-1} with probable J value of 0 or 2.



(a)



(b)

Fig. 5.4: Two-color photoionization mass spectra (a) when both λ_1 and λ_2 lasers have parallel linear polarization and (b) when λ_1 is circularly polarized and λ_2 is linearly polarized

These resonances are verified as two-color resonances by blocking the first-step laser so that the photoionization signal disappears completely. During these experiments, the second step dye laser fluence was kept low ($\sim 300 \mu\text{J}/\text{cm}^2$) so that it did not produce any single-color multi-photon ionization. It may be seen in Fig.5.5, that the resonance at 572.37 nm has appeared only in the spectrum of the odd isotope confirming the selective photoionization. It is observed that the isotopic-selectivity degrades with increasing power of the excitation lasers due to multi-photon ionization process.

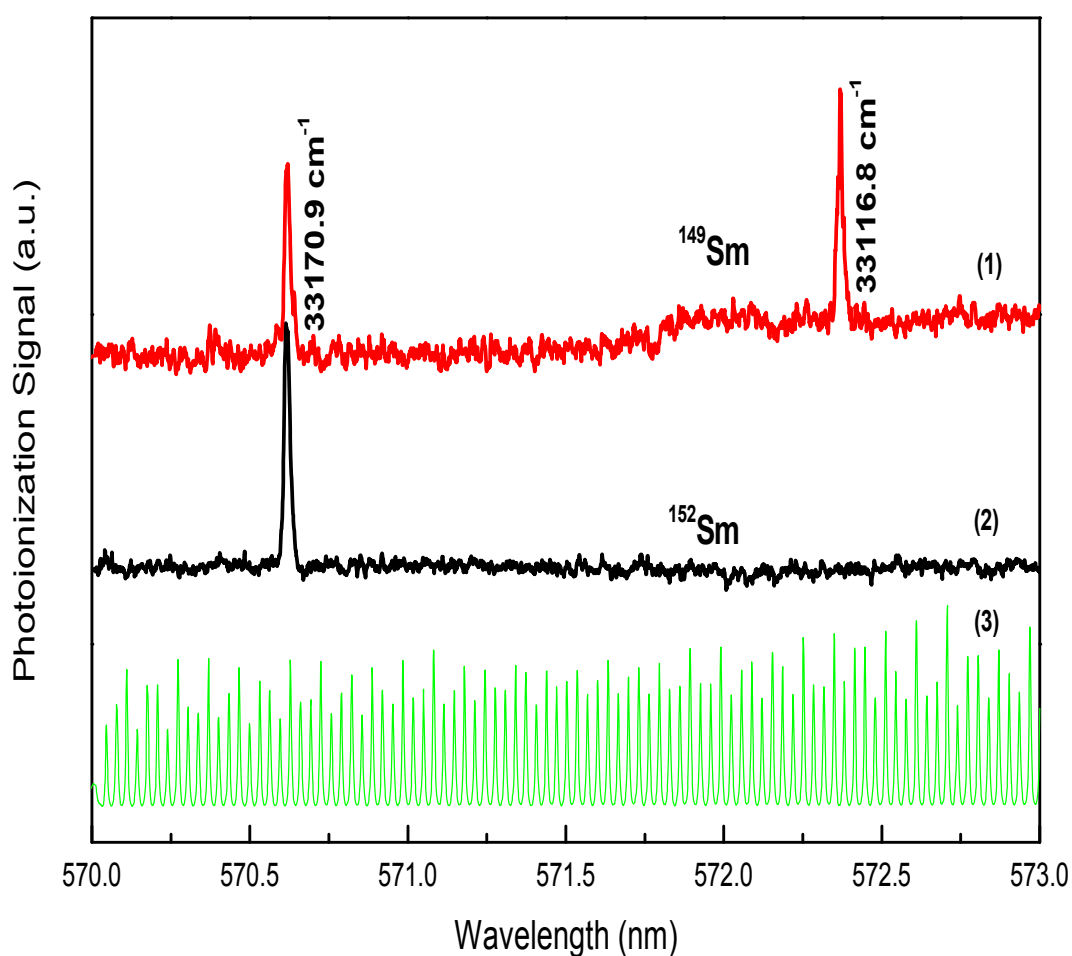


Fig. 5.5: Mass-resolved two-color photoionization spectra of Sm I. (1) Two-color photoionization spectra for the odd isotope (¹⁴⁹Sm) (2) Two-color photoionization spectra for the even isotope (¹⁵²Sm) and (3) Fabry-Perot etalon fringes

5.4.1 Population alignment on changing the quantisation axis

This section describes the effect of relative polarization angle between the two linearly polarized lasers on the ionization yield for even and odd isotopes. In this case, for the chosen excitation scheme, the first laser induces an electronic transition from an initially isotropic ground state $|jm\rangle$ to an excited state $|JM\rangle$. This creates an anisotropic population distribution among the magnetic sub-levels of the excited state due to the non-uniform distribution of the transition strength. Since the atom has an angular momentum ($J=0$) in the initial state, the linearly polarized excitation at the first step can populate only the second state with $J=1$ and $M=0$. The second state wave function is given by,

$$\Psi_{JM} = \Psi_{10} \quad (5.1)$$

This population alignment produced by the first laser is probed by a second laser for which, the electric field makes an angle θ with respect to the polarization axis of the first laser. Consequently, quantization axis is changed to the polarization axis of the second laser and hence the excited state wave function for which M is quantized along the polarization axis of the second laser and is obtained by the linear transformation [95, 102,103, 104, 82],

$$\Psi_{JM} = \sum_{M'=-M}^M D_{M'M}^J(\alpha, \beta, \gamma) \Psi_{JM'} \quad (5.2)$$

Where Ψ_{JM} is the old wave function and $\Psi_{JM'}$ is the new wave function quantized along the polarization axis of the second laser, $D_{M'M}^J(\alpha, \beta, \gamma)$ are the components of the finite rotation matrix and α , β and γ are the Euler angles. Hence, the second state wave function on changing the quantization axis becomes,

$$\Psi_{10}(\theta) = \left[\left(\frac{\sin \theta}{\sqrt{2}} \right) \psi_{1-1} + (\cos \theta) \psi_{10} - \left(\frac{\sin \theta}{\sqrt{2}} \right) \psi_{11} \right] \quad (5.3)$$

The above equation illustrates that the population gets realigned between the magnetic sub-levels ($M_J = -1, 0$ and 1) and this redistribution of population between the magnetic sublevels can be controlled by changing the relative polarization angle. In the special case of polarizations of $E_1 \perp E_2$,

$$\Psi_{10}(90^\circ) = \frac{1}{\sqrt{2}} [\psi_{1-1} - \psi_{11}] \quad (5.4)$$

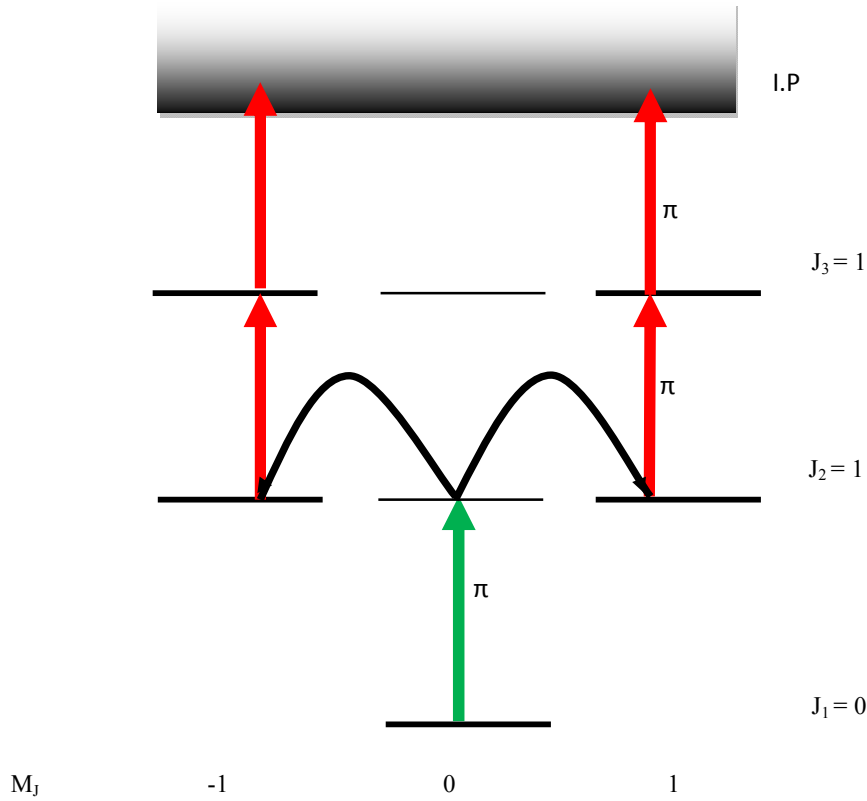


Fig. 5.6: Population alignments along the excitation ladder in case of an even isotope with cross polarizations of the excitation lasers

Thus, the population gets reoriented between the magnetic sublevels with $M_J = \pm 1$ as shown in Fig. 5.6 when the quantization axis is rotated by 90 degree. In the figure, the bent arrows show the redistribution of population among the magnetic sublevels and the bold lines differentiate the populated components on changing the quantization axis along the polarization axis of the second laser. The second-step transition obeys the selection rule $\Delta M = 0$. The third state wave function will have components with the same projection values as in the second state but with different coefficients. The square matrix element for the 2nd step transition $J_2 \rightarrow J_3$ is proportional to

$$|W_{J_2 J_3}|^2 \propto \sum_{M=-J_{\min}}^{M=J_{\min}} |D_M|^2 \begin{pmatrix} J_3 & 1 & J_2 \\ -M & 0 & M \end{pmatrix}^2 \quad (5.5)$$

where J_{\min} is the smaller of the two numbers J_2, J_3 . The sum in the above equation depends on the relative polarization angle through the coefficient D_M and the second factor, the $3j$ symbol gives the relative line strength.

$$|W_{J_2 J_3}|^2 \propto \left[\left(\frac{\sin \theta}{\sqrt{2}} \right)^2 \begin{pmatrix} 1 & 1 & 1 \\ 1 & 0 & -1 \end{pmatrix}^2 + (\cos \theta)^2 \begin{pmatrix} 1 & 1 & 1 \\ 0 & 0 & 0 \end{pmatrix}^2 + \left(-\frac{\sin \theta}{\sqrt{2}} \right)^2 \begin{pmatrix} 1 & 1 & 1 \\ -1 & 0 & 1 \end{pmatrix}^2 \right] \\ \propto \sin^2 \theta \quad (5.7)$$

Due to this redistribution of atoms between the magnetic sub-levels [96, 102, 36], the second step transition, which is forbidden for $E_1 \parallel E_2$ polarization in case of an even isotope,

becomes allowed for different orientations of E_2 with respect to E_1 , thus degrading the selectivity of the process.

5.4.2 Dependence of relative polarisation angle on selectivity

The photoionization yield for odd and even isotopes is measured as a function of relative polarization angle(θ) between first and second step lasers for the chosen photoionization scheme. The ion yield for the odd isotopes does not show significant dependence on the relative polarization angle whereas that of the even isotope was strongly dependant on θ . The ratio of even to odd isotope (^{152}Sm to ^{149}Sm) photoionization yields as a function of polarization angle between two lasers is shown in Fig.5.7. The dependence of the even mass isotope signal on the relative polarization angle followed $\sin^2\theta$, which is in excellent agreement with theoretical predictions. Degradation in the selectivity of the process as the relative polarization angle between the two lasers is rotated from linear to perpendicular is observed with a minimum selectivity at a relative polarization angle of 90 degrees between the two lasers.

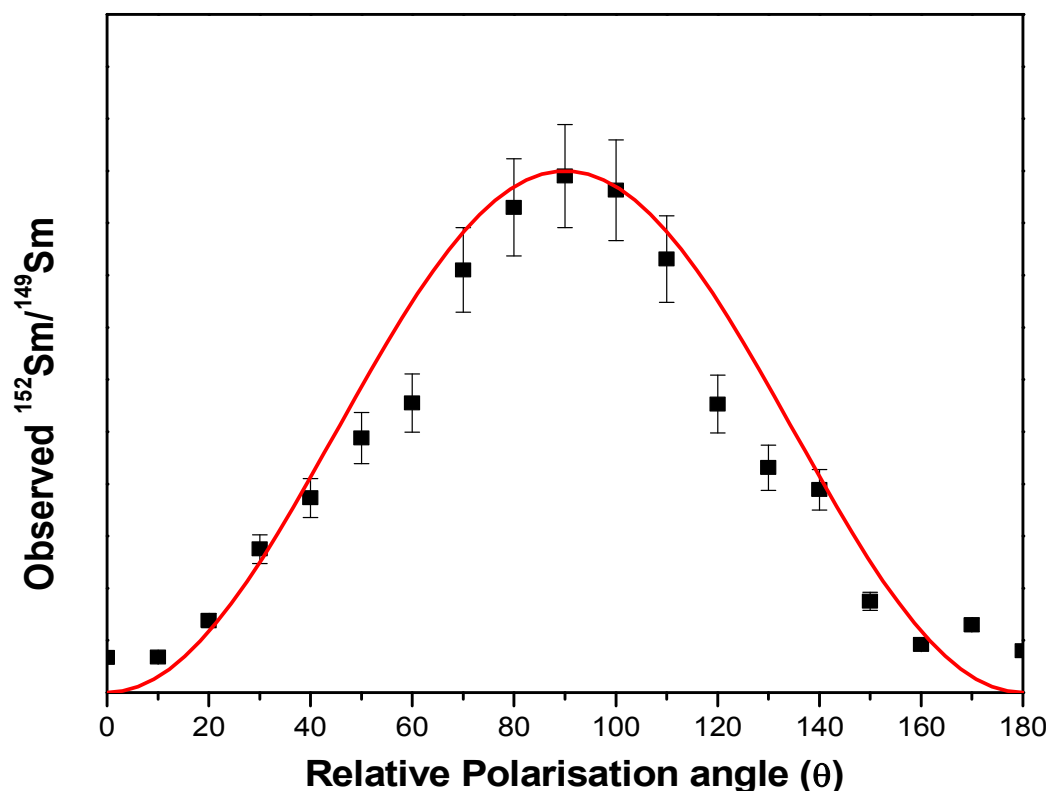


Fig. 5.7: Dependence of the ratio of the photoionization signal for the even isotope to that of the odd isotope ($^{152}\text{Sm}/^{149}\text{Sm}$) on relative polarization angle (θ) between the two dye lasers

5.5 Conclusions

Polarization-based isotope-selective photoionization of odd isotopes of Sm I has been investigated by using two-color three-photon photoionization spectroscopy with broad band lasers. Isotopic-selectivity of more than 40 between the odd and even isotopes of atomic Sm has been experimentally demonstrated by judiciously selecting proper excitation sequence and polarizations of the excitation lasers. To our knowledge, this is the first experimental

demonstration of isotope-selective excitation of odd isotopes of samarium using polarized laser beams. Since the technique has the advantage that the isotopic selectivity is not affected by the spectral broadening of the excitation lasers, it is highly useful for the separation of odd and even isotopes exhibiting overlapping spectra owing to small isotope shifts and broad hyperfine structures. Studies reported in this chapter also include the effect of different states of polarization of the excitation lasers and the relative polarization angle between them on the isotopic selectivity.

Chapter 6:

Conclusions and Future Prospects

Chapter 6

The applications of multi-step resonance ionization spectroscopic techniques for the measurement of various atomic parameters of samarium ($Z=62$) has been presented in this thesis. The work described here involves the determination of atomic parameters like energy values, total angular momenta, isotope shifts and radiative lifetimes of high-lying energy levels of atomic samarium. The knowledge of most of these atomic parameters find application in many areas of science such as atomic physics, laser physics, plasma physics, laser chemistry, atmospheric science, astrophysics etc. Particularly, in an isotope selective multi-step photoionization process, the choice of an efficient and selective photoionization scheme demands developing a complete data base of the atomic parameters of the energy levels with their detailed spectroscopic characterisation. Apart from this, a novel isotope selective photoionization technique based on polarisation selection rule for efficient isotope-selective photoionization of the odd isotopes of samarium using broad band lasers has been described in detail in this thesis.

The energy level values, total angular momenta and isotope shifts of the second excited levels of samarium has been measured using two-colour photoionization spectroscopy employing an atomic beam coupled with a time-of-flight mass spectrometer. Two-colour three-photon resonance photoionization spectra of atomic Sm were investigated in the energy regions $33136 - 33960 \text{ cm}^{-1}$ and $35450 - 35750 \text{ cm}^{-1}$. The analysis of the photoionization spectra recorded in these regions has resulted in the identification of twenty one new and confirmation of twenty previously reported energy levels in these regions. The energy values of the newly identified energy levels have been assigned with an accuracy of $\pm 0.3 \text{ cm}^{-1}$. Based on the excitation scheme used, most of the new levels have been identified with a

unique total angular momentum (J). In addition, by performing mass-resolved photoionization spectroscopy, the isotope shifts of twenty eight high-lying (second excited) levels of Sm I were measured.

The radiative lifetimes of the even-parity high-lying levels of atomic samarium has been measured by delayed photoionization measurements using pump-probe spectroscopy. The radiative lifetimes of fifteen even-parity high-lying levels in the energy range 34000-34815 cm^{-1} were measured for the first time. The measured values are in the range of 35 to 349 ns. The accuracy of the measurements was validated by measuring the lifetime of the first excited level used in the excitation scheme by employing two-colour pump-probe photoionization spectroscopy and comparing the measured value with that reported in the literature.

As discussed before, radiative lifetime is an important atomic parameter when combined with branching ratio can provide another vital atomic parameter, the absolute transition probability which finds application in many areas of science such as laser physics, plasma physics, astrophysics etc. These parameters also play crucial role in applications like laser isotope separation, trace elemental analysis, etc.

A polarization based isotope selective photoionization technique for selective photoionization of odd isotopes of samarium has been experimentally demonstrated using broad band lasers. Isotope-selectivity of more than 40 between the odd and even isotopes ($^{149}\text{Sm} / ^{152}\text{Sm}$) of atomic Sm has been experimentally demonstrated by judiciously selecting proper angular momentum sequence of the levels involved in the excitation scheme and laser polarizations. This is the first experimental demonstration of isotope-selective photoionization of the odd isotopes of samarium using polarized lasers. Since the technique

has the advantage that the isotopic selectivity is not affected by the spectral broadening of the excitation lasers, it is highly useful for the separation of odd and even isotopes exhibiting overlapping spectra owing to small isotope shifts and broad hyperfine structures. The effect of different states of polarization of the excitation lasers and the relative polarization angle between them on the isotope selectivity is also discussed in detail in this chapter. The future studies in this direction can include the effect of magnetic field and laser intensities on the selectivity of the photoionization process.

The techniques employed in the work presented in the thesis are universal and can be utilised for the determination of the atomic parameters of any element of interest. As previously mentioned, multi-step photoionization in general has diverse applications in many areas of science as well as in industry. The major applications of multi-step photoionization are in the fields of isotope selective photoionization processes such as laser isotope separation process, trace elemental/isotopic analysis etc. The isotope selective photoionization process is not restricted only to nuclear fuel cycle but finds equally important applications in the separation of isotopes which have medical significance as well. To summarise, augmenting the atomic data base related to the elements/isotopes of interest can give more insight into the understanding of basic atomic physics as well as it can provide necessary information required for developing novel isotope selective multi-step photoionization processes.

References

References

- [1] Wolfgang Demtröder, "*Laser spectroscopy - 1: Basis Principles*," (Springer, 2014).
- [2] William F Meggers, "*Review of Reviews of Atomic Spectroscopy*," *Applied Optics* 2 (7), 657-663 (1963).
- [3] Wolfgang Demtröder, "*Laser spectroscopy: basic concepts and instrumentation*," (Springer Science & Business Media, 2013).
- [4] AK Pulhani, "Laser Spectroscopic Investigations of Lanthanides and Actinides," Ph. D. Dissertation, Mumbai University, India (2011).
- [5] Richard W Solarz, "*Laser spectroscopy and its applications*," (Routledge, 2017).
- [6] ML Shah, "*Laser Spectroscopic Techniques and Related Instrumentation for Studies on Lanthanides and Actinides*," Ph. D. Dissertation, Homi Bhabha National Institute, India (2016).
- [7] Wolfgang Demtröder, "*Laser spectroscopy - 2 : Experimental Techniques*," (Springer, 2015).
- [8] Vladilen Letokhov, "*Laser photoionization spectroscopy*," (Elsevier, 2012).
- [9] BM Suri, "*High-Resolution Spectroscopy*," *Laser Physics and Technology* (Springer, 2015), pp. 223-251.
- [10] LR Carlson, SA Johnson, EF Worden, CA May, RW Solarz, and JA Paisner, "*Determination of absolute atomic transition probabilities using time resolved optical pumping*," *Optics Communications* **21** (1), 116-120 (1977).
- [11] VN Fedoseyev, VS Letokhov, VI Mishin, GD Alkhazov, AE Barzakh, VP Denisov, AG DERNYATIN, and VS Ivanov, "*Atomic lines isotope shifts of short-lived radioactive Eu studied by high-sensitive laser resonance photoionization method in "on-line" experiments with proton beams*," *Optics communications* **52** (1), 24-28 (1984).

-
- [12] Klaus Wendt, Norbert Trautmann, and Bruce A Bushaw, "*Resonant laser ionization mass spectrometry: an alternative to AMS?*," Nuclear Instruments and Methods in Physics Research Section B: Beam Interactions with Materials and Atoms **172** (1-4), 162-169 (2000).
- [13] Robert D Cowan, "*The theory of atomic structure and spectra*," (Univ of California Press, 1981).
- [14] Walter Albertson, "*The arc spectrum of samarium and gadolinium. Normal electron configurations of the rare earths*," Physical Review **47** (5), 370 (1935).
- [15] Walter Albertson, "*An Extension of the Analysis of the Spectrum of Neutral Samarium, Sm I*," Physical Review **52** (6), 644 (1937).
- [16] Arthur S King, "*Temperature classification of samarium lines*," The Astrophysical Journal **82**, 140 (1935).
- [17] William F Meggers, "*Atomic spectra of rare earth elements*," Reviews of Modern Physics **14** (2-3), 96 (1942).
- [18] William F Meggers, "*Electron Configurations of `Rare-Earth' Elements*," Science **105** (2733), 514-516 (1947).
- [19] JG Conway and BG Wybourne, "*Low-lying energy levels of lanthanide atoms and intermediate coupling*," Physical Review **130** (6), 2325 (1963).
- [20] Victor G Mossotti and Velmer A Fassel, "*The atomic absorption spectra of the lanthanide elements*," Spectrochimica Acta **20** (7), 1117-1127 (1964).
- [21] G Racah and U Ganiel, "*Subconfiguration $f^6 (7 F) sp$ in Sm I*," JOSA **56** (7), 893-895 (1966).
- [22] Joseph Reader and Jack Sugar, "*Ionization energies of the neutral rare earths*," JOSA **56** (9), 1189-1194 (1966).

-
- [23] KF Zmbov and JL Margrave, *"The First Ionization Potentials of Samarium, Europium, Gadolinium, Dysprosium, Holmium, Erbium, Thulium, and Ytterbium by the Electron-Impact Method,"* The Journal of Physical Chemistry **70** (9), 3014-3017 (1966).
- [24] U Ganiel, *"Comments on the study of the Zeeman effect in Sml,"* Zeitschrift für Physik **200** (4), 419-420 (1967).
- [25] GR Hertel, *"Surface Ionization. III. The First Ionization Potentials of the Lanthanides,"* The Journal of Chemical Physics **48** (5), 2053-2058 (1968).
- [26] Leo Brewer, *"Energies of the electronic configurations of the singly, doubly, and triply ionized lanthanides and actinides,"* JOSA **61** (12), 1666-1682 (1971).
- [27] WC Martin, *"Energy Differences between Two Spectroscopic Systems in Neutral, Singly Ionized, and Doubly Ionized Lanthanide Atoms,"* JOSA **61** (12), 1682-1686 (1971).
- [28] WC Martin, Lucy Hagan, Joseph Reader, and Jack Sugar, *"Ground levels and ionization potentials for lanthanide and actinide atoms and ions,"* Journal of Physical and Chemical Reference Data **3** (3), 771-780 (1974).
- [29] CH Corliss W. F. Meggers, and B. F. Scribner, *"Tables of Spectral-Line Intensities, Part I – Arranged by Elements, Part II – Arranged by Wavelengths,"* Natl. Bur. Stand. Monograph 145. Nat. Bur. Stand., U.S., 600 pp. (1975).
- [30] Albert C Parr and Mark G Inghram, *"Photoionization of samarium in the threshold region,"* JOSA **65** (5), 613-614 (1975).
- [31] Wolfgang Demtröder, *"Laser spectroscopy-1 basis principles,"* 5th edition, Springer-Verlag Berlin Heidelberg 2014.

-
- [32] EF Worden, R_W Solarz, JA Paisner, and JG Conway, "*First ionization potentials of lanthanides by laser spectroscopy*," JOSA **68** (1), 52-61 (1978).
- [33] VE Dobryshin, NA Karpov, SA Kotochigova, BB Krynetskii, VA Mishin, OM Stelmakh, and VM Shustryakov, "*Laser spectroscopy of atomic-samarium autoionization levels*," Optics and Spectroscopy **54**, 244-247 (1983).
- [34] Hu Sufen, Z nang Sen, Mei Shimin, Qui Jizhen, and Chen Xing, "*Investigation of highly excited states of Sm*," Journal of Quantitative Spectroscopy and Radiative Transfer **43** (1), 75-79 (1990).
- [35] Liejuan Jia, Chunyang Jing, Zhiyao Zhou, and Fucheng Lin, "*Studies of high-lying even-parity levels of Sm i: energies and isotope shifts*," JOSA B **10** (8), 1317-1320 (1993).
- [36] T Jayasekharan, MAN Razvi, and GL Bhale, "*Observation of new even-parity states of Sm I by resonance ionization mass spectrometry*," JOSA B **13** (4), 641-648 (1996).
- [37] T Jayasekharan, MAN Razvi, and GL Bhale, "*Investigations of new high-lying even-parity energy levels of the samarium atom below its first ionization limit*," JOSA B **17** (9), 1607-1615 (2000).
- [38] T Jayasekharan, MAN Razvi, and GL Bhale, "*Even-parity bound and autoionizing Rydberg series of the samarium atom*," Journal of Physics B: Atomic, Molecular and Optical Physics **33** (16), 3123 (2000).
- [39] Hyun Min Park, Hyun Chae Kim, Jong Hoon Yi, Jae Min Han, Yong Joo Rhee, and Jong Min Lee, "*The odd-parity autoionization states of Sm atom determined by three-step excitation*," Journal of the Korean Physical Society **33** (3), 288-291 (1998).

-
- [40] AI Gomonař and OI Kudelich, "*Resonance three-photon ionization of samarium atom by laser radiation in the range from 17200 to 17900 cm⁻¹*," *Optics and Spectroscopy* **93** (2), 198-207 (2002).
- [41] AI Gomonai and OI Plekan, "*Single-colour resonance three-photon ionization of samarium atoms*," *Journal of Physics B: Atomic, Molecular and Optical Physics* **36** (20), 4155 (2003).
- [42] Osamu Kujirai and Youichi Ogawa, "*Study of even-parity autoionization states of samarium atom by laser optogalvanic spectroscopy*," *Journal of the Physical Society of Japan* **72** (5), 1057-1068 (2003).
- [43] Takashi Wakui, Wei-Guo Jin, Kenji Hasegawa, Haruko Uematsu, Tatsuya Minowa, and Hidetsugu Katsuragawa, "*High-resolution diode-laser spectroscopy of the rare-earth elements*," *Journal of the Physical Society of Japan* **72** (9), 2219-2223 (2003).
- [44] BK Ankush, MN Deo, A Venugopalan, and SA Ahmad, "*Isotope shift studies in UV lines of Sm I on FTS: level isotope shifts and configuration assignments of the energy levels of neutral samarium atom*," *The European Physical Journal D-Atomic, Molecular, Optical and Plasma Physics* **30** (3), 303-316 (2004).
- [45] A Schmitt, Bruce A Bushaw, and Klaus Wendt, "*Determination of the 154Sm ionization energy by high-precision laser spectroscopy*," *Journal of Physics B: Atomic, Molecular and Optical Physics* **37** (8), 1633 (2004).
- [46] AK Pulhani, ML Shah, Vas Dev, and BM Suri, "*High-lying even-parity excited levels of atomic samarium*," *JOSA B* **22** (5), 1117-1122 (2005).
- [47] AK Pulhani, ML Shah, GP Gupta, and BM Suri, "*Measurement of total angular momentum values of high-lying even-parity atomic states of samarium by spectrally resolved laser-induced fluorescence technique*," *Pramana* **75** (6), 1135-1139 (2010).

-
- [48] Zhao Hong-Ying, Dai Chang-Jian, and Guan Feng, "*Photoionization spectra of an Sm atom with stepwise excitation*," *Journal of Physics B: Atomic, Molecular and Optical Physics* **42** (6), 065001 (2009).
- [49] Wen-Jie Qin, Chang-Jian Dai, and Ying Xiao, "*Multistep excitation of autoionizing states of the samarium atom*," *Journal of Quantitative Spectroscopy and Radiative Transfer* **111** (1), 63-70 (2010).
- [50] WJ Qin, CJ Dai, and Y Xiao, "*The study of autoionizing states of the samarium atom*," *Journal of Quantitative Spectroscopy and Radiative Transfer* **111** (7-8), 997-1004 (2010).
- [51] Ming Li, Chang-Jian Dai, and Jun Xie, "*Photoionization spectra of even-parity states of Sm atom with multistep excitation*," *Journal of Quantitative Spectroscopy and Radiative Transfer* **112** (5), 793-799 (2011).
- [52] Yan-Hong Zhao, Chang-Jian Dai, and Shi-Wei Ye, "*Study on even-parity highly excited states of the Sm atom*," *Journal of Physics B: Atomic, Molecular and Optical Physics* **44** (19), 195001 (2011).
- [53] AI Gomonai and E Yu Remeta, "*Investigation of highly excited states of samarium*," *Optics and Spectroscopy* **112** (1), 15-23 (2012).
- [54] JE Lawler, AJ Fittante, and EA Den Hartog, "*Atomic transition probabilities of neutral samarium*," *Journal of Physics B: Atomic, Molecular and Optical Physics* **46** (21), 215004 (2013).
- [55] ML Shah, AC Sahoo, AK Pulhani, GP Gupta, BM Suri, and Vas Dev, "*Investigations of high-lying even-parity energy levels of atomic samarium using simultaneous observation of two-color laser-induced fluorescence and photoionization signals*," *The European Physical Journal D* **68** (8), 235 (2014).
-

-
- [56] ML Shah, AC Sahoo, AK Pulhani, GP Gupta, B Dikshit, MS Bhatia, and BM Suri, "*Measurements of excited-state-to-excited-state transition probabilities and photoionization cross-sections using laser-induced fluorescence and photoionization signals,*" *Journal of Quantitative Spectroscopy and Radiative Transfer* **142**, 9-16 (2014).
- [57] VN Fedosseev, L-E Berg, DV Fedorov, D Fink, Olli J Launila, R Losito, BA Marsh, RE Rossel, S Rothe, and MD Seliverstov, "*Upgrade of the resonance ionization laser ion source at ISOLDE on-line isotope separation facility: New lasers and new ion beams,*" *Review of Scientific Instruments* **83** (2), 02A903 (2012).
- [58] Kyuseok Song, Hyungki Cha, and Jongmin Lee, "*Determination of samarium by the use of 2-color 3-photon resonance ionization mass spectrometry,*" *Journal of Analytical Atomic Spectrometry* **13** (10), 1207-1210 (1998).
- [59] Masabumi Miyabe, Masaki Oba, and Ikuo Wakaida, "*Isotope shift measurement for high-lying energy levels of atomic uranium by resonance ionization mass spectrometry,*" *Journal of the Physical Society of Japan* **70** (5), 1315-1320 (2001).
- [60] Masanori Wakasugi, Takayoshi Horiguchi, Wei Guo Jin, Hidefumi Sakata, and Yasukazu Yoshizawa, "*Changes of the nuclear charge distribution of Nd, Sm, Gd and Dy from optical isotope shifts,*" *Journal of the Physical Society of Japan* **59** (8), 2700-2713 (1990).
- [61] JA Ransohoff, J. A. Ransohoff, US Patent, 3,103,479 (1963).
- [62] JA Renier, J.-P. A. Renier and M. L. Grossbeck: "*Development of improved nuclear poisons for commercial nuclear power reactors,*" ORNL/TM-2001/238 63 (2001).
- [63] Orazio Svelto and David C Hanna, *Principles of lasers.* (Springer, 1998).
- [64] Balkrishna B Laud, "*Lasers and nonlinear optics,*" (1986).

-
- [65] WC Wiley and Ii H McLaren, "*Time-of-flight mass spectrometer with improved resolution*," *Review of scientific instruments* **26** (12), 1150-1157 (1955).
- [66] Ramesh Chandra Das "*Development of Mass Selective Ion Manipulation Techniques for Spectroscopic Studies*", Dr. K. G. Manohar and Prof. B. N. Jagatap, Ph. D. Thesis submitted to the University of Mumbai, December [2012].
- [67] MN Reddy, "*Laser optogalvanic spectroscopy: Experimental details and potential applications in R and D*," *Defence Science Journal* **44** (4), 279 (1994).
- [68] Byron A Palmer, Richard A Keller, and Rolf Engleman Jr, 1980.
- [69] Beniamino Barbieri, Nicolo Beverini, and Antonio Sasso, "*Optogalvanic spectroscopy*," *Reviews of modern physics* **62** (3), 603 (1990).
- [70] Joseph Ladislav Wiza, "*Microchannel plate detectors*," *Nucl. Instrum. Methods* **162** (1-3), 587-601 (1979).
- [71] JL Collier, BJ Goddard, DC Goode, S Marka, and HH Telle, "*A low-cost gated integrator boxcar averager*," *Measurement science and technology* **7** (9), 1204 (1996).
- [72] Hyunmin Park, Miran Lee, EC Jung, Jonghoon Yi, Yongjoo Rhee, and Jongmin Lee, "*Isotope shifts of Sm I measured by diode-laser-based Doppler-free spectroscopy*," *JOSA B* **16** (7), 1169-1174 (1999).
- [73] Hyunmin Park, Duck-Hee Kwon, and Yongjoo Rhee, "*High-resolution spectroscopy of Sm I performed with an extended-cavity violet diode laser*," *JOSA B* **21** (6), 1250-1254 (2004).
- [74] Pushpa M Rao, SA Ahmad, A Venugopalan, and GD Saksena, "*Isotope shifts and electronic configurations of the odd parity energy levels of singly ionised samarium*," *Zeitschrift für Physik D Atoms, Molecules and Clusters* **15** (3), 211-220 (1990).

-
- [75] William Holland King, *"Isotope shifts in atomic spectra,"* (Springer Science & Business Media, 2013).
- [76] KG.Manohar "*Development and applications of dye laser systems in multi-step photoionization spectroscopy of uranium atom*", Ph. D. Dissertation, Mumbai University, India (1991).
- [77] H Brand, B Seibert, and A Steudel, "*Laser-atomic-beam spectroscopy in Sm: isotope shifts and changes in mean-square nuclear charge radii,*" *Zeitschrift für Physik A Atoms and Nuclei* **296** (4), 281-286 (1980).
- [78] Hideaki Niki, Takaaki Kuroyanagi, Yasunobu Horiuchi, and Shigeki Tokita, "*Laser isotope separation of zirconium for nuclear transmutation process,*" *Journal of Nuclear Science and Technology* **45** (sup6), 101-104 (2008).
- [79] LC Balling and JJ Wright, "*Use of angular-momentum selection rules for laser isotope separation,*" *Applied Physics Letters* **29** (7), 411-413 (1976).
- [80] EA Den Hartog and JE Lawler, "*Radiative lifetimes of neutral samarium,*" *Journal of Physics B: Atomic, Molecular and Optical Physics* **46** (18), 185001 (2013).
- [81] Ch R Cowley and G Mathys, "*Line identifications and preliminary abundances from the red spectrum of HD 101065 (Przybylski's star),*" *Astronomy and Astrophysics* **339**, 165-169 (1998).
- [82] PT Greenland, "*Laser isotope separation,*" *Contemporary Physics* **31** (6), 405-424 (1990).
- [83] PK Mandal, RC Das, AU Seema, AC Sahoo, ML Shah, AK Pulhani, KG Manohar, and Vas Dev, "*Radiative lifetimes, branching ratios and absolute transition probabilities of atomic uranium by delayed photoionization measurements,*" *Applied Physics B* **116** (2), 407-413 (2014).

-
- [84] RC Das, PK Mandal, ML Shah, AU Seema, DR Rathod, Vas Dev, KG Manohar, and BM Suri, "*Measurements of radiative lifetime of high-lying odd parity energy levels of U1*," *Journal of Quantitative Spectroscopy and Radiative Transfer* **113** (5), 382-386 (2012).
- [85] Alan Corney, "*Atomic and laser spectroscopy*," (Clarendon Press Oxford, 1978).
- [86] Charles H Corliss, "*Experimental transition probabilities for spectral lines of seventy elements*," NBS monograph **53**, 80-81 (1962).
- [87] E Handrich, A Steudel, R Wallenstein, and H Walther, "*Level crossing experiments in the Tm I and Sm I spectra*," *Le Journal de Physique Colloques* **30** (C1), C1-18-C11-23 (1969).
- [88] Wei Zhang, Yanyan Feng, and Zhenwen Dai, "*Radiative lifetime measurements of odd-parity moderately excited levels belonging to $J= 0, 1, 2, 3$ series in Sm I*," *JOSA B* **27** (11), 2255-2261 (2010).
- [89] Wei Zhang, Yanyan Feng, Guijuan Sun, and Zhenwen Dai, "*Radiative lifetime measurements of odd-parity moderately excited levels belonging to $J= 4, 5, 6$ and 7 series in Sm I*," *Journal of Physics B: Atomic, Molecular and Optical Physics* **43** (23), 235005 (2010).
- [90] ML Shah, AK Pulhani, GP Gupta, and BM Suri, "*Measurements of radiative lifetimes, branching fractions, and absolute transition probabilities in atomic samarium using laser-induced fluorescence*," *JOSA B* **27** (3), 423-431 (2010).
- [91] AC Sahoo, ML Shah, PK Mandal, AK Pulhani, GP Gupta, Vas Dev, and BM Suri, "*Measurement of radiative lifetime in atomic samarium using simultaneous detection of laser-induced fluorescence and photoionization signals*," *Pramana* **82** (2), 403-408 (2014).

-
- [92] AU Seema, PK Mandal, Asawari D Rath, and Vas Dev, "*New even-parity high-lying levels of Sm I and measurement of isotope shifts by two-color resonance ionization mass spectrometry,*" *Journal of Quantitative Spectroscopy and Radiative Transfer* **145**, 197-204 (2014).
- [93] C-M Gao, C-F Wang, C-T Jin, Y-X An, and D-F Zhou, "*Natural radiative lifetime measurement of excited states of Sm atoms,*" *Kexue Tongbao(Chinese Science Bulletin)(USA)* **38** (5), 393-395 (1993).
- [94] P Hannaford and RM Lowe, "*Some recent developments in atomic lifetime determinations,*" *Australian Journal of Physics* **39** (5), 829-844 (1986).
- [95] H Niki, "*Two-Color Ionization Spectroscopy and Laser Isotope Separation of Zirconium for Efficient Transmutation of Long-lived Fission Products,*" *J. Korean Phys. Soc.* 56. **190** (2010).
- [96] E Le Guyadec, J Ravoire, R Botter, F Lambert, and A Petit, "*Effect of a magnetic field on the resonant multistep selective photoionization of gadolinium isotopes,*" *Optics communications* **76** (1), 34-41 (1990).
- [97] CA Haynam, BJ Comaskey, J Conway, J Eggert, J Glaser, Edmund W Ng, JA Paisner, RW Solarz, and EF Worden, "*Gadolinium enrichment technology at Lawrence Livermore National Laboratory,*" *Proc. SPIE* **1859**, 24 (1993).
- [98] Hideaki Niki, Kazunori Motoki, Masateru Yasui, Yasunobu Horiuchi, Shigeki Tokita, and Yasukazu Izawa, "*Selectivity and efficiency of laser isotope separation processes of gadolinium,*" *Journal of nuclear science and technology* **43** (4), 427-431 (2006).
- [99] Hideaki Niki, Takaaki Kuroyanagi, and Kazuhiro Motozu, "*Isotopic Selectivity in Two-Color Multi-photon Ionization Spectroscopy of Zirconium,*" *Japanese Journal of Applied Physics* **48** (11R), 116510 (2009).

-
- [100] GI Bekov, AN Zherikhin, VS Letokhov, VI Mishin, and V Fedoseev, "*Differences in the yields of even and odd Yb isotopes in multi-step photoionization by polarized laser beams,*" JETP Lett **33** (9) (1981).
- [101] R Zalubas W. C. Martin, and L. Hagan, "*Atomic Energy Levels – The Rare-Earth Elements,*" in Nat. Stand. Ref. Data Ser. NSRDS-NBS 60, 422 pp. (Nat. Bur. Stand., U.S., 1978). (1978).
- [102] WC Martin, R Zalubas, and L Hagan, "*Atomic Energy Levels—The Rare Earth Elements, Natl. Bur. Stand. Ref. Data Ser., Natl. Bur. Stand.(US) Circ. No. 60,*" (1978).
- [103] MP Chernomorets, MV Dubov, and GV Klishevich, "*Determination of the Pu autoionizing level angular momenta by a multistep excitation with linearly polarized laser light,*" Optics communications **171** (4-6), 253-261 (1999).
- [104] RN Zare, "*Angular Momentum Wiley,*" New York.[5] (1988).